1-1-2018

Photochemistry of Polycyclic Aromatic Hydrocarbons with Environmentally Relevant Metals

John P. Haynes
University of Denver

Photochemistry of Polycyclic Aromatic Hydrocarbons with Environmentally Relevant Metals

_____

A Dissertation

Presented to

the Faculty of Natural Sciences and Mathematics

University of Denver

_____

In Partial Fulfillment

of the Requirements for the Degree

Doctor of Philosophy

_____

by

John P. Haynes

June 2018

Advisor: Brian J. Majestic

Author: John P. Haynes
Title: Photochemistry of Polycyclic Aromatic Hydrocarbons with Environmentally Relevant Metals
Advisor: Brian J. Majestic
Degree Date: June 2018

ABSTRACT

The details of the work presented in this dissertation focus on simulated reactions in the atmosphere and water systems between persistent aromatic compounds and varying species of metals with an emphasis on iron. Bulk water suspensions of a standard soil and polycyclic aromatic hydrocarbons (PAH) were analyzed for soluble iron by inductively-coupled plasma mass spectroscopy (ICP-MS) following a 16 hour reaction period using simulated sunlight. Significant increases in soluble iron were only seen with 2-3 ring linear PAH and carboxylic acids.

A two-stage study was conducted to investigate the potential for and possible mechanisms involving the photo-oxidation of PAH into humic-like substances (HULIS). Aqueous suspensions of PAH and oxidized PAH products are illuminated by a bench solar simulator and resulting samples are analyzed by high-pressure liquid chromatography (HPLC), UV-Vis, attenuated total reflectance Fourier transformer infrared spectroscopy (ATR-FTIR), solid-phase extraction (SPE), and electrospray ionization/atmospheric pressure chemical ionization mass spectroscopy (ESI/APCI-MS). HULIS production is based on comparison to SRFA and is observed in short chain PAH following a surface dependent path through naphthalene derivative intermediate structures. These results help explain brown carbon and health effects observed in areas affected by urban emissions.

ACKNOWLEDGEMENTS

I would like to take this time to give a very special thank you to my advisor and mentor Dr. Brian J Majestic. I very much appreciate the time, patience, and understanding that you have given to help me grow as a scientist.

A very special thanks is also given to my co-advisor Dr. Keith Miller, whose guidance has always proven very helpful, and the other members of my committee, Drs. Alex Huffman and Shannon Murphy.

My great appreciation also goes out to the many University of Denver faculty members who have offered their time and advice for me and my many constant questions. Thank you very much to Dr. Michelle Knowles, Dr. Todd Wells, Dr. Bryan Cowen, Dr. Gary Bishop, and Dr. John Latham.

I would also like to acknowledge my appreciation for the University of Denver and the National Science Foundation for their funding and support over my time here.

I would also extend my warm regards and special thanks to the undergraduates. Thank you very much to Eva Cutler, Elizabeth Kepl, and Sarah McDonald.

A very special thank you and gratitude to all of my friends and cohorts for your support and words of encouragement! Thanks to my fellow project members Dr. Benton Cartledge, Dr. Nitika Dewan, Molly Haugen, Joe Salazar, Rachel Marini, and Heather Runberg. And to everyone to whom we could lean on for support: Michael Holden, Emily Hager, Amani Alhalwani, Taylor Firman, and Ben Swanson.

And, of course, thank you to my family both near and far for your support.

.

TABLE OF CONTENTS

LIST OF FIGURES

CHAPTER ONE: INTRODUCTION

1.1 Persistent Pollutants

Anthropogenic pollutants such as polycyclic aromatic hydrocarbons (Kim et al. 2013) (PAH) are considered persistent due to their consistent tendency to remain in the environment for extended periods of time. They are often observed to remain stable in the environment up to several days. They are consistently difficult to capture and remove, therefore they are labeled as persistent organic pollutants (POP) (Joss et al. 2005; Andreae and Gelencser 2006). These POP are introduced to the environment directly through many methods, but primarily via combustion of carbon-based fuels. Despite their inherent stability in the environment, POP poses a toxic threat to biological systems (Kim and Aga 2007; Corcoran et al. 2010). The association with oxy-radical generation of atmospheric PAH implicates them with respiratory illness and some are considered highly carcinogenic (Graber and Rudich 2006; Kim et al. 2013). POPs in wastewater are historically difficult to remove from urban water supplies (Joss et al. 2005). Presentations of these in water systems are known to cause mutations in aquatic life (Corcoran et al. 2010) and are potentially linked with altered or accelerated biological processes in humans (Kim and Aga 2007). PAH released into the atmosphere can be difficult to remove and traditional filtration systems in wastewater renewal processes are not able to capture other POP. Therefore these waste products can only be removed or transformed via chemical oxidation processes (Joss et al. 2005; Graber and Rudich 2006).

1.2 HULIS and Humic Character

Humic material is defined as groups of organic compounds which are highly oxidized hydrocarbons with strongly aromatic olefin systems (Andreae and Gelencser 2006; Graber and Rudich 2006). Humic-like substances (HULIS), fulvic, and humic acids all share structure, functionality, and behavior despite their difference in mass range. These differences are seen as being due to their respective environments of development, i.e. atmospheric, aqueous, and terrestrial-borne. Humic and fulvic acids are known to form from aliphatic hydrocarbons by oxidative pathways mediated via bacterial processing (Graber and Rudich 2006). The exact formation pathways for HULIS in the atmosphere are unknown. Shared functional groups include significant aromatic regions connected by and to oxidized groups, such as ether, ester, carboxylic acid and hydroxyl groups (Graber and Rudich 2006). All humic samples collected in the field will contain some remaining aliphatic regions from the organic material from which they were produced. This wide array of functionality allows humic species to be both water and methanol soluble, lending to their ability to facilitate a diverse number of aqueous and organic phase processes. Behaviorally, dissolved humic substances demonstrate a characteristic light absorption gradient (Andreae and Gelencser 2006) from high absorption in the UV wavelength region to lower absorption in higher wavelengths throughout the visible region, allowing them to be considered a principle component of brown carbon (Andreae and Gelencser 2006). The combination of regions of aromaticity and oxidation allows them to be implicated in interactions involving the reaction with and production of highly oxidizing compounds as well as acting as nutrient mobilizers in

biological systems (Canellas et al. 2015). The effect of electron shuttling to reduce ferric oxides on biological processes has led some to connect humic substances with the development of abiogenesis (Piepenbrock et al. 2014).

1.3 Environmentally Relevant Iron Species

Humic substances have a known relationship with environmental metals, including iron. In atmospheric and aqueous systems humics have been connected with aiding in bringing insoluble metals into a soluble and bioavailable state (Piepenbrock et al. 2014). Metals in the environment pose a significant risk to biological systems (Valavanidis et al. 2008). Most redox active metals in their soluble state are potentially bioavailable and can act as catalysts (Anipsitakis and Dionysiou 2004) to disrupt naturally occurring energy cycles or can act as metal poisoning by direct toxic pathways inherent in their character. The solubility of iron can be affected by several factors; however the two main features include reduction of ferric iron in the environment into a soluble ferrous state (Levar et al. 2017) and complexation of water soluble organic ligands (Willey et al. 2015), similar to siderophore-like behavior. Ferrous iron is very soluble and easily participates in Fenton behavior (Anipsitakis and Dionysiou 2004) with available oxygen in producing highly reactive radicals (Valavanidis et al. 2008). Other metals known for their redox activity in the environment may also readily participate in these electron-transfer reactions and are therefore considered similarly harmful. Along with metals, PAH are also heavily correlated with the production of reactive oxygen species (ROS) (Valavanidis et al. 2008).

1.4 Reactive Oxygen Species

ROS compounds are generally defined as oxygen-centered radicals, such as hydroxyl radical (OH) and superoxide radical (O_2^-) (Valavanidis et al. 2008), but can also include other high-energy state oxygen reagents, including singlet oxygen ($^1O_2$), hydroperoxyl (HO_2), and ozone (O_3). OH is considered to be the strongest oxidizer among ROS, and typically operates by homolytically cleaving acidic hydrogens (Wols and Hofman-Caris 2012) to form water and thus creating an unstable hydrocarbon radical. Further reactions between these radicals can casue a radical cascade (Wols and Hofman-Caris 2012) and lead to atmospheric light absorbing compounds, affecting the Earth's energy balance (Andreae and Gelencser 2006; Wols and Hofman-Caris 2012). Superoxide is also a strong oxidizing radical. It may produce peroxide bridge intermediate structures within hydrocarbon chains and peroxy acids on oxidized end groups. These can easily breakdown to form other oxygen-centered radicals, including OH. Singlet and hydroperoxyl species are comparatively milder as oxidizers, but are known to react with dienes and alkenes (Wols and Hofman-Caris 2012; Zhu et al. 2013) to form hydroperoxides and alkylperoxide radicals, respectively. ROS can evolve from a variety of sources and generally result from oxygen supplied to high energy environments, as is discussed next.

1.5 Radical Generating Environments

The production of ROS is not entirely known but is typically seen as evolving from redox processes (Wols and Hofman-Caris 2012) due to the presence of locally increased electron density, such as aromatic species and transition metals or from known

oxidizing organic acids. These conditions may be more efficient with this production with exposures to UV or high temperatures and pressures producing high energy environments. OH is produced mainly from redox-active metals and PAH using surrounding oxygen sources, such as dissolved oxygen and water (Valavanidis et al. 2008), to create hydrogen peroxide intermediates. Ferrous iron is a highly prominent source for OH, however ferric iron can also be used by becoming reduced in a more complex chain of oxidation reactions (Anipsitakis and Dionysiou 2004). This process is understandably slower. Dissolved oxygen and peroxides exposed to UV can create superoxide and hydroxyl radicals, respectively. This exposure can also promote elemental oxygen electrons to an excited-state to create singlet oxygen (Wols and Hofman-Caris 2012).. The addition of oxygen to this system allows for robust radical generation and therefore may enhance oxidation of these compounds.

1.6 Analytical Techniques

Metal content of samples are analyzed by inductively-coupled plasma mass spectroscopy (ICP-MS) following acid-assisted microwave digestion. Acidity of bulk samples are tested unfiltered and unacidified by pH-meter measured by a microprobe. Light absorbance character for these samples is tested by UV-vis spectroscopy from wavelengths of 220 to 700 nm. Quantity and overall product character of organic materials are evaluated by high-performance liquid chromatography (HPLC) using reversed-phase columns packed with C18-coated silica beads containing 80 Å pore size. Identification of organic functional groups are performed by attenuated total reflectance Fourier-transformer infrared spectroscopy (ATR-FTIR) using an evaporative application

process on a diamond crystal for sample analysis. Separation of HULIS-specific products is accomplished by solid-phase extraction (SPE) using multifunctional retention groups on silica beads. Overall mass of organic products is analyzed by electrospray-ionization and atmospheric pressure chemical ionization mass spectroscopy (ESI/APCI-MS) using both positive and negative modes. The largely varying compounds that make up HULIS material does not allow for a standard reference material (Graber and Rudich 2006) for a comparison. Therefore this project will use the most common humic material used by other bench and field studies, Suwannee River Fulvic Acid (SRFA) (Graber and Rudich 2006). Despite the fulvic acid nature, this material is known to display similar character to observed HULIS. This study represents the culmination of bench studies and observations of these techniques in the conversion of metal species during the oxidation and transformation of organic material. These experiments are meant to represent naturally occurring reactions, with a focus on the transition of persistent organic pollutants from atmospheric aqueous environments which may be mediated by reactive oxygen species.

CHAPTER TWO: ROLE OF POLYCYCLIC AROMATIC HYDROCARBONS ON THE PHOTO-CATALYZED SOLUBILIZATION OF ATMOSPHERIC IRON

2.1 Abstract

Deposition of soluble atmospheric iron plays an essential role in the carbon, sulfur, and other biogeochemical cycles, affecting the Earth's energy balance and human health. Anthropogenic iron emissions are observed to be much more soluble than within collected dust samples. Global production of soluble iron may be due, in part, to atmospheric processing of soil and polycyclic aromatic hydrocarbons (PAH) emitted as anthropogenic and biomass burning products. The production of soluble iron is monitored by illuminating an aqueous suspension of a soil within various PAH bulk water matrices. Significant increases in soluble iron from soil are observed with oxidized and short-chain PAH, including phthalic acid, naphthalene, and anthracene. In terms of soluble Fe formation, the most photo-sensitive PAH observed is anthracene as these samples in the dark demonstrate little-to-no produced soluble iron. Results of these reactions show some correlation, but no dependence upon, system acidity or dissolved organics. Also comparisons of reactions between PAH demonstrate patterns of stability related to the individual aromatic structures of the organic reagents. The data presented in this study suggest that the solubilization of atmospheric iron is likely due to surface-interaction catalysis on PM containing PAH. To our knowledge, this is the first bench study

investigating the specific impact of PAH on the photo-catalyzed production of soluble elements from a soil source.

2.2 Introduction

Every year, 50-60 Tg of iron (Fe) enters the atmosphere, with 90-95% coming from wind-swept sand and soil (Jickells et al. 2005; Mahowald et al. 2005; Mahowald et al. 2009), collectively called dust. The presence of iron in ecosystems has major implications on carbon and sulfur cycles (VanCappellen and Wang 1996), redox environments (Lecuyer and Ricard 1999), and nutrient availability (Jickells et al. 2005). There are very few studies which have investigated how Fe solubility is affected by specific organic components of PM in atmospheric conditions (Chuang et al. 2005). Iron deposition in water systems is implicated with the viability of ocean biota (Takeda 1998), as a limiting nutrient for phytoplankton production in about half the world's oceans (Martin and Fitzwater 1988; Boyd et al. 2000; Moore et al. 2013). In both environmental and biological fluids, soluble metals, including iron, contribute to the production of reactive oxygen species, such as superoxide and hydroxyl radical (Shafer et al. 2010; Verma et al. 2010), which contribute to oxidative damage in lung tissue (Meneghini 1997; Fenoglio et al. 2001; Knaapen et al. 2002). The presence of iron in radical producing environments, such as sunlight, may catalyze the cleavage of water molecules and possibly excite pi-system electrons in aromatic organic compounds, ultimately producing solubilized iron and the previously mentioned radicals (Babu et al. 2001). An overall reaction involving electron transfer processes between radicals and iron-containing particles, analogous to a Fenton reaction, would contribute to soluble iron and

oxidized organic species (Chacon et al. 2006; Baba et al. 2015). For the atmosphere, there are only very limited studies which have monitored how the production of these oxygenated species affect other PM components (Akhtar et al. 2010).

There are several environmental pathways that convert insoluble iron to a soluble form. The major mechanisms involve reduction from the insoluble ferric to the more soluble ferrous iron through an electron donor (Diaz-Quintana et al. 1998; Levar et al. 2017). Ligand complexation of ferrous and ferric iron with soluble organic compounds can bring otherwise insoluble iron into a soluble state (Bridge and Johnson 1998; Willey et al. 2015). The production of soluble iron can also be inherent in the emissions of combustion reactions (Sedwick et al. 2007; Sholkovitz et al. 2009). Electron donor reduction processes typically involve oxygen radicals such as the superoxide radical (Valavanidis et al. 2000; Garg et al. 2007) or electron-rich aromatics such as anthraquinone (Vile et al. 1987; Faiola et al. 2011). Complexation reactions of iron use water soluble organic species with oxygen-containing groups, carboxylic acids for example, to chelate the typically insoluble ferric iron and bring the iron into a soluble state (Paris et al. 2011; Baba et al. 2015). Combustion sources are considered as direct contributors of atmospheric soluble iron (Luo et al. 2008). Formation of soluble iron on aged particles have been monitored by the ratio of ferrous and ferric iron composition based on XANES studies (Majestic et al. 2007; Schroth et al. 2009; Oakes et al. 2012) while other direct emission sources, such as from vehicle exhaust, are less well known.

Globally, major contributions of soluble iron have been attributed to biofuel burning (Oakes et al. 2012) and combustion processes, including biomass burning (Guieu

et al. 2005; Sholkovitz et al. 2009). However, the higher observed total iron deposition, uncertainty, and temporal variability of soluble iron from these regions are not accounted for by solely these emissions (Fung et al. 2000; Hand et al. 2004; Jickells et al. 2005; Luo et al. 2005; Johnson et al. 2010; Luo and Gao 2010) and therefore are likely due to the addition of soluble iron from external sources such as atmospheric processing of insoluble iron in transported dust (Mahowald et al. 2009; Longo et al. 2016; Rizzolo et al. 2017).

Polycyclic aromatic hydrocarbons (PAH) are ubiquitous in PM sourced from combustion reactions, particularly biomass burning (BB) emission (Ravindra et al. 2008; Zhang and Tao 2009; Balachandran et al. 2013), with PAH concentrations at about 500 ppm by mass (Balachandran et al. 2013). PAH produced in these reactions range from two to five ring centers, with a majority containing 2-3 rings (Zhang and Tao 2009). Due to the stability of the aromatic ring, PAH parent chains and their oxidized byproducts can sustain extended lifetimes and remain in the atmosphere from hours to weeks (Bamforth and Singleton 2005; Reisen and Arey 2005; Zhang and Tao 2009). In oxidizing environments naphthalene can be rapidly converted to naphthol and other oxidized derivatives (Cerniglia et al. 1983; Pei et al. 2013; Kim et al. 2016) and anthracene is readily oxidized to anthraquinone (Faiola et al. 2011). As persistent pollutants, atmospheric PAH experience longer exposures to sunlight, entrainment into clouds, and therefore potentially undergo many oxidizing reactions (Bamforth and Singleton 2005; Lundstedt et al. 2007; Tsapakis and Stephanou 2007). In these conditions PAH can further oxidize to form an array of more complex oxidized PAH (oxPAH). These

additional functional groups may include one or combinations of multiple carboxylic acid groups, carbonyl and hydroxide groups, ring-openings and linkage via condensation reactions (Perraudin et al. 2007; Ringuet et al. 2012; Paris and Desboeufs 2013; Baba et al. 2015).

Naphthalene, for example, has been shown to convert to phthalic acid (a dicarboxylic acid) with a silica catalyst under 300 nm irradiation (Barbas et al. 1993). Previous studies have demonstrated a significant decrease in iron oxidation in the presence of phthalic acid (Santana-Casiano et al. 2004), suggesting an affinity to soluble iron and perhaps increased complexation relative to the unoxidized PAH. This further suggests that phthalic acid and other dissolved organic matter may stabilize the more soluble ferrous ion (Willey et al. 2008) and possibly enhance the solubilization of iron in reductive conditions.

This project is among the first to test how components of primary organic emissions, specifically PAH, affect Fe solubility in atmospheric cloud water processes, particularly in the presence of sunlight (i.e., photochemistry). Specifically, this study aims to determine the impact that sunlight may provide to the interaction between insoluble iron and aqueous PAH suspensions. Saturated PAH suspensions, ranging from 2-5 aromatic centers, are combined with a soil suspension as an iron source and illuminated with sunlight provided by a solar simulator. Any production of soluble iron due to oxPAH would be expected to increase over longer exposure times and decrease for shorter times. In an effort to evaluate an overall effect based solely between different organic matrices, each assay is treated under identical conditions using a set exposure

time. Our preliminary experiments showed that soluble iron tended to peak around 12 hrs into the light. Therefore, we apply a total illumination time of 16 hours; this also represents expected sunlight on the longest day of the year. Soluble iron from these assays focus on the comparison of pre and post reaction soluble iron between lighted samples and control samples kept in the dark.

2.3 Experimental

2.3.1 Materials

All experiments and sample preparation were performed under a laminar-flow hood using HEPA-filtered air. Plastic tubes, bottles, and syringes were cleaned and prepared using a series of overnight acid baths. The first of these was a reagent grade 10% nitric acid (Fisher Scientific, Waltham, MA) bath, followed by reagent grade 10% hydrochloric acid (Fisher Scientific, Waltham, MA), and a final resting bath of trace-metal grade 3% nitric acid (EMD, Gibbstown, NJ). Between each bath, these materials were put through a rigorous triplicate rinse using ultrapure water with a resistance of 18.2 MΩ (ThermoScientific Nanopure, Waltham, MA).

To reduce the potential for reagent residue contamination of the reaction vessel, a revised version of the plastic cleaning method was developed. This cleaning method was used to remove residual iron and organic material from the reaction liner walls, resulting in a decrease in blank iron data to below detection limits. Teflon beaker liners were cleaned through a succession of solvent treatments. This process starts with an acetone rinse followed by an overnight bath of 100% HPLC-grade acetonitrile, then a final

overnight bath in 5% trace-metal grade nitric acid including a pre and post-bath triplicate rinse with 18.2 MΩ purified water.

0.20 micron syringe filters (Whatman, Marlborough, MA) were prepared by flushing a series of 5 mL aliquots of dilute acid and clean water. An initial rinse of 10% trace-metal grade hydrochloric acid is followed by a rinse with 18.2 MΩ purified water, then a 5% nitric acid rinse is followed by five flushes of 18.2 MΩ purified water.

2.3.2 Reagents

The iron source for this study was the NIST standard San Joaquin soil (NIST SRM 2709a), certified 3.3% iron by mass. 99% naphthalene, 99% anthracene, 97% phenanthrene, 98% pyrene, and 98% benzo(e)pyrene (Sigma, Fisher), in addition to concentrated formic acid (Sigma) and 99.5% phthalic acid (Sigma) were the organic components for these reactions. All of these reagents were used as received without further purification. Simulated sunlight was provided by an Oriel Sol 1A solar simulator using an Air Mass, AM 1.5 Global Filter (Newport). This simulator is calibrated to partition light into 5.4% UV, 54.7% visible, and 39.9% IR spectra at an overall flux of 1550 Wm^{-2} (Newport), considered to be equivalent to one sun at sea level at its zenith. All samples are illuminated for 16 hours to reflect the total exposure of sunlight during summer solstice.

2.3.3 Methods

An appropriate amount of NIST soil was added to purified water to produce a stock suspension containing 25 ppm total iron. Aqueous solvents of PAH were created by adding 100 mg of organic crystals to 200 mL of purified water to obtain a total

concentration of 500 ppm, with benzo(e)pyrene tested at 100 ppm. Note that organic buffers were not used in these solvents in order to avoid potential interferences and preserve the specific reactivity of the target PAH compounds (Spokes et al. 1994). Similar to previous studies (Pehkonen et al. 1993), the soluble organic acids formic and phthalic acid were individually tested at a concentration of 6mM correlating to 276 and 996 ppm, respectively. These mixtures are then capped, inverted ten times, and stored at room temperature in the dark. Preliminary experiments showed extremely high variability when the organic fraction was not allowed to equilibrate prior to adding the iron source. Thus, each organic reagent suspension is held in the dark for 24 hours to allow the very slightly soluble solids to reach equilibrium with the ultrapure water.

The reaction vessels are comprised of 100 mL Teflon liners inside jacketed glass beakers which are temperature controlled at 25° Celcius by water flow from a chiller pump. Each sample solution is prepared by spiking 100 mL of aqueous organic solvent with 1 mL of soil stock. Soil suspensions are homogenized by rigorous agitation using a Teflon stir bar. To avoid significant sedimentation, soil aliquots are drawn within 10 seconds of agitation. Illuminated samples were held at 25 degrees Celsius with stirring open to the atmosphere for 16 hours under a controlled light using the calibrated solar simulator lamp. Control samples were conducted under identical conditions, except were kept in the dark. Simultaneous reactions of dark samples were conducted by covering an additional reaction vessel with a commercially available aluminum foil. Sample loss by evaporation was reduced by temperature control and tracked gravimetrically. Loss from

dark samples was insignificant and light sample losses were found to be less than 10% which were included in the analysis calculations.

Sample aliquots of 2 mL were removed at the beginning and end of the reaction period. Samples are prepared for analysis of soluble iron by adding directly into a syringe and filtered at 0.2 μm into a 15 mL polypropylene centrifuge tube. These samples were acidified to 5% nitric acid and analyzed by inductively coupled plasma mass spectrometry (ICP-MS, Agilent 7700) using indium as an internal standard. Values of each assay represent triplicate data collected using identical methodologies as described above.

Total iron values in these samples are consistent with listed SRM values and were confirmed by preparing an unfiltered aliquot of sample using acid-assisted microwave digestion and analyzed by ICP-MS. This digestion process uses concentrated trace-metal grade acids followed by ultrapure water addition to 2% nitric, resulting in a 5:1 total dilution for recovery analysis. Iron concentrations in samples were determined via inductively-coupled plasma mass spectroscopy (ICP-MS) with active calibration to 50 ppb, other metal concentrations were similarly analyzed with calibrations to 5 ppb. Overall reaction systems are analyzed for pre- and post-reaction conditions with a focus on quantitative changes in various dissolved metals, although the focus here is iron. Acidic content of post-reaction samples are determined using raw unfiltered sample aliquots and evaluated by pH meter model Orion Star A111 (Thermo Scientific) with an ultra slim probe.

The metal source for this project was a standard reference material (SRM) soil 2709a, supplied by the National Institiute of Standards and Technology (NIST). The total metal concentrations of this soil are determined and certified by NIST and must be taken into account during each iteration of sample preparation for use in our reaction assays. An appropriate amount of dry soil is suspended in ultrapure water to create a standard soil stock suspension. An aliquot of this suspension is introduced to a suspension of PAH and ultrapure water. This total suspension represents the reaction system subjected to the solar simulator. Aliquots of this total suspension are removed, acidified with concentrated trace-metal grade nitric and hydrochloric acid, digested via microwave digestion, and diluted further with ultrapure water to produce a prepared sample for ICP-MS analysis of total metal concentration.

Table 2.1 shows the total concentrations of major metals present in these soil reactions and the analysis parameters used for this study. These metals represent a sample of the major component of potentially redox-active metals in the soil (Warner et al. 1996; Voelker et al. 1997; McLennan 2001; Belous et al. 2008; Murakami et al. 2008). The magnitudes of these metals were based on target iron concentrations consistent with expected entrainment of atmospheric dust into clouds found in the troposphere (Duce et al. 1980; Prospero et al. 1996). Other known environmentally relevant metals in the soil, such as copper and lead, are an order of magnitude lower in concentration; therefore soluble fractions of these would fall below detection. Total recoveries of all analyzed elements were found to be 96.5 ± 5.4% over 44 trials.

Table 2.1: Certified total major metal composition of standard soil, suspensions, and instrument calibration parameters. [a] total metal concentration of dry soil supplied by NIST, SRM 2709a. [b] total metal concentration of soil stock suspension at 7.4 mg/10 mL. [c] total metal concentration of reaction sample using 1 mL soil stock in 99 mL aqueous reagent. [d] total metal concentration of digested sample which incorporates a 5:1 dilution. Total recovery was 96.5 ± 5.4%, n = 44.

Element	[a] Total metal in dry soil, %	[b] Total metal in soil stock, ppm	[c] Total metal during reaction, ppb	[d] Total metal after digestion, ppb	ICP-MS calibration range, ppb	ICP-MS limit of detection, ppb
Fe	3.36	24.92	249	50	5-50	0.18
Ti	0.336	2.492	24.9	5.0	0.5-5	1.77
Ba	0.0979	0.726	7.26	1.45	0.5-5	0.02
Mn	0.0529	0.392	3.92	0.78	0.5-5	0.03

2.4 Results

2.4.1 Iron solubility

Figure 2.1 shows the component of soluble iron, as a percent of total iron, for every reaction scenario. Many of the tested organic assays, specifically formic and phthalic acids, naphthalene, and anthracene, demonstrate an increase in percent iron solubility compared to the soil blank reaction using purified water. The effect is enhanced further with the addition of light for all assays compared to the dark. Blank reactions were performed using the NIST soil against purified water; these blank samples represent the transformation of insoluble iron in the soil into solubilized iron due only to solar irradiation and any reactive species inherent in the soil. Blank samples produced soluble iron, at 1.8% under light and 0.8% in the dark, similar to previous iron studies under light (Pehkonen et al. 1993). Reactions using 6mM formic acid, with 11.7% in light and 5.2% in the dark, also demonstrated similar iron solubility as previous reports (Pehkonen et al. 1993). Here, formic acid is used as an analog for the expected organic content of cloud water. Formic acid therefore acts as the proxy for redox-active short-chain organic acids present in atmospheric conditions.

Phthalic acid, a PAH dicarboxylic acid derivative, is used as a representative oxPAH product and resulted in an iron solubility of 11.0% in light and 6.8% in the dark, demonstrating the highest percentage of solubilized iron among the aromatic organic compounds tested. This coincides well with soluble iron increases near BB regions (Mahowald et al. 2009; Paris et al. 2010), and fits with the expected characteristics of

oxPAH including phthalic acid's greater aqueous solubility and carboxylic acids groups as potentially iron-complexing functional groups (Kappler et al. 2004).

Among the tested PAH reaction systems, the degree of produced soluble iron appears to be structure dependent. Naphthalene in the light generates the greatest iron solubility among PAH with 6.5%, followed by the 3-ring linear anthracene showing 5.1 % soluble iron. The remaining PAH, 3-ring bent-shaped phenanthrene, 4-ring pyrene, and 5-ring benzo(e)pyrene, display a statistically similar (t-test, $p<0.95$) sharp drop in iron activity with soluble iron values of 1.06%, 0.85%, and 1.71%, respectively. Control reactions in the dark demonstrate an enhanced iron solubilization in the presence of some reagents, starting from 0.8% using only water to 6.8% using phthalic acid. While Figure 2.1 also shows the other aromatic controls in the dark, phenanthrene, pyrene, and benzo(e)pyrene, producing 0.29%, 0.18%, and 0.06% soluble iron, respectively, representing a significant decrease (t-test, $p<0.95$) in soluble iron compared to water.

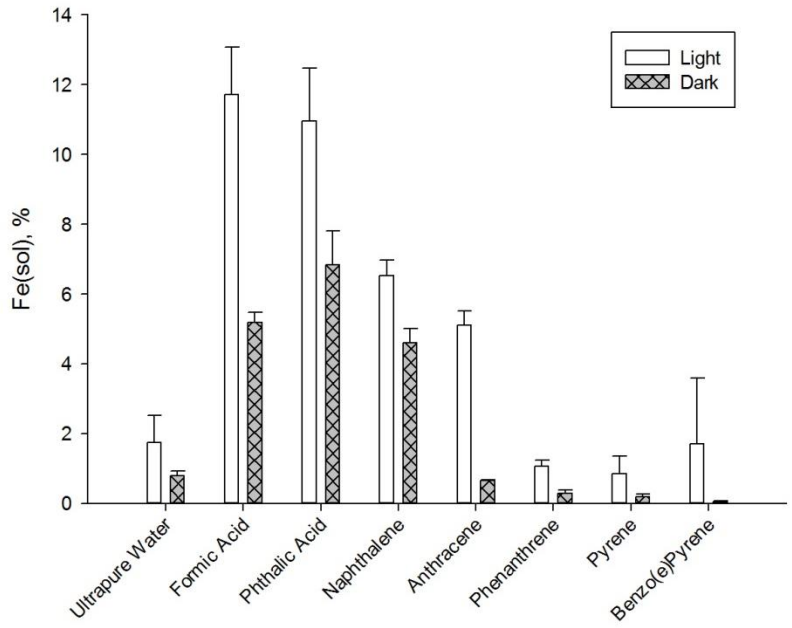

Figure 2. 1: Soluble iron as a percent of total iron in photoreaction samples.
Total iron is a standard value of an SRM soil source and confirmed by microwave digestion in replicate samples. Ultrapure water is supplied as water filtered to 18.2MΩ. Soluble iron is determined via 0.2 μm filtration, error bars represent 1s of calculated average, n = 3.

2.4.2. Light Factor, L

$$L = (\%\ Fe_{(light)})/(\%\ Fe_{(dark)})$$

To better understand the importance of light on these reactions, the ratio between the amounts of produced soluble iron in illuminated samples against soluble iron in dark samples was calculated using the above equation. This introduces a value, L, which can be interpreted as the enhancement factor that light contributes to the inherent process in the dark. Water is included in this analysis as a reference baseline point for comparisons in activity to the organic reagents. Reactions with naphthalene, formic and phthalic acids (Figure 2.2) demonstrate that the enhancement of sunlight on iron-active suspended soil samples are statistically similar (t-test, $p<0.95$) to water and are nearly doubling the amount of soluble iron compared to the dark, while anthracene shows a light factor of almost eight. Note that phenanthrene, pyrene, and benzo(e)pyrene are not shown in Figure 2.2 as they are observed to be inactive towards iron solubility.

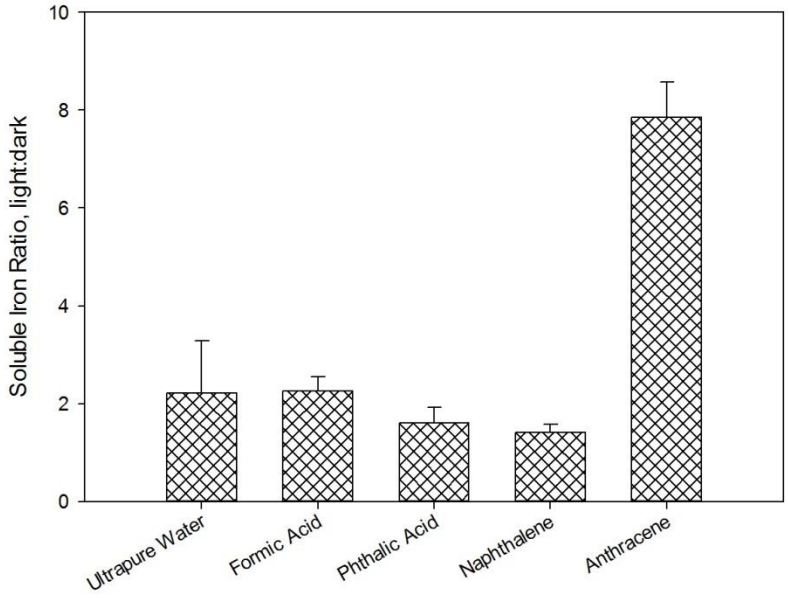

Figure 2. 2. Iron response as a ratio of percent soluble iron in light.
Ratio of light to dark samples presented show the response from observed iron-active reagents. Note that phenanthrene, pyrene, and benzo(e)pyrene, with respective L values of 3.70, 4.65, and 30.16, are not included here as these values are considered artificially high due to their overall inactivity to iron. Ultrapure water is supplied as water filtered to 18.2MΩ. Error bars represent 1s of calculated average values, n = 3.

Figure 2.3 displays the differences in soluble metals due only to the presence of sunlight. In all cases illuminated iron shows the highest total solubility response among tested metals. This suggests a high specificity to iron for these photo-reactions. Both manganese and barium show slight but similar increases in soluble concentration in nearly all of the assays. While these low concentrations are susceptible to higher reported percent soluble values with small perturbations, it is interesting to note that Mn and Ba display solubilities up to 60% and 40%, respectively; these are similar to previous studies (Boyle et al. 2005; Baker et al. 2006) and are in marked contrast to the lesser redox active titanium which displayed virtually no solubility. This demonstrates an overall specificity to redox active metals relating to a larger total iron deposition in environmental conditions.

Figure 2.3 also shows that illuminated formic acid displayed a small but consistent inverse solubility effect compared to the dark on all metals except iron; this response, compared to phthalic acid, suggests that sunlight seems to inhibit solubilization of non-iron metals in samples with short chain organic acids. The increase in iron solubilization in illuminated formic acid and the decrease in solubilization of other metals suggests a solubilization pathway which is specific to iron in sunlight reactions.

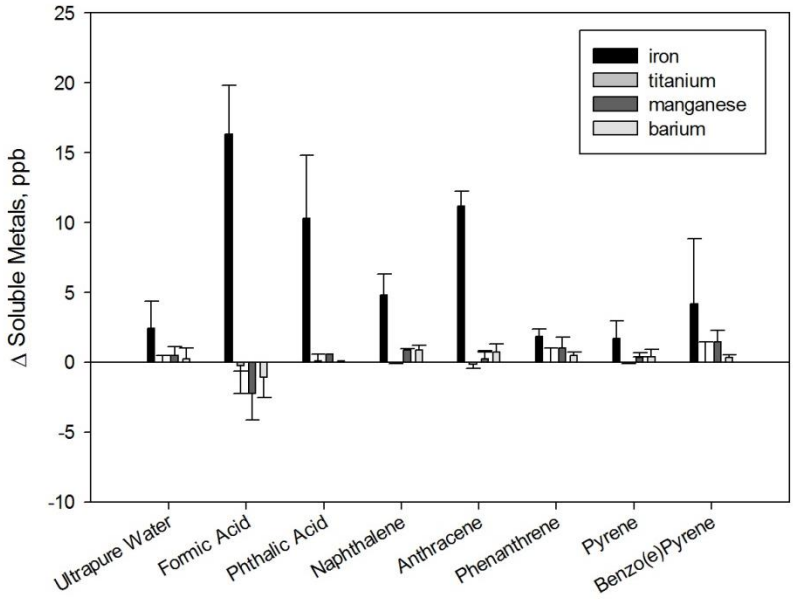

Figure 2. 3. Difference in average ppb concentrations of soluble metals.
Change of reactions between light and dark samples. Ultrapure water is supplied as water filtered to 18.2MΩ. Error bars represent 1s from the reported values, n = 3.

2.4.3. Reaction characteristics

Every assay was conducted in ultrapure water without buffering. This allows for the evaluation of interactions only between pure PAH, soil, and the ultrapure water. Therefore, any reactions occurring due to acidic processes, or the production of acidic products, can be assessed without interference from the buffer. To evaluate the acidic component of PAH processing of soluble iron within bulk aqueous samples, raw unfiltered samples without acidification are analyzed for pH. Quality control pH analyses of cleaned sample tubes confirm the complete removal of acid from these containers following the acid treatment process described above. Note that starting pH values for PAH assays were found to be 5.5 ± 0.3 (n = 24). Figure 2.4 compares two sets of dependent variables, i.e. observed soluble iron with the resultant acidity of the individual samples, and therefore represents a two-variable plot where these values can be evaluated for their dependence upon each other, if any. The x-axis in Fig. 2.4 plots the percent soluble iron, which has herein been defined for these assays and therefore serves as the independent variable, against the resultant pH values on the y-axis. Despite a wide range of soluble iron, i.e. 0% to 8%, pH values range from 3.5 to 5.5 with the large majority within pH of only 4 to 5. The pH values for these bulk aqueous samples closely represent the expected range for cloud water (Guo et al. 2012).

This scatter plot shows no statistical difference (t-test, $p<0.95$) in the pH of samples with lower soluble iron and those of higher soluble iron. The overall lack of trend between pH and soluble iron is further shown as these plotted points demonstrate little statistical correlation ($r^2 = 0.2181$) between these factors. Light soluble iron data in

Figure 2.4 demonstrate a minor slope (m = -0.1133, r^2 = 0.4199) with respect to pH, however the high variability within values observed in the dark samples lowers the confidence in this trend, and the dark samples display virtually no correlation (m = 0.0440, r^2 = 0.0523) with pH values. Despite the downward trend for lighted samples this plot presents no statistical difference (t-test, $p<0.95$) between the light and dark data. The relatively high pH correlation of light samples, compared to the dark, suggests that the products of illuminated reactions have a small difference in their acidic dissociation properties that have a greater connection to produced soluble iron.

The left side of the plot shows the major clustering of points from these assays, representing the high number of low iron solubilization tests at a comparatively high range of pH values. Observing the trend of increasing iron solubility shows roughly even spread of pH data points. This suggests that there is no optimal pH within this soluble iron environment which relates to the reaction of these samples. The high variability in pH along the range of percent soluble iron demonstrates that pH alone is not a sufficient predictor of soluble iron in these samples. This suggests a mechanism based on iron reduction or organic complexation rather than a purely acid-driven process.

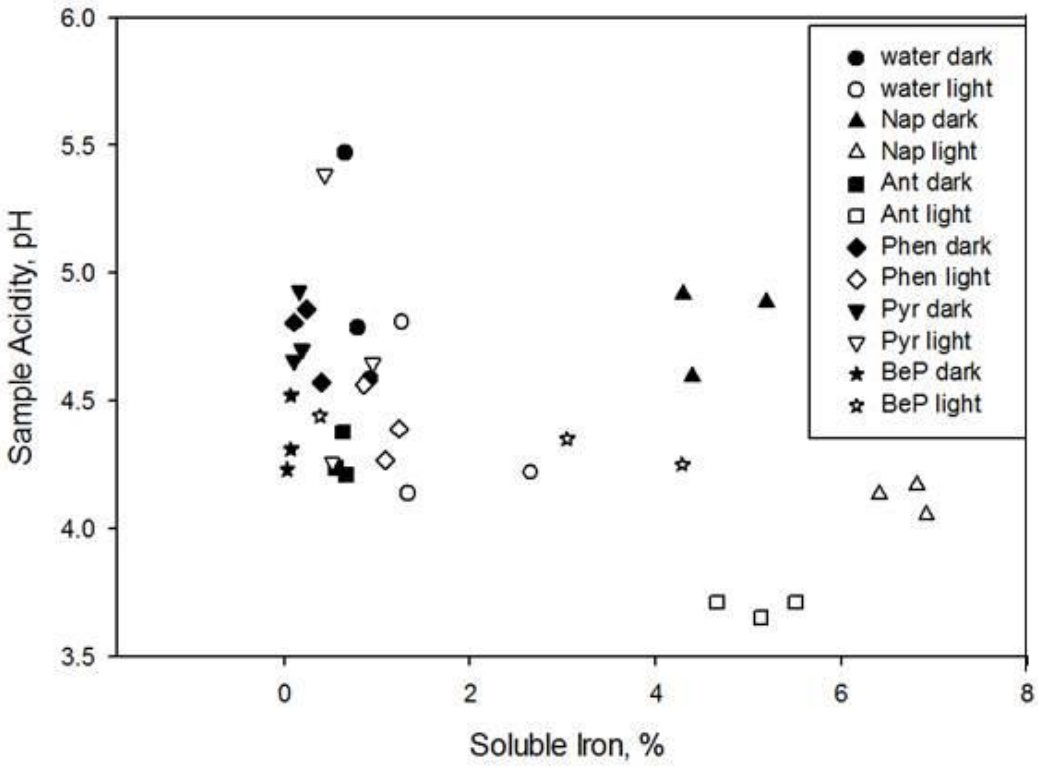

Figure 2. 4**.** Acidity of unbuffered PAH samples with soil.
Open markers represent light samples, filled markers represent dark samples. The total scatter plot shows individual triplicate data showing a statistical correlation of 0.2181 between pH and soluble iron. Light samples show a linear regression of $y = -0.1133x + 4.6254$, $r^2 = 0.4199$; dark samples show a linear regression of $y = 0.0440x + 4.6001$, $r^2 = 0.0523$. "water" refers to ultrapure water samples; Nap, naphthalene; Ant, anthracene; Phen, phenanthrene; Pyr, pyrene; BeP, benzo(e)pyrene.

Any complexation of iron with soluble ligands is thought to be dependent on the amount of dissolved organics. Figure 2.5 shows the relationship between observed percent iron solubility against the listed ppb values of the aqueous solubility of the un-oxidized organic reagents (Ministry of Environment-Province of British Columbia). Note that the data points for formic and phthalic acid samples are based on their 6 mM concentrations. The plotted points of the more dissolved organics, naphthalene, formic acid, and phthalic acid, appear to have a good direct correlation of their own solubility and iron production though percent soluble iron seems to plateau at higher dissolved organics, while most of the lesser dissolved organics display activities similar to or less than water. This low solubility inactive trend is broken by anthracene whose aqueous solubility is an order of magnitude lower than phenanthrene, yet produces a significant amount of soluble iron in its lighted assays.

An evaluation between moles of soluble iron against the expected molar solubility of PAH (SI Figure A.1), further elucidates this lack of dependency on dissolved PAH. The same spike in soluble iron for anthracene in the light occurs in the midst of data points of more soluble, yet less iron-active, pyrene and phenanthrene. Given that these PAH solubilities are only listed for the un-oxidized parent structures, a clearer picture may be made by identifying and quantifying any produced oxPAH that are expected to have a greater aqueous solubility, which is currently underway.

Among the tested PAH, naphthalene, at 12.5 ppm (Ministry of Environment-Province of British Columbia), has the highest water solubility and demonstrates the highest iron solubility in both sunlight and the dark, while anthracene demonstrates

similar iron solubility to naphthalene in sunlight yet with a very low aqueous solubility of 59 ppb (Ministry of Environment-Province of British Columbia). Pyrene and phenanthrene's low iron activity with their listed solubilities of 133 and 435 ppb (Ministry of Environment-Province of British Columbia), respectively, strongly suggest that iron solubilization does not depend simply upon freely dissolved aromatic species. The presence of redox-active PAH and oxPAH, despite their highly varying solubilities in water, demonstrate an observable correlation with iron solubility. The negligible amount of dissolved anthracene suggests that the aromatic-based iron solubilization reaction is not dependent solely on dissolved organics, but a reliance on a combination of dissolved organics with the un-dissolved portion of suspended PAH, and therefore aqueous suspensions of particles containing redox-active PAH.

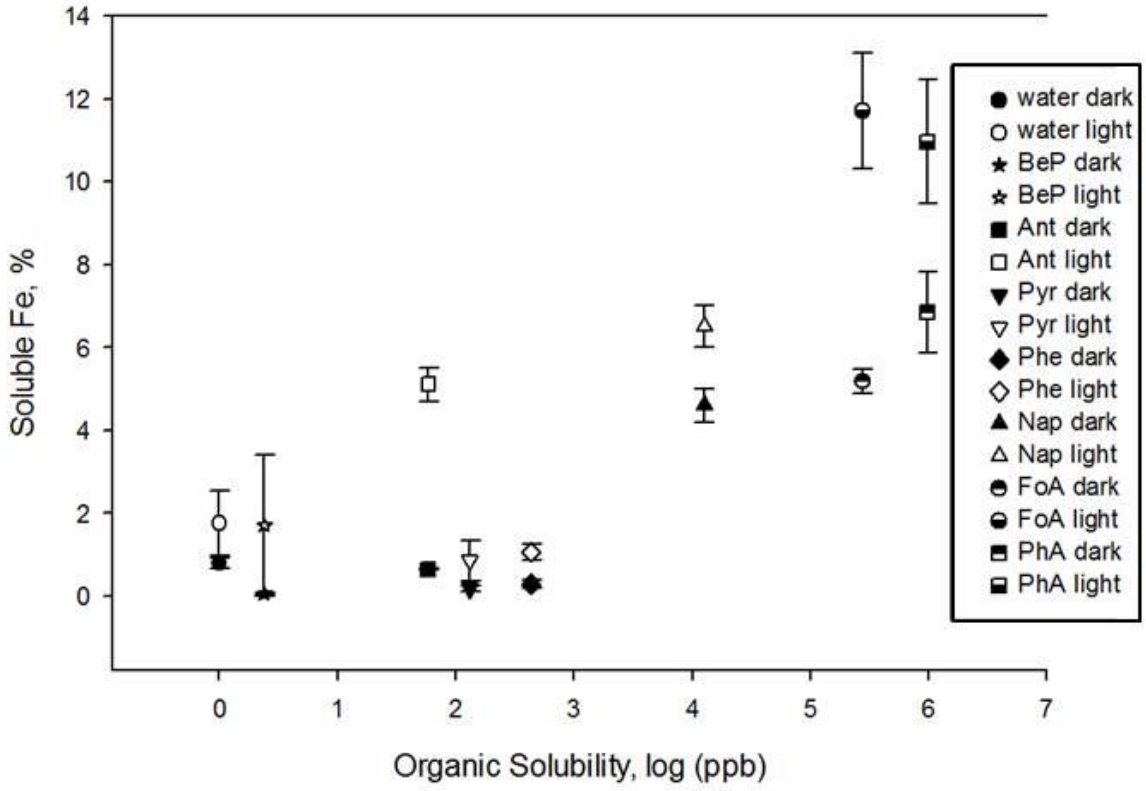

Figure 2. 5**.** Comparison of dissolved organic reagents and resulting solubilized iron. For PAH assays open markers represent light samples, filled markers represent dark samples. Split markers represent carboxylic acid assays, where open tops are light samples and closed tops are dark. Dissolved content of organics are based on listed aqueous solubilities in ppb which are plotted in log scale. Soluble iron data is based on average values of triplicate 16-hour reactions in the light and the dark and is reported as percent of total iron. Error bars represent 1s from the reported values, n = 3. "water" refers to ultrapure water samples; BeP, benzo(e)pyrene; Ant, anthracene; Pyr, pyrene; Phe, phenanthrene; Nap, naphthalene; FoA, formic acid; PhA, phthalic acid.

2.5 Discussion

In this study, we have demonstrated that the presence of aromatic organics enhances the solubility of iron from a soil suspension. Soluble iron presents itself to the environment through a variety of observed mechanisms. Atmospheric iron in rural dust is less than 0.5-1% soluble (Mahowald et al. 2009; Sholkovitz et al. 2012), iron in biomass burning (BB) areas are observed to increase as high as 45% iron solubility (Oakes et al. 2012), while iron in urban areas are observed at a wide range of 2-80% iron solubility (Sedwick et al. 2007; Mahowald et al. 2009). In addition to elevated soluble Fe in urban environments, dust processing is another mechanism which has been shown to yield soluble Fe. Observed produced iron represents the cumulative soluble iron over a continuous 16 hour exposure. Evaluations of the mechanism and kinetics of these reactions are currently underway. Products emitted from combustion sources, such as biomass burning and automobile exhaust, commonly contain particulate matter with varying amounts of aromatic composition, including PAH (Jenkins et al. 1996). The PAH chosen for this bench study comprise the simple non-oxidized parent structures that may act as the building blocks for more oxidized and branched combustion-based aromatics (Baek et al. 1991; Bamforth and Singleton 2005). Naphthalene and anthracene have observed atmospheric lifetimes ranging from hours to days (Bamforth and Singleton 2005) creating oxidized products, including naphthol (Cerniglia et al. 1983) and anthraquinone (Faiola et al. 2011), which act as intermediate structures to more complex aromatic species. Phenanthrene and pyrene have extended observed lifetimes that allow

transport across the globe and are observed in their parent forms in atmospheric field samples (Yunker et al. 1996; Bamforth and Singleton 2005; Zhang and Tao 2009).

Wind swept natural iron sources, such as dust, has been observed to undergo counterion exchange with the nitrate anion from nitric acid vapors resulting in a significant increase in soluble metals including iron (Duvall et al. 2008). Aerosolized particles mixing with air pollution are also found to produce soluble iron in the form of ferrous sulfate (Li et al. 2017), although interactions with SO_2 are not seen as a source of soluble iron (Cartledge et al. 2015). There are other studies that demonstrate an increase in bioavailable iron by a complexation reaction between dust-borne insoluble iron and short-chain and large oxidized organic acids (Kappler et al. 2004; Paris and Desboeufs 2013).

Atmospheric conversion reactions for soluble iron have several potential mechanisms and are generally classified into two separate major categories, acid-driven aerosol processes and organic complexing cloud water processes. Acid processing is associated with PM2.5 emissions from urban and combustion sources which have calculated pH values ranging from 0 to 2 (Fang et al. 2017). These values are consistent with the classic acid-driven protonation mechanism in the solubilization of insoluble ferric hydroxides with nitric acid resulting in dissolved free ferric ions. The sulfuric acidity of these aerosolized fine particles are connected with increased production of soluble ferrous sulfates (Li et al. 2017) and are shown to reduce and stabilize ferrous ions in soil suspensions (Shi et al. 2015). These undertake the protonation of loosely associated iron oxides in the release of freely soluble ions (Fang et al. 2017).

The focus of this study is on a potential aqueous-phase aromatic cloud processing reaction. These environments have a relatively higher pH range from 3 to 5 (Spokes et al. 1994; Paris et al. 2011; Guo et al. 2012) and allow for the mixing of dust and organic compounds over the duration of their long range transport. These mixtures have been observed in bench studies to produce soluble iron via reduction and complexation reactions with formate (Pehkonen et al. 1993) and oxalate systems (Paris et al. 2011). The implications of cloud mixing of terrestrial dust and emitted PAH (Allen et al. 1996) is of particular interest here, this is strengthened by the occurrences of PAH and oxPAH compounds found on atmospheric dust particles (Falkovich et al. 2004).

Previous studies have shown that iron in certain forms can solubilize in the presence of some short chain organic acids (Mahowald et al. 2009; Baba et al. 2015). Formic acid was chosen as the starting reagent for this project due to the ubiquitous nature in environmental atmospheric conditions (Pehkonen et al. 1993). Phthalic acid is used as the expected product of PAH oxidation and therefore serves as the standard for likely oxPAH in environmental samples. BB regions providing heavy combustion activity experience higher percentages of soluble iron, therefore the contributions from emitted aromatic organics may explain the strong increase in soluble iron near these areas.

Control assays in the dark show that some organics alone contribute to soluble iron. Phthalic acid and naphthalene in the presence of soil, containing insoluble iron, represent the only aromatic reagents which were able to form a significant amount of soluble iron in dark assays. The carboxylic acid groups on phthalic acid may be able to

chelate and complex with the iron to facilitate bringing it into a soluble state (Barbeau et al. 2003; Baba et al. 2015). This would be similar to siderophore compounds that aid organisms in the uptake of iron (Barbeau et al. 2003; Searle et al. 2015). The naphthalene reaction in the dark may be explained by its propensity, in aqueous suspensions, to convert to oxidized forms like phthalic acid (Barbas et al. 1993) and the hydroxylated naphthol species (Baba et al. 2015).

In addition to the PAH alone, this study shows that sunlight significantly enhances the solubility of iron in redox active environments by approximately a factor of two in half of our assays, and anthracene which shows a factor of eight. The overall degrees of generated soluble iron relate to the reactive nature of the aromatic compounds. The lowest iron solubilities observed were displayed by the lowest predicted redox-active structures of phenanthrene, pyrene, and benzo(e)pyrene (Cho et al. 2005). The lack of iron response of these PAH can be related to their predicted reactivity based on Clar's rules for aromatic stability (Clar and Schmidt 1975). Stated briefly, Clar and Schmidt have postulated that the overall stability of PAH is based on the number of complete benzene rings depicted in an aromatic compound's structure; where the higher number of complete rings in the structure leads to lower energies of the aromatic system, and therefore greater stability and lower reactivity. This is particularly evident in the relatively large soluble iron response from the 3-ring anthracene compound containing only a single complete benzene structure, and the lack of iron response from the 3-ring phenanthrene, containing two complete benzenes.

The electron-rich environments of the oxygen-containing groups on these products make attractive centers for bonding or coordinating with available iron (Kappler et al. 2004). The ultraviolet radiation (UV) environment of sunlight may catalyze the formation of aqueous-phase radicals via atmospheric photochemistry within cloud water droplets, particularly those containing oxidized organic compounds (Baba et al. 2015). These may experience cleavage with exposure to UV to produce hydroxyl radicals (OH). Surface ferric ions may participate in these electron transfer reactions and become reduced to ferrous iron in the process. Additionally, oxPAH may use their oxygenated groups to complex with ferric iron in a siderophore-like reaction (Hersman et al. 1995; Paris and Desboeufs 2013). This can draw iron into a dissolved state despite remaining in the otherwise insoluble ferric form (Winkelmann 2002).

Anthracene and naphthalene showed the highest overall iron solubilizations among the PAH parent compounds tested, with anthracene demonstrating the highest response factor to sunlight among all tested reagents. This reactivity fits well with the PAH known to be highly reactive with hydroxyl radical in gas phase and readily oxidized in the atmosphere (Biermann et al. 1985). In biological oxidation systems naphthalene is thought to convert to naphthol as a precursor for more complex structures (Cerniglia et al. 1983; Bamforth and Singleton 2005), while anthracene has been known to transform between its 9,10 diol form and anthraquinone (Faiola et al. 2011). Soluble iron produced by reactions in the dark suggest that soil may participate in the oxidation of naphthalene spontaneously, while an analogous catalyzation reaction of anthracene may require sunlight to drive the conversion to anthraquinone before iron solubilization. With only

one complete benzene ring in their structures, their propensity to oxidize may contribute to the higher iron responses they displayed. The interactions between sunlight, suspended soil, PAH and the resulting oxPAH products are currently being evaluated in a concurrent study by our group.

The reagents containing carboxylic acid groups, formic and phthalic acids, demonstrate the highest iron response both in the light and dark. Whether by reduction or complexation with iron, the fact that formic and phthalic acids showed significantly higher soluble iron strongly suggests that the structures needed for iron solubility will include oxygen-containing functional groups, including carboxylic acids and possibly ketones, and hydroxyl groups (Paris and Desboeufs 2013; Baba et al. 2015).

Although previous studies have shown environmental soluble iron to have a relationship with the acidity of the environment (Meskhidze et al. 2003; Cwiertny et al. 2008; Mahowald et al. 2009), the overall iron solubilization results in this study are shown to be independent upon acidity of the resultant samples based on linear correlation coefficients of percent soluble iron and measured pH values following reaction periods. Studies have discussed that acid-driven processes of soluble iron will require an aerosol environment of pH less than 2 (Kendall and Hochella 2003; Baker et al. 2006). To evaluate this as a possible mechanistic pathway, these reactions were prepared in ultra-pure water (18.2 MΩ) to facilitate only reactions between pure PAH and insoluble iron. Each sample was tested for pH values following the reaction periods. The observed relationship between produced iron and pH are not well correlated in the dark assays and show a minor relationship with good correlation in the light. Resultant pH values in dark

samples show no slope or correlation to iron values, where light samples show a modest downward slope which shows a much greater agreement with soluble iron. This low but well correlated trend could be explained by an increase in expected weakly dissociating carboxylic acid groups in produced oxPAH via processing by PAH of soil-bound iron. These pH values would then represent acidic character as a product as opposed to a driver of the reaction. The variations in found pH within the pyrene and water assays were somewhat surprising. If interactions in this study have any surface dependence then these differences may be attributable to varying particle sizes in either or both the soil and the saturated PAH. In an attempt to characterize the nature of this produced soluble iron we may look at the environmental effects to differentiate either free or complexed iron species. The acidic nature of free iron would be expected to produce a 3-to-1 ratio of hydronium ion which would have a direct impact on pH, however given the nanomolar scale of the iron in these solutions this would be insignificant compared to the auto-dissociation of water. However, since the observed pH values using PAH were well above this region, demonstrating the pH 3.5 to 5.5 character of cloud water, then mechanisms that involve organic chelation reduction to form soluble ferrous ions or siderophore-like behavior, such as complexation with dissolved aromatics, must be considered as reaction pathways.

Soluble iron shows a complex relationship with potentially available dissolved organics. The previously studied mechanisms of siderophores demonstrate interactions with soluble organic ligands given their high affinity for iron (Rose and Waite 2003; Willey et al. 2008). These reactions are described as interactions of individual, and

therefore unencumbered, ligands which would be the equivalent of dissolved aromatic species in our assays. The semi volatile nature of environmental PAH would allow for partitioning onto ambient particles (Garban et al. 2002; Chen et al. 2006; Galarneau 2008) lending themselves to be available as dissolved species in cloud water droplets. However, the absolute concentrations of all the dissolved tested PAH do not completely correlate to the amounts of observed iron solubility. Little to no iron responses were observed with assays of benzo(e)pyrene, pyrene, and phenanthrene; illuminated assays using anthracene and naphthalene produced a significant amount of soluble iron. The most striking activity comparison is between anthracene and phenanthrene, given that phenanthrene is substantially more soluble than anthracene. A strong direct correlation is observed between iron and the solubilities of the known redox-active aromatics (ie, anthracene, naphthalene, phthalic acid). This suggests a connection with highly oxidized organic species where reactivity is structure-dependent. The strong iron reactivity of illuminated anthracene samples is in contrast to the non-reaction of its dark samples and the small component of dissolved material. This strongly suggests a mechanism that relates to a photo-oxidation surface interaction of the remaining solid that contains a redox-active aromatic structure, leading to the production of soluble iron complexes (Paris et al. 2011). Given the great excess of dissolved organic reagent in the naphthalene, formic, and phthalic assays to observed soluble iron, this study also further suggests that only surface-bound iron in dust particles are susceptible to this mechanism pathway. This mechanism fits well with the observed production of soluble ferric and

ferrous organic complexes in the long range transportation of Saharan dust (Rizzolo et al. 2017).

Creation of soluble iron from soil based solely upon interactions with PAH appears to be dependent on solid particles of redox-active aromatics and sunlight illumination. Previous studies of PAH and metal-oxides have shown a dependence on surface interactions (Tombacz et al. 2004). The coordination of soil-based iron, PAH oxidation, and sunlight assisted pi electron excitation may be aided by particulate matter acting as a surface catalyst. This pathway fits with the expected emissions of combustion sources, focusing specifically on emitted PM and the varying aromatic nature of these particles (Khalili et al. 1995; Ravindra et al. 2008; Mahowald et al. 2009; Lee et al. 2011).

Finally, this study is also directly related to anthropogenic urban emissions. Increased Fe solubility (up to 80%) has been commonly observed in urban centers. Although the reason for this has not been elucidated, it is known that automobiles emit PAH as a primary pollutant (Marr et al. 1999; Lee et al. 2001).

This is one of the first studies to examine the interactions of terrestrial-borne iron, PAH, and sunlight to monitor the contribution of soluble iron in these reactions. The connection of increased soluble iron fits well with observed iron increases near urban regions as well (Sedwick et al. 2007; Mahowald et al. 2009) as these processes also emit aromatics to the atmosphere. Reactions of this type appear to be strongly specific to redox active materials, especially iron, and may therefore follow a mechanism similar to a Fenton electron transfer reaction to facilitate soluble iron production and PAH

conversion. Studies are ongoing to evaluate the fate and identity of the aromatic products formed during these reactions.

2.6 Conclusions

Here, we report our evaluation of the specific role of PAH on the cloud processing formation of soluble iron from terrestrial-borne atmospheric particles. Production of soluble iron via this reaction pathway is heavily dependent on the presence of redox-active PAH and further influenced by sunlight, particularly in anthracene samples. Differing from the acid-driven source of soluble iron, this process is observed in aqueous environments of relatively high pH suggesting a ligand-based complexation mechanism. The results of this study suggest a promising complimentary solubilization pathway to the aerosol-based acid process. The atmospheric cloud mixing of terrestrial insoluble iron and combustion-based PAH particles may contribute a significant portion of soluble iron toward global temporal observations.

2.6.1 Acknowledgements

We thank Drs. Benton Cartledge, Keith Miller, and Gary Bishop for their help and advice on the installation of the photosimulation reactor components. Dr. Bryan Cowen is thanked for his advice on materials preparation for the reactions involving organic aromatic compounds. Eva Cutler is thanked for her help in performing photoreactions and analysis. NSF award 1342599 supported this work.

CHAPTER THREE: PHOTO-INDUCED AUTO-OXIDATION OF POLYCYCLIC AROMATIC HYDROCARBONS RESULTING IN HUMIC-LIKE SUBSTANCE PRODUCTION

3.1 Abstract

Humic-like substances (HULIS) are a collection of oxidized atmospheric compounds detected worldwide with functionality and behavior resembling humic acids. This multifunctional nature allows HULIS to be water soluble, bioavailable, and to demonstrate light absorption at multiple wavelengths. The association of oxyradicals with HULIS has implications on human health via lung tissue damage; and its absorption character may add to radiative forcing processes in the atmosphere. Polycyclic aromatic hydrocarbons (PAH) are major primary products of combustion emissions and have long been known to oxidize in the environment as a component of secondary organic aerosols. In this study we have exposed aqueous PAH suspensions to simulated sunlight to investigate oxidized PAH as HULIS precursors. Illuminated samples of naphthalene and anthracene have demonstrated growth of several new products with absorptions and oxidation consistent with humic character. These results offer a new perspective on secondary formation pathways of HULIS from anthropogenic pollution sources.

3.2 Introduction

Humic-like substances (HULIS) are a class of oxidized organic light-absorbing compounds found in atmospheric samples around the world. Atmospheric darkening

conditions such as smog and brown clouds around urban areas are comprised of brown carbon species in which HULIS is considered a major component (Andreae and Gelencser 2006). Field PM samples have found high correlations between HULIS fraction and proximity to combustion events including vehicle emissions and forest fires (Lin et al. 2010). The gradient light absorption of HULIS, which differentiates it from black carbon, is believed to be due to individual absorption sharing and Rayleigh scattering across the UV-vis spectrum between several structurally similar compounds (Graber and Rudich 2006; Ravindra et al. 2008). When all of these products are present, the combined individual absorptions will create an overall pattern resembling a smooth continuous gradient of UV-vis absorption across the entire region (Andreae and Gelencser 2006; Dinar et al. 2008).

The HULIS fraction of environmental samples is defined by its chemical properties and has been characterized by evaluating several different parameters, including patterned light absorption and overall functionality. These have been identified by analyzing for characteristic absorption gradients within the UV-vis region (Andreae and Gelencser 2006; Graber and Rudich 2006) as well as identifying specific functional groups by FTIR and Raman spectroscopy (Kristensen et al. 2015). HULIS behavior has also been determined by retaining organic compounds using a solid-phase extraction technique unique to these compounds (Varga et al. 2001).

HULIS materials, being structurally similar to humic acids, are presented as a collective of compounds containing significant aromatic and oxidized character (Graber and Rudich 2006). The propensity for atmospheric HULIS material to evolve from

combustion processes dictates that the bulk structures will contain aliphatic regions of unburned organic fuels (Hoffer et al. 2004) and significant aromatic areas formed from inefficient combustion (Jenkins et al. 1996; Balachandran et al. 2013). HULIS samples observed from field campaigns have demonstrated increased average oxidation states of carbon from -2.0 to -0.4 (Kroll et al. 2011) and contain enhanced oxygen:carbon ratios ranging from 0.69 to 1.0 (Aiken et al. 2008; Altieri et al. 2008) presented as oxygen-containing functional groups. Production of these oxidized groups may be due to oxidation during combustion or down field oxidation by atmospheric oxyradicals (Pillar et al. 2014), such as hydroxyl and superoxide radicals.

Several studies have suggested oxidizing humification processes, similar to compost degradation for humic acids (Domeizel et al. 2004), on primary combustion emissions in the atmosphere due to interactions with reactive oxygen species (ROS) (Pillar et al. 2014). These reactions result in the formation of varying levels of oxidized regions, including the formation of olefin groups (Wentworth and Al-Abadleh 2011) and direct oxidation by oxygen-containing molecules (Arangio et al. 2016). The structure of these products are found to have aromatic character coated with oxidized groups including hydroxyl, carbonyl, and connected by ether bridges (Altieri et al. 2008), supplying the water solubility of these otherwise nonpolar molecules.

HULIS is associated with several atmospheric and biologically relevant processes which may have a significant impact on the global energy balance and may involve both direct and indirect reactions that adversely affect human health. First, HULIS has the ability to strongly absorb in the UV decreasing into the IR regions (Hoffer et al. 2004).

This wide range of light absorbing properties of HULIS may exacerbate the radiative forcing of incident light and heat and promote climate anomalies (Dinar et al. 2008). Second, organics with HULIS character are also strongly correlated with the solubilization of metals due to complexation (Tipping et al. 2002; Gonzalez et al. 2017). The intake of these compositions may aggravate the production of ROS and increase the risk of respiratory illness and oxidative damage to healthy tissue (Lin and Yu 2011; Yue et al. 2016).

HULIS and polycyclic aromatic hydrocarbons (PAH) are commonly observed in particles sourced from pyrogenic processes, e.g. biomass burning (Ravindra et al. 2008) and vehicle exhaust (Tsai et al. 2004). PAH are commonly known to be produced directly from combustion sources and comprise a significant fraction of the total organic carbon present in these collections (Balachandran et al. 2013; Bandowe et al. 2014; Ma et al. 2016). Anthropogenic particulate matter has been shown to contain mainly larger PAH while smaller PAH are dominant in aqueous environments, such as cloud and fog water droplets (Li et al. 2010). This partitioning between particle and water phases is seen as a function of vapor pressure due to the semi-volatile nature of shorter chain PAH (Allen et al. 1996). The strong tendency for observing PAH, along with enhanced HULIS material, in combustion samples adds an intriguing connection between the production of humic compounds and the presence of complex aromatics in the atmosphere.

The exact character and formation of atmospheric HULIS molecules are not completely understood, though several recent lab studies have successfully produced behaviorally similar compounds by oxidizing simple aromatics in both air-particle phase

(Vione et al. 2014; Zanca et al. 2017) and aqueous phase reactions (Chang and Thompson 2010). Several laboratory studies have shown significant HULIS production from single ring aromatics, such as phenol (Chang and Thompson 2010) and dihydroxybenzoic acid (Hoffer et al. 2004), as starting materials in photoreactions. However these reactions require the addition of oxidizing agents, such as hydrogen peroxide and ozone, to complete the reaction. Some recent studies have demonstrated the production of HULIS from the extended aromatic character of soot particles with the addition of generated ozone (Decesari et al. 2002).

The extended atmospheric lifetimes of PAH lend themselves to longer exposure times to sunlight and oxidants, producing branched and oxidized PAH (oxPAH) (Collett et al. 2008), potentially becoming building blocks for HULIS formation. PAH are associated with the creation of ROS in environmental conditions (Fu et al. 2012). The addition of ROS in these systems would result in the oxidation of PAH (Lee and Lane 2009), which may act as intermediates to further aggregate into more complex structures.

Particles containing PAH may use ultraviolet radiation as a catalyst in an electron transfer process with elemental oxygen or water molecules to produce radicals such as superoxide or hydroxyl radicals, respectively. Naphthalene has been shown to oxidize to form naphthols (Preuss et al. 2003) and phthalic acids (Barbas et al. 1993) in the presence of sunlight and oxidizers, and anthracene has been found to form carbonyl groups during oxidation resulting in equilibrium between anthraquinone and anthracenediol (Faiola et al. 2011). Further reactions between these species as well as remaining ROS may involve diol condensation reactions to form ether groups (Altieri et al. 2008) and ring-splitting

nucleophilic substitution at ketone sites to form esters and carboxylic acids (Altieri et al. 2008).

This study evaluates the formation of HULIS via aqueous photo-oxidation of simple PAH. Saturated suspensions of various PAH are tested for reaction by applying simulated sunlight in an open air environment. This will allow for similar expected dissolved oxygen as would be experienced in an atmospheric cloud water droplet. Analyses for the production of HULIS content in these reactions include UV-vis, HPLC, attenuated total reflectance-based FTIR, and HULIS-specific solid phase extraction (SPE). These evaluations allow for a complete cache of evidence toward the number of products created and sufficient knowledge of their character to properly determine true HULIS formation.

3.3 Experimental

3.3.1. Materials

All experiments and sample preparation were performed under a laminar-flow hood using HEPA-filtered air. To reduce cross-contamination in the reactor between assays, Teflon beaker liners were cleaned through a succession of solvent treatments. This process starts with an acetone rinse followed by an overnight bath of 100% HPLC-grade acetonitrile, then a final overnight bath in 5% trace-metal grade nitric acid including a pre and post-bath triplicate rinse with 18.2 MΩ purified water. Plastic tubes, bottles, and syringes were prepared using a rinse with 100% acetone and dried before sample addition.

Whatman 0.20 μm syringe filters were prepared by flushing a series of 5 mL aliquots of dilute acid and ultrapure water. An initial rinse of 10% trace-metal grade hydrochloric acid is followed by a rinse with 18.2 MΩ purified water, then a 5% nitric acid rinse is followed by five flushes of 18.2 MΩ purified water.

3.3.2. Reagents

Naphthalene (NAP), anthracene (ANT), phenanthrene (PHE), and pyrene (PYR) (Sigma, Fisher) were the PAH used for these reactions. Suspected reaction products, including 1-naphthol, naphthoquinone, anthraquinone, phthalic acid, and phthalic anhydride (Sigma) were analyzed as standards dissolved in 100% acetonitrile (Sigma). All of these compounds were used as received without further purification. Ultrapure water was obtained from a Thermo Scientific Nanopure water deionization system and was collected during a resistance value of 18.2 MΩ. Simulated sunlight was provided by an Oriel Sol 1A solar simulator using an Air Mass, AM 1.5 Global Filter (Newport) producing 5.4% UV, 54.7% visible, and 39.9% IR spectra light equivalent to sunlight, and calibrated for a flux of 1550 Wm^{-2} to simulate one sun at sea level at its zenith.

3.3.3. Methods

Aqueous suspensions of PAH were created by adding 100 mg of organic crystals to 200 mL of ultrapure water to obtain a total concentration of 500 ppm. These mixtures are then capped, inverted ten times, and stored at room temperature in the dark. Each organic suspension is aged for 24 hours to allow the solids to fully dissolve to equilibrium. The reaction vessels are comprised of 100 mL Teflon liners inside jacketed

glass beakers which are temperature controlled at 25°C by water flow from a chiller pump.

During the reaction, illuminated samples were held at 25^{o}C with stirring for 16 hours under a controlled light using the calibrated solar simulator lamp. Control samples of identical composition were conducted in the dark by covering an additional reaction vessel with a commercially available aluminum foil. Sample aliquots of 4 mL were removed at the beginning and end of the reaction period. Samples evaluated for bulk aqueous properties, such as acidic character, UV-vis spectra, and liquid chromatographic separation, are analyzed raw without filtration or acidification. Samples analyzed for functional groups are performed on resultant solid residues prepared by evaporation of the water solvent using a clean air flow in a HEPA-filter hood. Reaction products tested for HULIS-specific retention behavior are prepared and evaluated using a revised method described in a previous study (Varga et al. 2001). Briefly, sample aliquots are filtered at 0.2 μm and acidified to pH 2 using HCl before application to an extraction procedure as described below.

UV-vis absorption patterns in samples are analyzed using a Shimadzu UV-1800 spectrophotometer. Bulk aqueous samples are added to 1 cm quartz cuvettes after baseline calibration using ultrapure water. All samples are analyzed from 220 to 700 nm with maximum absorbance set to 4.0 absorbance units.

HPLC (Agilent 1100) analysis was performed using a reversed-phase separation, employing a gradient mobile phase method. Separation was obtained using 1 mL/min flow rate, 0.1% TFA:ACN gradient of 90:10 to 0:100 over 22.5 min plus hold to 28 min,

100 μL sample injection through a Hydro-RP 250 x 4.6 mm column (Phenomenex), and detection at 254 nm. The chosen column uses a C18 stationary phase on beads with 80Å pore size; this creates a method that may retain substances in part by polarity component which may separate individual HULIS compounds. Therefore each peak will represent a compound or set of compounds that match a particular hydrodynamic diameter and degree of oxidation (i.e, polarity). To allow for mobile phase system reset between samples, each analysis was followed by a hold-time of 5 minutes.

Aliquots from the naphthalene and anthracene reactions were evaporated and tested for functional groups using attenuated total reflectance Fourier transform infrared spectroscopy (ATR-FTIR) on a ThermoScientific iS5, analyzed from 700 to 4000 cm^{-1}. The diamond crystal was cleaned and prepared for analysis using a swab of isopropanol and background set after drying. Obtained residues were applied directly to the crystal and firm contact was attained by a torque-controlled plunger.

Speciation of HULIS-specific organic compounds used a revised SPE method (Varga et al. 2001) wherein 2 mL of filtered and acidified sample is drawn through a multi-modal SPE cartridge (Oasis HLB), followed by a 1% methanol wash. Retained material is eluted with 100% methanol and evaluated for HULIS products by UV-vis and HPLC using the methods detailed above.

3.4 Results

3.4.1 UV-vis Absorption

The spectra in Figure 3.1 show the changes in light absorption for PAH samples across the UV-vis range due to the influence of simulated sunlight. NAP and ANT

spectra in the light demonstrate a dramatic increase in absorption, displaying a featureless decay from the UV and throughout the visible range resulting in yellow to orange colored solutions at the end of the reaction period. This is contrasted by the same assays in the dark which maintain a single absorption peak in the UV region and shows no absorption in wavelengths higher than 300 nm, resulting in a clear and colorless solution.

The resultant colorless samples with the dark PHE and PYR assays display a similar single peak in the UV without absorbance into the visible region. The results of these samples in the light create similar discolored solutions to the NAP and ANT light samples. The elevated absorbance from the light allows for an elevated baseline into the near-UV region of the visible spectrum. The single peak in the PHE light sample is shown to increase in intensity and shift slightly from 237 to 243 nm, while the PYR sample has similarly shifted its peak at 238 nm in the dark to a shoulder at 253 nm in the light.

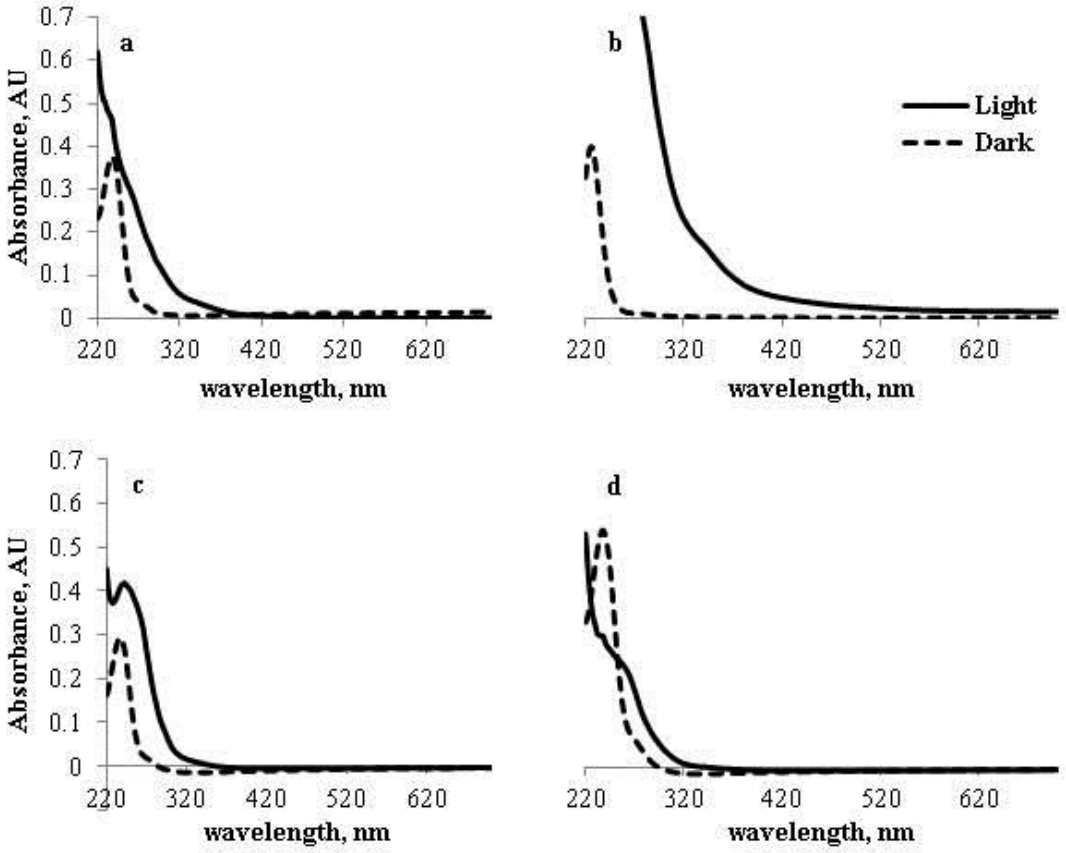

Figure 3. 1: UV-vis analysis of saturated suspensions of PAH.
(a) naphthalene, (b) anthracene, (c) phenanthrene, (d) pyrene, in ultrapure water following 16 hour reaction period. Lighted samples are represented in the solid spectra, the dashed spectra represents the samples kept in the dark.

3.4.2 High Performance Liquid Chromatography

The HPLC chromatograms in Figure 3.2 display the separations of individual products formed from the 16 hour reaction time. The NAP and ANT assays display response production of many new products from sunlight irradiation. This is in contrast to their PHE and PYR counterparts who display the production of very few products in sunlight. NAP light samples demonstrate a wide range of products across the elution gradient; ANT light samples also show products across this region but display some changes in the chromatographic pattern as well as some major peaks during the later retention times. These are compared to the very few peaks obtained from the same assays kept in the dark.

The analyses of PHE and PYR are also shown to produce a small number of peaks in both assays, which relate to the formation of very few products. The propensity for NAP and ANT in the light to produce several products correlates well with the expansive UV-vis absorption evaluation, as well as the connection between the comparatively uneventful responses in UV-vis and HPLC from PHE and PYR samples.

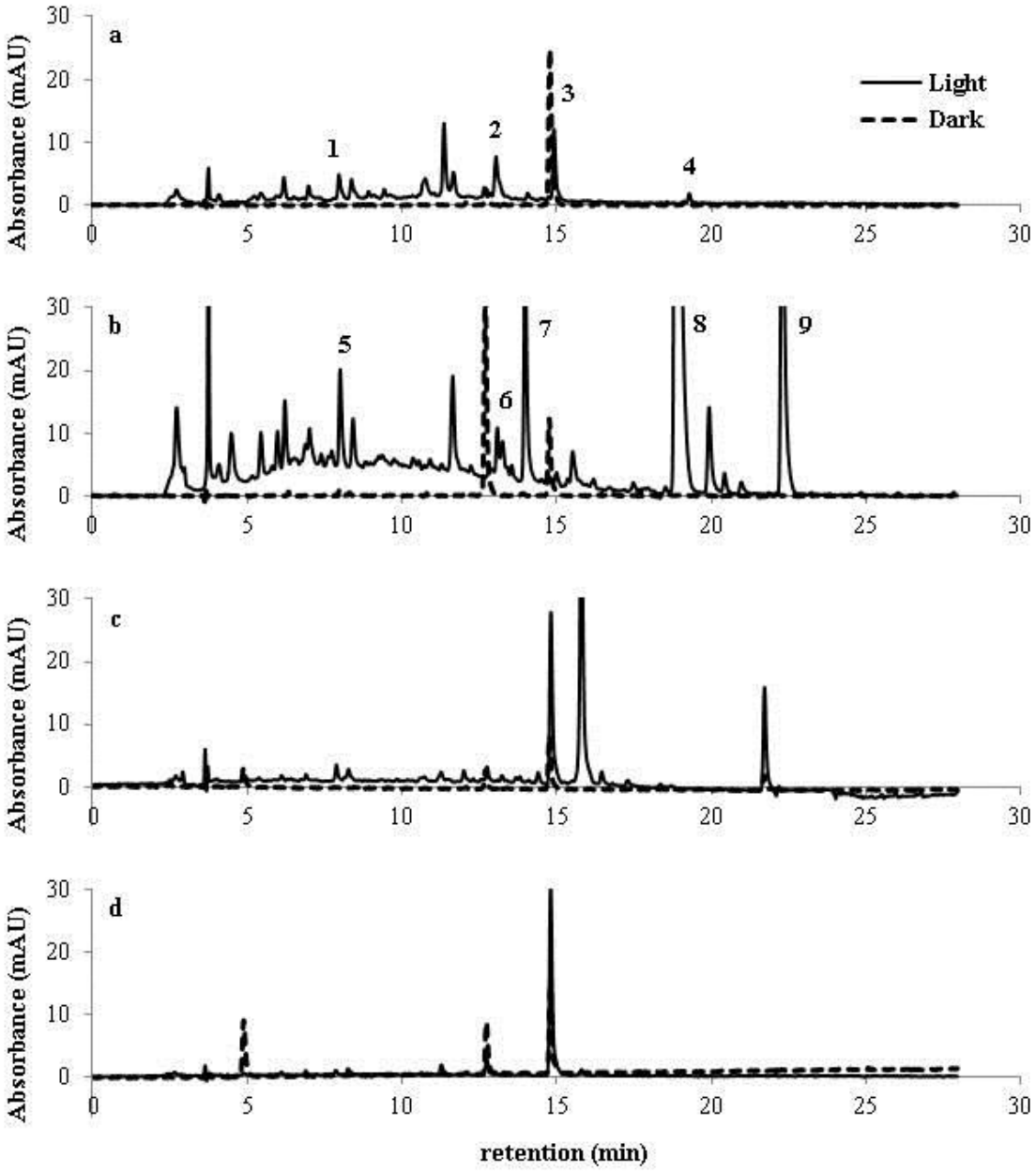

Figure 3. 2: HPLC analysis of post-reaction samples of saturated PAH.
(a) NAP, (b) ANT, (c) PHE, (d) PYR. Lighted samples are represented in the solid spectra, the dashed spectra represents the samples kept in the dark. Numbered peaks are identified products based on retention times of standards dissolved in acetonitrile.1. phthalic anhydride, 2. phthalic acid, 3. naphthol, 4. naphthalene, 5. phthalic anhydride, 6. phthalic acid, 7. naphthoquinone, 8. anthraquinone, 9. anthracene.

3.4.3 Infrared Spectroscopy

Figure 3.3 shows the analysis of functional groups on light and dark samples using ATR-FTIR. These analyses are performed on solid residues following aqueous evaporation. Both NAP and ANT dark samples display single peaks at 3048 cm^{-1} and a group of several peaks from 1600 to 900 cm^{-1}, correlating to poly-aromatic hydrogen stretches and bends, respectively. One difference with the NAP dark sample is the small dip centered at 3343 cm^{-1} which may indicate a hydroxyl hydrogen bend or adsorbed water species.

The top spectra in Figure 3.3 display the growth of functional groups on illuminated NAP and ANT assays. Comparing these spectra with the dark samples allows for the determination of sunlight-specific growth in bulk water media. The NAP light spectrum shows significant growth of new peaks at 3219, 1717, and large baseline dip from 1360 to 950 cm^{-1}. These would indicate the formation of hydroxyl alcohols, carbonyl groups, and ether bridges, respectively. The ANT spectrum displays new groups with modest absorbance peaks at 1673 and stretch from 1317 to 1175 cm^{-1}, which correlate to carbonyl and ether groups, respectively. An intriguing difference in functional group character between lighted NAP and ANT samples is the lack of hydroxyl stretches in the 3000-3500 cm^{-1} region of the ANT spectrum.

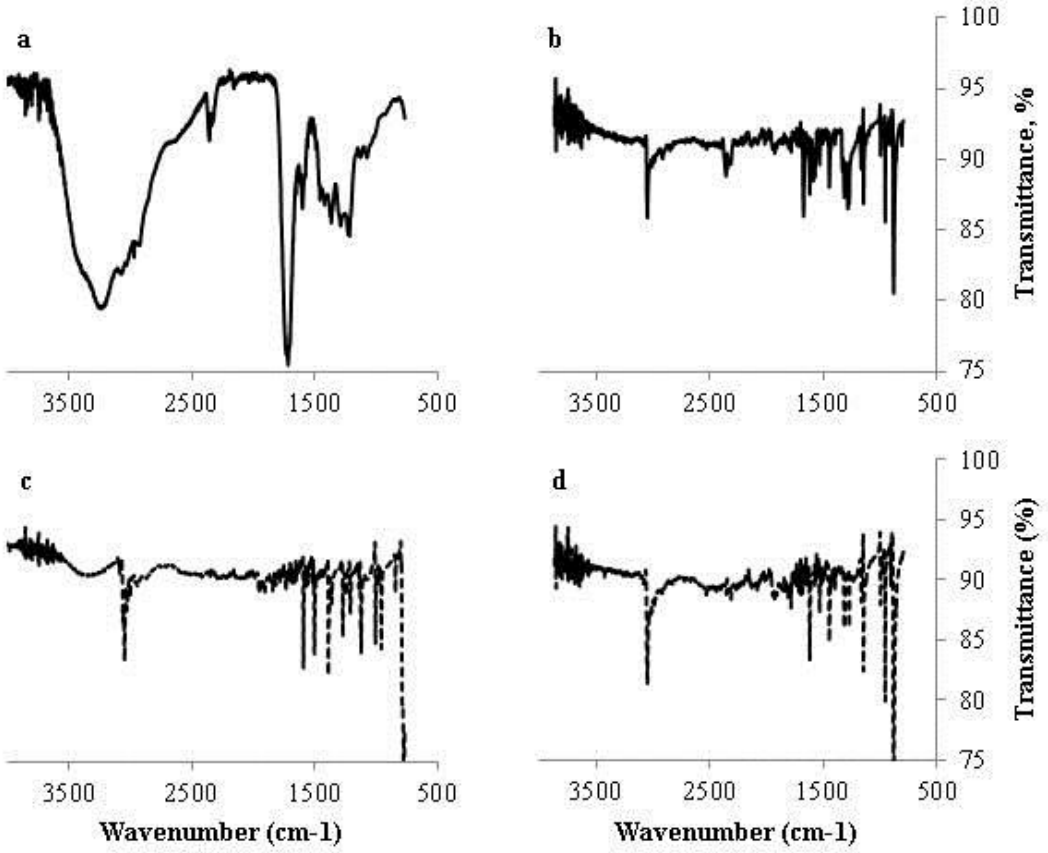

Figure 3. 3: ATR-FTIR analysis of NAP and ANT products.
Light and dark conditions of illuminated samples are presented for naphthalene (a) and anthracene (b). Samples kept in the dark are presented for naphthalene (c) and anthracene (d). Light and dark product analyses are represented by the solid and dashed spectra, respectively. These are performed on a diamond crystal, therefore peak activity in the 2400 cm^{-1} region is considered background uncertainty.

3.4.4 Solid Phase Extraction

Figure 3.4 presents the evaluation of potential products in the elution stage of the solid-phase extraction method specific to HULIS. Any products retained using this method are detected by UV-vis and HPLC methods as described above, except that these extractions are evaluated in the methanol matrix used for the elution.

The UV-vis analysis for the NAP sample demonstrates a similar absorption curve as the original aqueous lighted sample with an added shoulder, suggesting a similar composition of HULIS products with a slight rise in a major product. The elution of HULIS products is further confirmed in the HPLC analysis for NAP, where significant product peaks are observed.

UV-vis evaluation of the ANT extraction displays an overall similar decaying absorbance as its aqueous light sample, but with added significant peaks. These peaks bear no resemblance to the single peak in the aqueous dark sample; therefore this maintains evidence of various HULIS material with some major products of similar composition. Similar to the HULIS extraction analysis of the NAP sample, the HPLC evaluation on the ANT extraction demonstrates the presence of individual HULIS-like products.

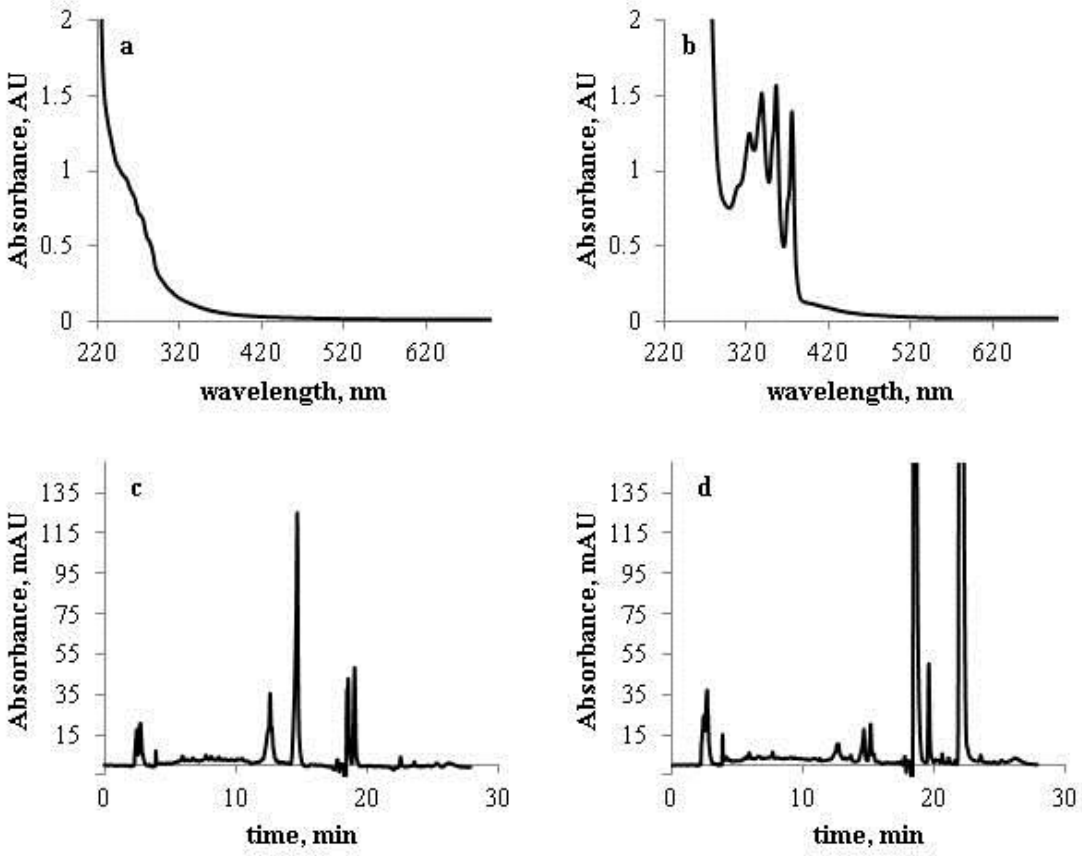

Figure 3. 4: Solid phase extraction spectra of UV-vis and HPLC data.
UV-vis data for NAP (a) and ANT (b) and HPLC data for NAP (c) and ANT (d). These represent HULIS on Light samples of NAP and ANT following 16 hour reaction time. UV-vis spectra and HPLC chromatograms are obtained using the same methods previously described for the raw samples. UV-vis absorbance is obtained from 220 to 700 nm. HPLC detection is obtained using wavelength 254 nm. Samples are analyzed in their methanol elution matrix.

3.5 Discussion

Aqueous suspensions of NAP and ANT have demonstrated their capacity to form a wide array of compounds in simulated sunlight. HPLC separation of NAP and ANT lighted samples displayed the creation of numerous new oxidized products. This separation followed a dual-retention technique where the C18 stationary phase on the beads, retaining compounds of varying nonpolar character, is combined with an 80Å pore size, preferentially retaining compounds with hydrodynamic diameters of 8 nm and smaller. The variety of peaks between the void and end points demonstrate the diversity of compounds of varying levels of oxidation, diameter, and composition. Comparing retention times of product peaks with pure standards demonstrates that both NAP and ANT lighted assays contain phthalic acid and phthalic anhydride, with NAP favoring the acid product and ANT the anhydride. This demonstrates a pattern of products where ANT has shown a preference for producing primarily ketone-containing products, such as anthraquinone and naphthoquinone, while NAP shows the hydroxylated product naphthol. The dissimilar pattern of peaks between the NAP and ANT chromatograms attest to the observed differences between HULIS character sourced from different fuel types in field samples (Jenkins et al. 1996; Kristensen et al. 2015).

Evaluations of these products on FTIR clearly display the formation of oxidized groups, including carbonyls, ethers, and hydroxyl groups. NAP sample assays clearly show produced peak dips at 3300 cm^{-1} indicating OH character, strong peak at 1725 cm^{-1} indicating the growth of carbonyl groups, and a baseline dip within the 1100-1300 cm^{-1} region which coincides with ether moieties. In the IR spectrum, ANT products contain

similar features to the NAP products with respect to the produced spectra character for ether and carbonyl content, but show no indication of OH group formation. This may explain the high degree of quinone character found in environmental HULIS samples (Lin and Yu 2011) as anthracene, along with naphthalene, is one of the major exhaust compounds seen in primary emission samples (Tsai et al. 2004). The chemical composition, size distribution, and number of products in these assays coincide with expected HULIS character.

These PAH reaction systems create the characteristic absorption decay observed in environmental HULIS. While all illuminated assays created overall discolored aqueous samples, only the NAP and ANT assays displayed UV-vis spectra containing continuous absorption from 220 through 700 nm. The PHE and PYR lighted samples showed a similar discoloration due to a slight shift in maxima and an enhanced baseline, which allowed absorption into the near-UV portion of the visible spectrum. This coincides with the observance of several products demonstrated on the HPLC for the NAP and ANT assays with few new products on the PHE and PYR assays.

The solid-phase extraction method for produced HULIS involves stationary phases of divinylbenzene and N-vinylpyrrolidone (Varga et al. 2001) acting as both hydrophobic and hydrophilic stationary phase groups, respectively, to account for inherent varying functionality. Both NAP and ANT products show significant retention using this method as demonstrated by the characteristic UV-vis and HPLC analyses. Each assay contained the previously described observed absorbance decay in the UV-vis analyses. Products which were extracted by the SPE cartridge and recovered by elution

are also seen as collected peaks in the HPLC. The UV-vis spectrum for ANT differs from the NAP as there are significant peaks within the decay baseline. This may be due to the aggregation of quinone products within the methanol matrix, leading to a small number of major absorptions and concentrated retained peaks along the column.

Irradiated PAH products demonstrate types of behavior consistent with HULIS obtained from field samples (Kiss et al. 2005; Dinar et al. 2008) and lab-generated bench methods (Wentworth and Al-Abadleh 2011). Typical photochemical bench methods for HULIS formation start with simple oxidized aromatics, e.g. phenol (Vione et al. 2014), introduced to photosensitizers and oxidants, e.g. sulfates and hydroxyl radical (Liao et al. 2014; Pillar et al. 2014). Several studies have investigated products from organic precursors exposed to hydrogen peroxide or ozone in the presence of UV light (Chang and Thompson 2010). These assays require a photosensitizer to aid in the excitation of the reagent, creating a more reactive environment to the ROS leading to varying compositions of HULIS. PAH are known to be inherently photosensitive (Bamforth and Singleton 2005) and are strongly correlated with ROS production in aqueous systems with available dissolved oxygen (Fu et al. 2012).

Results in this study fit the expected reactivity of NAP and ANT given their inherent redox potential and photosensitivity (Bamforth and Singleton 2005). NAP and ANT are the only PAH tested in this study that are known to be susceptible to oxidation in atmospheric conditions, as PHE and PYR are found to be highly stable in environmental samples taken at greater distances from their source (Zhang and Tao 2009). This susceptibility would be essential for the addition of oxygen-containing

groups onto the parent structures and potentially ring-cleavages leading to a large variety of oxidized products.

This study looks to the possibility of PAH alone oxidizing and aggregating to form HULIS with simulated sunlight. Since there were no additional oxidants supplied for these reactions, the HULIS content formed in this purely aqueous PAH environment has significant implications on the inherent threat that anthropogenic and biomass burning emissions have on air quality and atmospheric absorption. Given that there are several pathways in the production of environmental light absorbing compounds (Andreae and Gelencser 2006), this study has demonstrated the potential long-term effect of PAH on the production of HULIS in the atmosphere and therefore on radiative forcing and climate change.

3.5.1 Acknowledgements

We thank Drs. Benton Cartledge and Gary Bishop for their help and advice on the installation of the photosimulation reactor components. NSF award 1342599 supported this work. This paper uses reference and primary research data which are presented in Figures 3.1-4. All authors declare that this research contains no conflict of interest.

CHAPTER FOUR: INVESTIGATION INTO HUMIC-LIKE SUBSTANCE PRODUCTION VIA AQUEOUS PHOTO-OXIDATION OF POLYCYCLIC AROMATIC HYDROCARBONS

4.1 Abstract

The production of Humic-Like Substances (HULIS), the atmospheric-borne component of brown carbon, from solar simulated oxidation of polycyclic aromatic hydrocarbons (PAH) is studied. Using Suwannee River Fulvic Acid (SRFA) as a reference for HULIS, reactions of aqueous naphthalene, anthracene, and oxidized derivatives of naphthalene were found to produce chromatographic and spectroscopic evidence of HULIS formation when exposed to sunlight. Overall product character from naphthalene and anthracene indicate reaction mechanism pathways using oxidized naphthol and naphthoquininone as intermediate species. This is the first study to propose some major reaction pathways involving PAH and brown carbon materials.

4.2 Introduction

Polycyclic aromatic hydrocarbons (PAH) are produced by the inefficient burning of organic fuels and display extended lifetimes in the atmosphere (Ravindra et al. 2008). These aromatics are toxic to human health and many structures are considered highly carcinogenic (Bamforth and Singleton 2005; Kim et al. 2013). Although PAH have many atmospheric reaction pathways, one unexplored endpoint is the formation of humic-like substances (HULIS). Aerosolized HULIS are consistently correlated with reactive

oxygen species and soluble metals (Tang et al. 2014), and as such, they are implicated with respiratory problems, oxidative stress, and Earth's energy balance (Andreae and Gelencser 2006). This study evaluates the mechanistic pathways of HULIS production by oxidation of aqueous suspensions of PAH with only exposure to sunlight.

HULIS material is a class of light absorbing compounds and is presented as a collective of organic species, each containing significant aromatic and carboxylic acid character (Graber and Rudich 2006). They are found to be a major component of brown carbon and are implicated with radiative forcing in the atmosphere (Andreae and Gelencser 2006). PAH and HULIS are commonly observed in particles sourced from pyrogenic processes, e.g. biomass burning and vehicle exhaust (Ravindra et al. 2008). The long range transport of PAH lend themselves to extended exposures to sunlight and oxidants, potentially producing other branched and oxidized PAH (oxPAH) products such as anthraquinone and naphthol, which may then act as intermediates for larger structures, e.g. HULIS. Environmental PAH and HULIS are correlated with reactive oxygen species in cloud water and aerosolized particles (Bamforth and Singleton 2005). Particle surfaces containing aromatics may use ultraviolet radiation as a catalyst in an electron transfer interaction with elemental oxygen or water molecules to produce radicals, such as superoxide or hydroxyl radicals. These radicals are highly reactive oxidation agents and may initiate several oxidizing pathways (Wols and Hofman-Caris 2012), resulting in the further production of HULIS via oxPAH.

Reaction parameters use varying PAH reagent and matrix composition, oxidizing agents, and time duration. Analytical techniques for detecting organic products include

UV-vis, HPLC, ESI/APCI-MS, and FTIR. These analyses will help to define the spectroscopic properties, growth in mass, and elucidate the number and structure of these products. Initial oxPAH data include the evolution of discolored samples demonstrating an exponential featureless decay within the UV-vis analysis and the growth of many new HPLC peaks during and following light exposure periods, which indicate the production of several new species. These UV-vis spectra and arrays of HPLC products are symptomatic of HULIS materials. Our project has observed the growth of peaks at specific retention times throughout these reactions, which demonstrate the evolution of explicit reaction pathways toward predictable products. Evaluating the formation of products from identified oxidation products of PAH assays allows for the determination of specific reaction mechanisms. A higher understanding of the creation of HULIS in atmospheric conditions will greatly aid in predictive models for air quality and human health downwind of pollution sources.

The category of humic substances is a broadly defined term which is meant to describe collections of similarly highly and diversely functionalized organic molecules. Traditional humic acids are named from the region of their transformation (Graber and Rudich 2006), ie the humus layer of soil, in a process called humification (Tuomela et al. 2000). Groups of these molecules formed in aquatic regions are described as fulvic acids. A very recently discovered form of these molecules is formed in the atmosphere and is less understood, and is therefore more broadly termed Humic-Like Substances (HULIS). Despite their varying origins, all types are classified as humic based upon shared functionality and environmental activity. These hydrocarbons all contain significant

aromatic regions and have a high degree of oxygenation in the form of ether bridges, carbonyl groups, and hydroxide (Graber and Rudich 2006). Several of these oxidized groups are paired together to create ester chains and carboxylic acids.

These groups give the collection of these compounds multiple similar activities. Humics are implicated with the production and sequestration of reactive oxygen species (ROS), their carbonyl and hydroxyl groups give them the ability to complex metals (Tang et al. 2014), the multimodal structure allows for nutrient mobilization in biological systems (Canellas et al. 2015), and when dissolved in aqueous solutions, including cloud water droplets, they demonstrate a translucent effect wherein a high absorbance at low wavelengths becomes progressively lower at longer wavelengths across the UVvis spectrum. This defines their considerable contribution to brown carbon (Andreae and Gelencser 2006). It is in the nature of humic substances to encompass a broad range of individual compounds and therefore represent a large range of masses. As such, these masses generally trend larger for humic acid, lower for fulvic acid, and HULIS represents the smallest masses (Graber and Rudich 2006).

Formations of atmospheric compounds are highly susceptible to several ever-changing factors, e.g. patterns of combustion emissions, varying wind speed and direction, temperature and humidity. Therefore there has been no established standard reference material for HULIS in bench or field studies. To this end, the most commonly accepted reference for HULIS character is Suwannee River Fulvic Acid (SRFA) (Graber and Rudich 2006).

Several bench studies of HULIS production have used single aromatic compounds and strong oxidizer reagents as starting materials in aqueous phase generation. Previous studies have investigated pre-oxidized benzene structures that have been observed in the atmosphere (Andreae and Gelencser 2006), mainly phenol and cathehol, representing compounds released by biological and combustion processes. To initiate these reactions previous projects typically add a known environmental oxidizing agent (Andreae and Gelencser 2006), such as hydrogen peroxide, ozone, and ferrous iron. These systems react robustly with UV irradiation (Wols and Hofman-Caris 2012) to produce reactive oxygen species (ROS) in the form of hydroxyl radical (OH) and superoxide radical (O2-). Each of these will act upon the aromatic compounds to form hydroxides and carbonyl groups, respectively.

Our project has previously observed HULIS formation in solar simulations from aqueous suspensions of polycyclic aromatic hydrocarbons (PAH) in the absence of oxidizing agents. Both of these compounds are sourced from combustion and anthropogenic regions and therefore are likely connected in their formations. PAH are a major primary emission product from biomass burning and vehicle emissions. They are commonly observed to oxidize in the atmosphere in the presence of ROS (Bamforth and Singleton 2005). Our bench studies have previously demonstrated that the products of these oxidations share several characteristics that are consistent with HULIS. One main factor we observed was the ability for oxidized PAH to produce soluble iron from insoluble iron in a standard reference soil.

Due to the highly varying nature of humic substances, there are likely several mechanistic pathways for atmospheric HULIS, many of which may involve multiple steps. The extended aromatic systems of PAH are strongly implicated with the generation of OH radical, these radicals are typically borne out of a peroxide intermediate structure that gets homolytically cleaved by UV light or react through a Fenton-like electron transfer mechanism resulting in an oxide and the OH radical (Zhu et al. 2013). Superoxide radicals are associated with elemental oxygen and regions of high electron density, such that extended aromatic systems may supply. Similar to alpha oxidation mechanisms, PAH reactions with OH are likely to produce structures with hydroxides at alpha positions to fused rings, such as 1-naphthol and 9,10-anthracene-diol. Elemental oxygen species, e.g. superoxide and singlet oxygen, are commonly observed to oxidize opposite ring positions (Bamforth and Singleton 2005) into symmetrical ketone structures, including 1,4-naphthoquinone and 9,10-anthraquinone. Our project has previously identified a handful of structures from aqueous PAH oxidations which include the previously mentioned hydroxyls and quinones, as well as more simple aromatics including benzoic and phthalic acids. The determination of any of these structures to behave as intermediate species, instead of end products, will greatly help in elucidating preliminary mechanism steps.

This study aims to examine the reaction of potential intermediate structures and system alterations in order to introduce some major reaction pathways involved in the transformation of PAH into HULIS. The number and behavior of products are evaluated by HPLC and UVvis. The overall structural qualities are analyzed by ATR-FTIR and

ESI/APCI-MS. Each of these tests are compared to data obtained from SRFA for HULIS content.

4.3 Experimental

4.3.1 Materials

All experiments and sample preparation were performed under a laminar-flow hood using HEPA-filtered air. To reduce cross-contamination in the reactor between assays, Teflon beaker liners were cleaned through a succession of solvent treatments. This process starts with an acetone rinse followed by an overnight bath of 100% HPLC-grade acetonitrile, then a final overnight bath in 5% trace-metal grade nitric acid including a pre and post-bath triplicate rinse with 18.2 MΩ purified water. Plastic tubes, bottles, and syringes were prepared using a rinse with 100% acetone and dried before sample addition.

4.3.2 Reagents

Reagents used for these reactions include the PAH, naphthalene (NAP), anthracene (ANT), phenanthrene (PHE), and pyrene (PYR), and found oxPAH products benzoic acid, phthalic acid, 1-naphthol, 1,4-naphthoquinone, 9,10-anthracenediol, and 9,10-anthraquinone (Sigma, Fisher) were all used as received without further purification. The structures for these organic reagents can be seen in Fig. 4.1. Suwannee River Fulvic Acid (SRFA) III (IHSS) was used as the analytical standard for HULIS and was used as received.

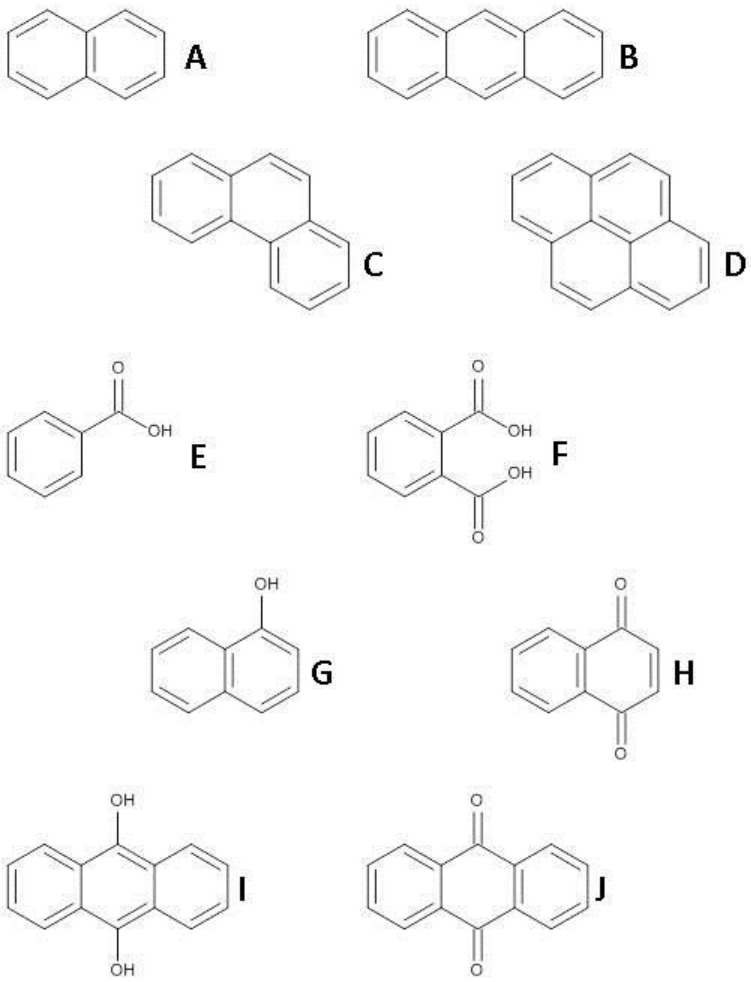

Figure 4. 1: Structures of PAH and oxPAH reagents.
(A) naphthalene, (B) anthracene, (C) phenanthrene, (D) pyrene, (E) benzoic acid, (F) phthalic acid, (G) 1-naphthol, (H) 1,4-naphthoquinone, (I) 9,10-anthracene-diol, (J) 9,10-anthraquinone. All structures are created by the author using MarvinSketch software.

Ultrapure water was obtained from a Thermo Scientific Nanopure water deionization system (ThermoScientific Nanopure, Waltham, MA).and was collected during a resistance value of 18.2 MΩ. Simulated sunlight was provided by an Oriel Sol 1A solar simulator using an Air Mass, AM 1.5 Global Filter (Newport) producing 5.4% UV, 54.7% visible, and 39.9% IR spectra light equivalent to sunlight, and calibrated for a flux of 1550 Wm^{-2} to simulate one sun at sea level at its zenith.

4.3.3 Methods

Aqueous suspensions of organic samples were created by adding 100 mg of organic crystals to 200 mL of ultrapure water to obtain a total concentration of 500 ppm. These mixtures are then capped, inverted ten times, and stored at room temperature in the dark. Each organic suspension is aged for 24 hours to allow the solids to fully dissolve to equilibrium. The reaction vessels are comprised of 100 mL Teflon liners inside jacketed glass beakers which are temperature controlled at 25°C by water flow from a chiller pump.

During the reaction, illuminated samples were held at 25^{o}C with stirring for 16 hours under a controlled light using the calibrated solar simulator lamp. Control samples of identical composition were conducted in the dark by covering an additional reaction vessel with a commercially available aluminum foil. Sample aliquots of 4 mL were removed at the beginning and end of the reaction period. Samples evaluated for bulk aqueous properties, such as acidic character, UV-vis spectra, and liquid chromatographic separation, are analyzed raw without filtration or acidification.

4.3.4 Analysis

Sample solutions following photoreaction are evaluated for HULIS character by qualitative comparison of analytical data to data obtained from the chosen standard material, namely SRFA. This fulvic acid standard is stored and handled in the same manner as the PAH and oxPAH reagents. HULIS character inherent in the SRFA, including retention, spectroscopic, functionality, and size are based on the HPLC, UVvis, ATR-FTIR, and ESI/APCI-MS analyses described below.

UV-vis absorption patterns in samples are analyzed using a Shimadzu UV-1800 spectrophotometer. Bulk aqueous samples are added to 1 cm quartz cuvettes after baseline calibration using ultrapure water. All samples are analyzed from 220 to 700 nm with maximum absorbance set to 4.0 absorbance units.

HPLC (Agilent 1100) analysis was performed using a reversed-phase retention gradient mobile phase method. Separation was obtained using 1 mL/min flow rate, 0.1% TFA:ACN gradient of 90:10 to 0:100 over 22.5 min plus hold to 28 min, 100 μL sample injection through a Hydro-RP 250 x 4.6 mm column (Phenomenex), and detection at 254 nm. The chosen column uses a C18 stationary phase on beads with 80Å pore size; this creates a method using a polarity component. Therefore each peak will represent a compound or set of compounds that match a particular degree of oxidation (i.e, polarity). To allow for mobile phase system equilibration between samples, each analysis was followed by a equilibrium time of 5 minutes.

Aliquots from photoreaction assays which indicate potential HULIS character are evaporated and tested for functional groups using attenuated total reflectance Fourier

transform infrared spectroscopy (ATR-FTIR) on a ThermoScientific iS5, analyzed from 700 to 4000 cm^{-1}. The diamond crystal was cleaned and prepared for analysis using a swab of isopropanol and background set after drying. Obtained residues were applied directly to the crystal and firm contact was attained by a torque-controlled plunger.

ESI/APCI-MS analysis was performed using an Agilent 1260 LC-MS system fitted with a coupler in the place of a column, allowing for direct injection into the detector. Sample injections of 10μL are carried through the system at a rate of 0.2 mL/min using 100% methanol.Tracking the sample analyte is done by single wavelength UVvis absorption set at 250nm, allowing for proper analysis of the MS spectra. Ionization and detection of analyte masses are attained by setting the MS to simultaneously capture existing ions in electrospray mode and induced ions in atmospheric pressure chemical ionization mode set for fragmentation at 150V. Positive and negative ion modes are run together with scanning mass values of 60-1000 m/z to capture several possible ionizations due to the multifunctional nature of the HULIS.

4.4 Results

4.4.1 HULIS characteristics

Figure 4.2 shows the analytical profiles of SRFA, which is herein used as the standard reference activity for HULIS character. Frame A shows the HPLC chromatogram, a significant early peak at 3.5 minutes is clearly evident. The remainder of the standard produced a broad Gaussian product peak ranging from 5 to 17 minutes.

Frame B has the UV-vis analysis, here a smooth curve is seen starting with high absorption at low wavelengths and lower absorptions at higher wavelengths.

The FTIR spectra in frame C demonstrates the 3 main function peaks expected for HULIS material: a broad peak at 3300 cm^{-1}, sharp peak at 1700 cm^{-1}, and a pronounced broad peak between 1300-1100 cm^{-1}. Finally the MS spectra demonstrates a large number of peaks showing mass:charge (m/z) 150 and smaller, the mass peaks generally evens out from 150 to 1000 m/z. This mass distribution represents the bulk profile of SRFA from a direct injection into the mass analyzer.

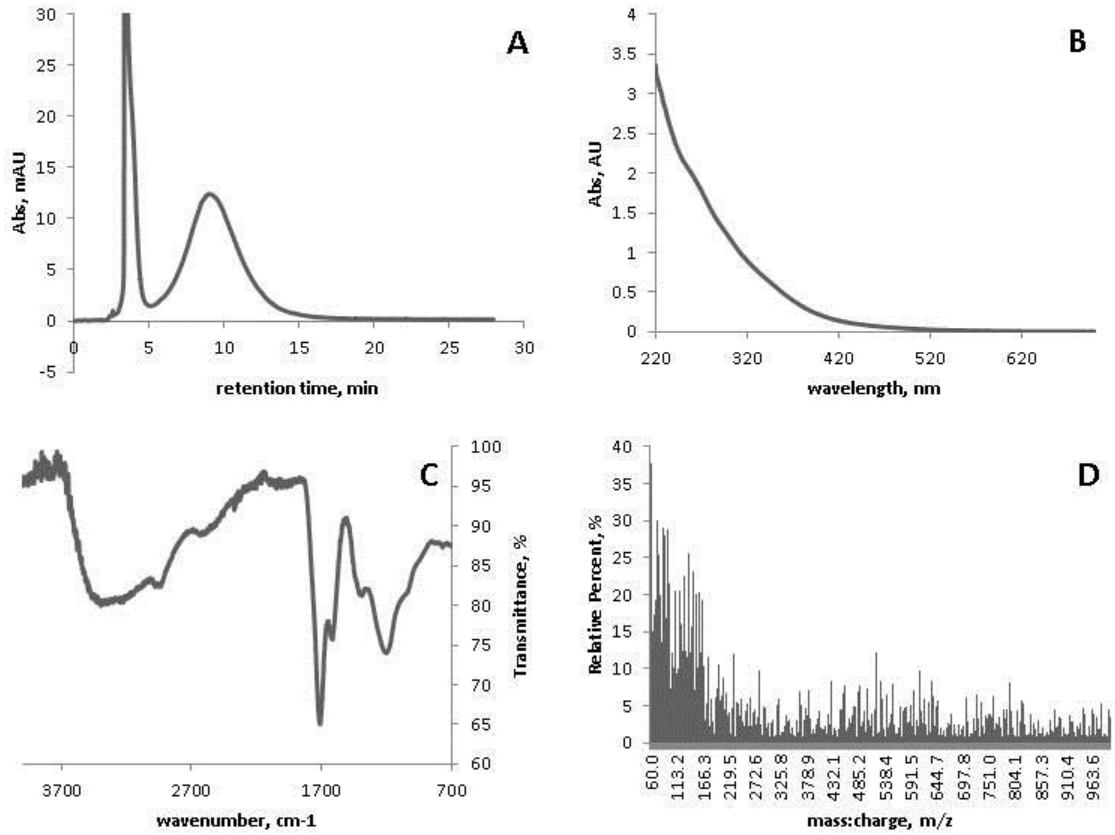

Figure 4. 2: Analytical data of SRFA.
(A) HPLC chromatogram, (B) UVvis spectra, (C) ATR-FTIR spectra, (D) ESI/APCI-MS spectra

4.4.2 HPLC product profiles

Figure 4.3 shows the HPLC profile of products of reactions from the potential intermediate structures identified from NAP and ANT reactions. Frames A and B show the chromatograms for post-reaction samples for benzoic and phthalic acid, respectively. These simple aromatic acids are shown to produce very few new products in the light. Similarly, anthracene-diol and anthraquinone in frames E and F show a product profile from the light to be essentially unchanged from the dark side of the reaction.

By contrast frames C and D show that photo-reactions of napthol and naphthoquinone, respectively, have produced a large number of robust products. the major production of naphthol reactions look to start eluting at 11 minutes and continuing a raised baseline until 28 minutes. Naphthoquinone photoreaction shows production of several products eluting from about 5 minutes until 20 minutes.

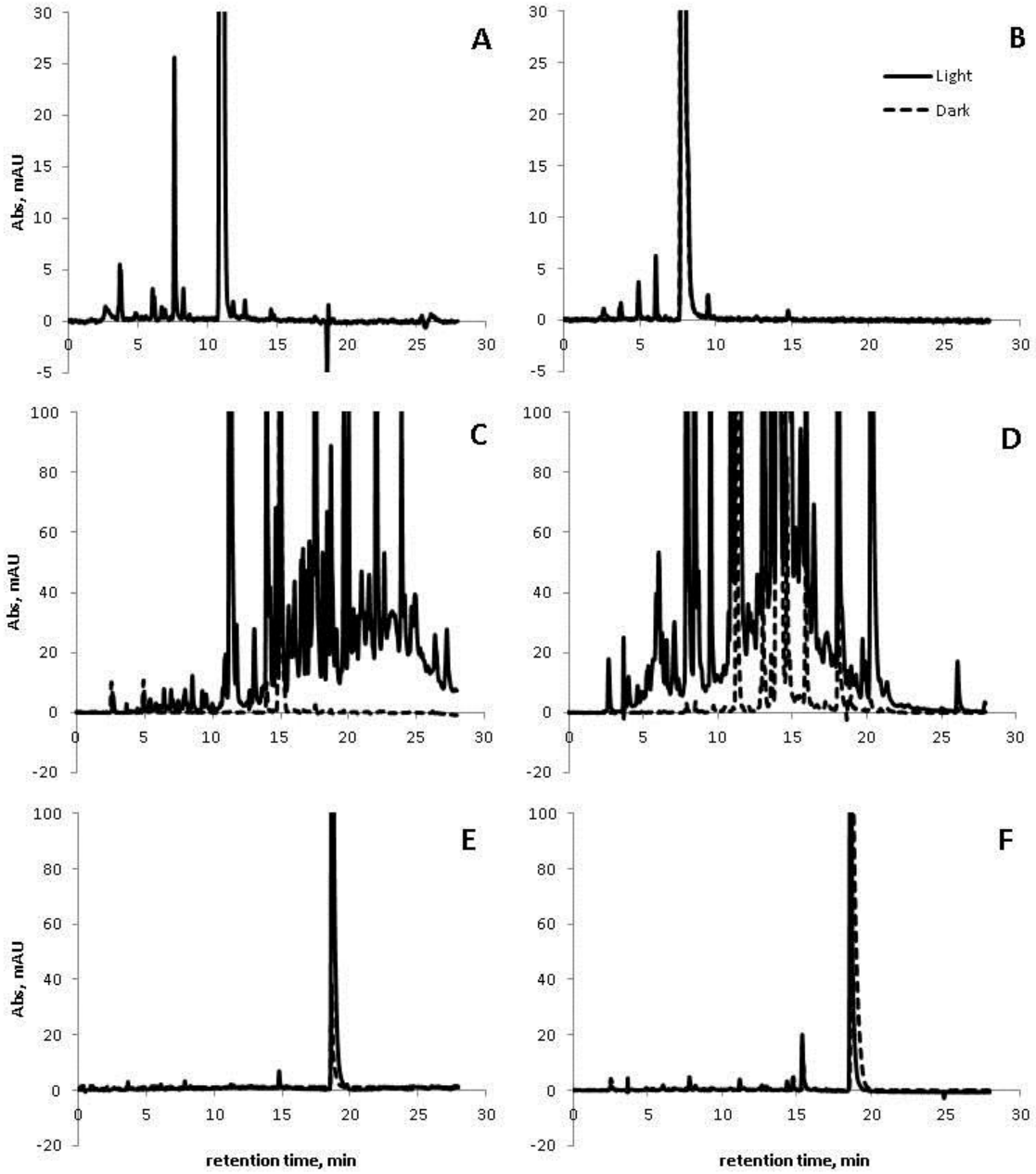

Figure 4. 3: HPLC chromatograms of post-reaction samples of oxidized reageants. Solid lines represent samples in the light, dashed lines represent samples in the dark, (A) benzoic acid, (B) phthalic acid, (C) 1-naphthol, (D) 1,4-naphthoquinone, (E) 9,10-anthracene-diol, (F) 9,10-anthraquinone.

4.4.3 UVvis character

Figure 4.4 shows the absorption character of saturated aqueous suspensions of oxPAH after photoreactions. The occurence of spectral change across these assays follow very closely with the reagents observed to create peaks in the previous HPLC data. Fig. 4.4A and B show the spectra for post-reaction samples for benzoic and phthalic acid, respectively. The only change observed between light and dark samples of these simple aromatic acids were a more enhanced absorption near 260nm in the light sample versus the dark. Interestingly, anthracene-diol and anthraquinone in frames E and F not only show profiles from the light to be essentially unchanged from the dark, but there exists nearly no absorption in this region of light at all.

By contrast Fig. 4.4C and D show that photo-reactions of napthol and naphthoquinone, respectively, have produced a significantly greater absorbance profile. These spectra in the dark already contain robust absorption peaks; the naphthol assay, Fig. 4.4C, has perfectly reproduced the UV-vis gradient seen with the SRFA standard in Fig. 4.2B. The naphthoquinone, Fig. 4.4D, has a strong baseline that fits with the SRFA gradient, however there also includes a pronounced shoulder on this spectra curve.

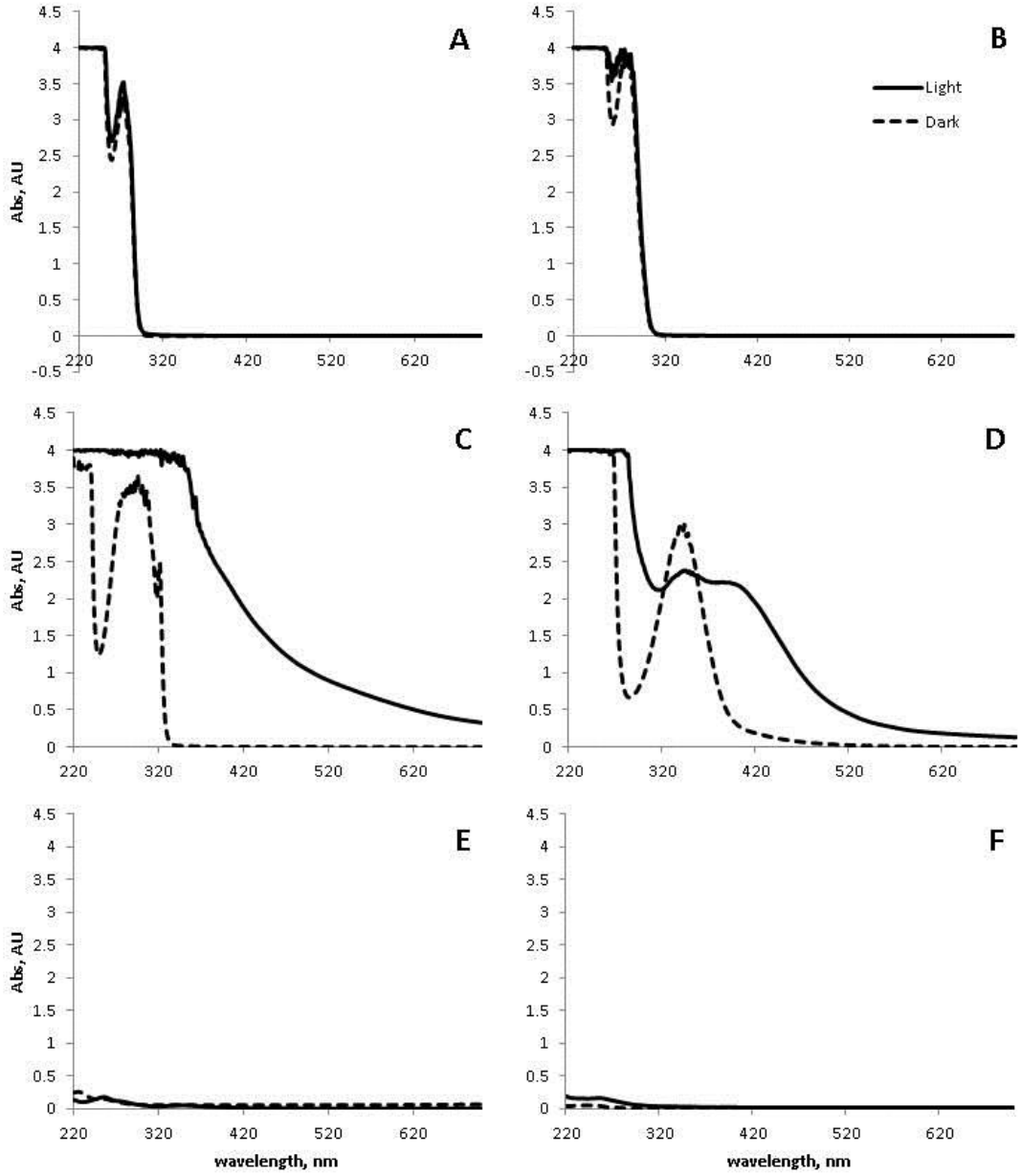

Figure 4. 4: UVvis spectra of post-reaction samples of oxidized reageants.
Solid lines represent samples in the light, dashed lines represent samples in the dark, (A) benzoic acid, (B) phthalic acid, (C) 1-naphthol, (D) 1,4-naphthoquinone, (E) 9,10-anthracene-diol, (F) 9,10-anthraquinone. All spectra are displayed in the 500 ppm concentration in which each assay was produced.

4.4.4 IR spectra

Figure 4.5 shows bulk functionality on potentially HULIS-active systems. Since only active samples under light produced any character related to HULIS, this analysis is focused on structurally characterizing those products. Naphthol and naphthoquinone, frames A and B, display the 3 main pillars of HULIS bulk functionality as demonstrated by SRFA. These peaks of interest are the broad peak at 3300 cm^{-1}, sharp peak at 1700 cm^{-1}, and a pronounced broad peak between 1300-1100 cm^{-1}.

The inclusion of anthracene derivatives in frames C and D, despite the low activity detected in HPLC, is based on the UVvis is inconclusive. Like the above naphthalene derivatives these spectra are virtually identical to each other, except that these show very little structure. The FTIR of these samples show spectra very similar to a parent-chain anthracene with regular sharp peaks from 1200 and lower cm^{-1}, yet with the inclusion of a sharp peak at 1700 cm^{-1}.

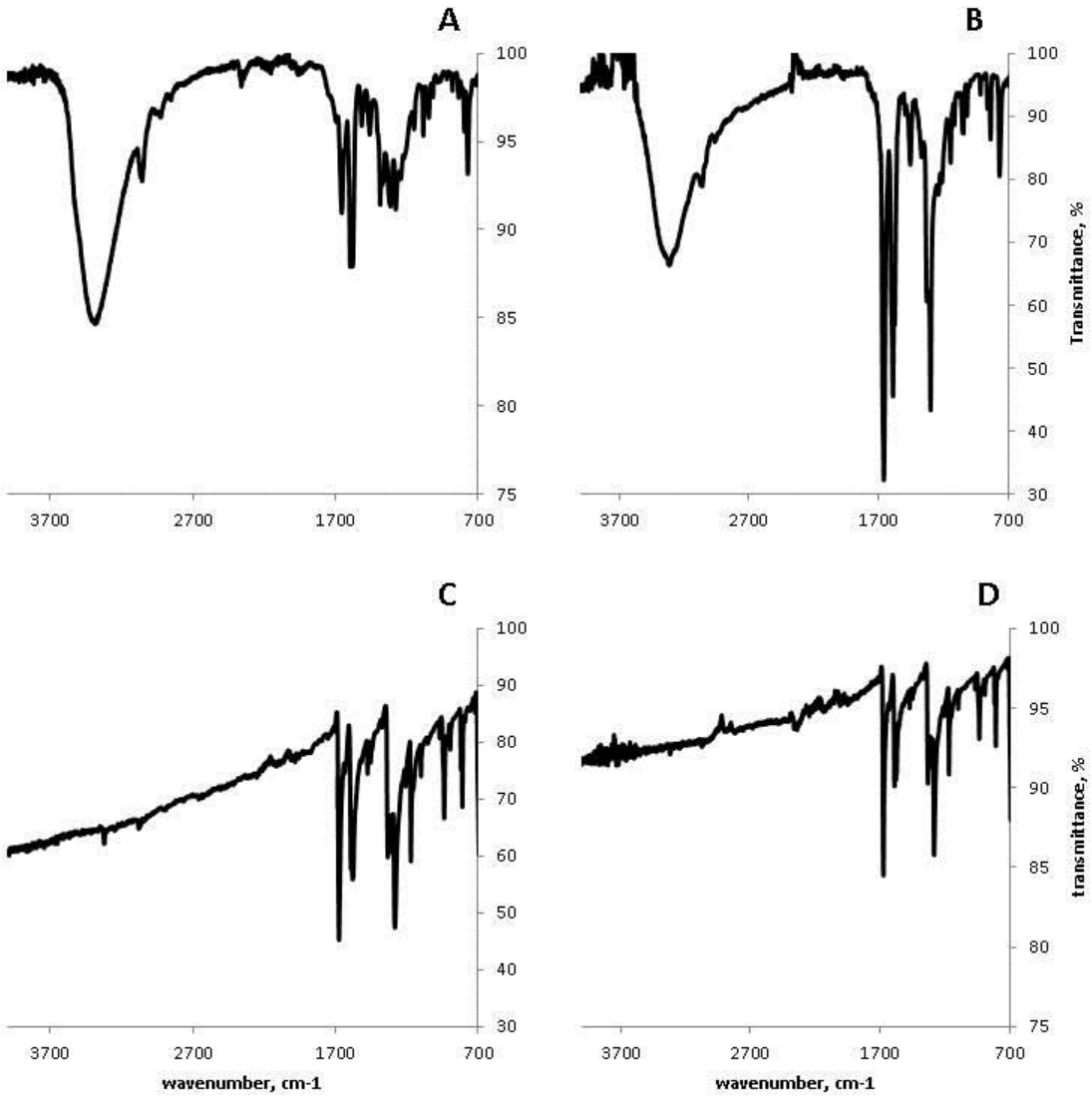

Figure 4. 5: ATR-FTIR of post-reaction products of oxPAH reactions in the light. (A) 1-naphthol, (B) 1,4-naphthoquinone, (C) 9,10-anthracene-diol, (D) 9,10-anthraquinone.

4.4.5 Mass Spec profiles

Figure 4.6 shows the mass range of saturated aqueous suspensions of PAH and oxPAH reactions. Again, the focus here is on characterizing PAH-based HULIS products. Frames A and B represent oxidized naphthalene and anthracene products; While the peaks are more pronounced in the naphthalene masses than the anthracene, their range and overall spread of masses look to be very similar.

The differences between the naphthol, frame A, and naphthoquinone, frame B, are few but pronounced. They both have a similar baseline spread of products across the range of masses, however the naphthol has shown interesting bumps in peaks at the 115 and 301 m/z values.

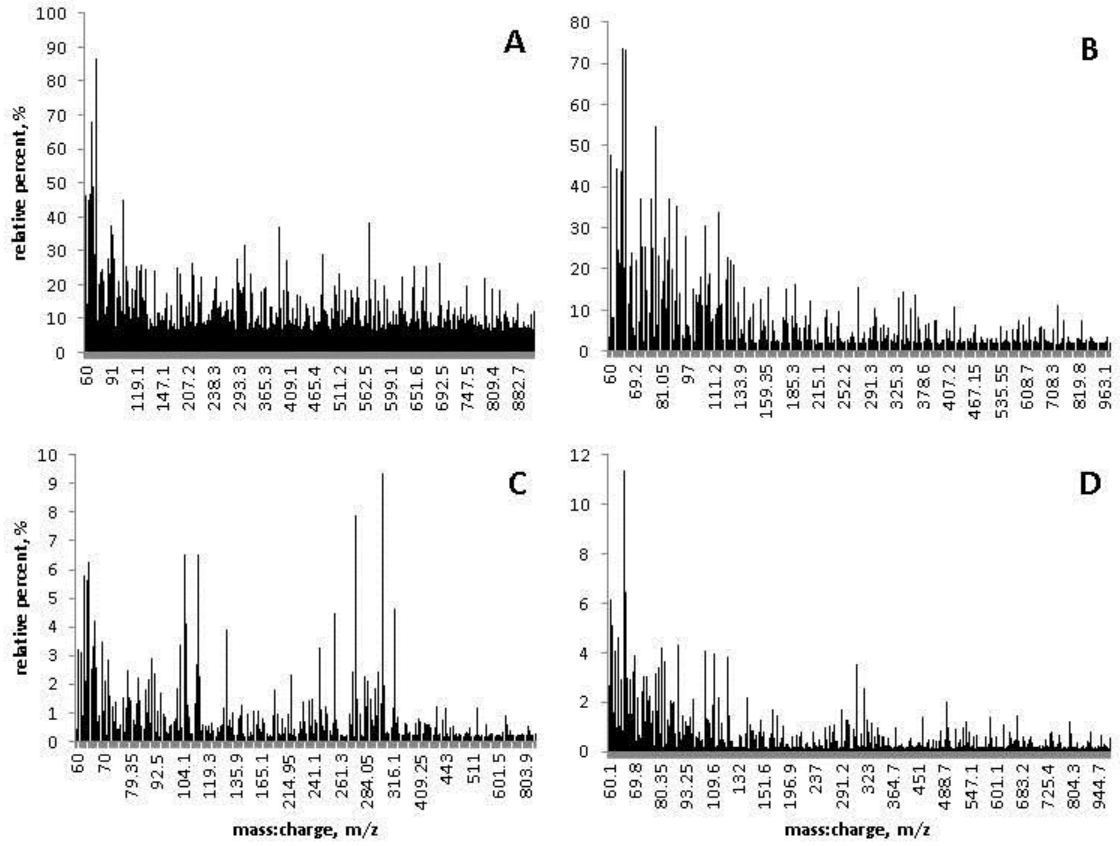

Figure 4. 6: ESI/APCI-MS spectra of HULIS-active reactions in the light.
(A) naphthalene, (B) anthracene, (C) 1-naphthol, (D) 1,4-naphthoquinone.

4.5 Discussion

4.5.1 Validity of analyses and SRFA evaluation

This study was able to confirm not only that HULIS is formed from simple PAH in a variety of environments, but some major details of the mechanistic pathways were demonstrated as well. The overall confirmations of HULIS character in active reactions are based on similarity to a common SRM in bench studies, mainly SRFA. Despite the fact that SRFA is widely used and therefore its analytical data is well characterized, it would only be helpful to showcase our found data using the same instrumentation and techniques as for the samples.

The HPLC analyses used standard reversed-phase silica beads coated with a C18 stationary phase for retention. The combination of a monodisperse 8 nm pore size with a polar-nonpolar mobile phase gradient results in a process that may separate compounds based on their individual degrees of oxidation. Wherein products will flow into crevices and channels throughout the beads and will experience either more or less retention based on their interactions with the coated bead surfaces. Higher oxidation will significantly decrease the final retention times by reducing the interactions with the nonpolar C18 coating.

SRFA, being a type of humic acid, is expected to encompass a wide range of structures, this also encompassing a wide range of sizes and amounts of oxidation. The observed chromatogram for this HULIS character demonstrates these attributes with a broad retention peak at three minutes representing large oxidized structures and a significant rise in baseline from 5 to 20 minutes. This would represent a large gaussian

distribution of products with varying oxidations and sizes including very small up to 8 nm in hydrodynamic diameter.

The typically expected absorption pattern for HULIS is a featureless decay including high absorption in the UV and lower absorption throughout the visible spectrum. This results in the translucent yellow-brown coloration seen in aqueous solutions. This is seen as an aspect of the presence of large numbers of products with varying absorption properties. This is also what defines atmospheric HULIS as a major factor in brown carbon and smog conditions.

The UVvis spectra for SRFA clearly demonstrates this expected pattern. This fits very well with the observed products in the HPLC profile. At its core humic material including HULIS is aromatic hydrocarbon in nature, however it is the makeup of the oxidized groups that gives these compounds their functionality. Their increased size allows for absorption at higher wavelengths and is due to the formation of branches and ether bridges, including esters. Their complexation role in metal solubilization and nutrient mobility is due to the presence of available carbonyl and hydroxyl groups.

These groups are observed in the FTIR spectra of SRFA, creating a validation for comparison with the produced samples in this study. Specifically, the focus is on the large peak dip at 3300 cm^{-1} signifying hydroxyl groups, the pronounced peak at 1700 cm^{-1} demonstrating carbonyl function, and the dip in the overall baseline ranging from 1300-1100cm^{-1}, which is characteristic of carbon-oxygen bonds forming ether groups.

From the HPLC spread of compounds to the absorption pattern within the UVvis spectrum, the masses of these structures will also be a wide range. Known HULIS masses

are found from 250-450 m/z, however it could be easily imagined that the actual mass spread of HULIS is dependent on the region and pace of formation.

The soft ionizations of electrospray (ESI) and atmospheric pressure chemical ionization mass spectroscopy (APCI-MS) make ideal conditions to observe the complete masses of these bulk structures. Running both ionization methods allows for the capture of highly acidic deprotonated groups, via ESI, and to add a protonation charge via APCI. To maximize the detection of all compounds, both ESI and APCI are used for mass analysis.

In this project using a fragmentation voltage of 150V, SRFA solutions have given a percent relative mass spread starting with many large mass peaks near 150 and dwelling into smaller but regular peaks into the range of 600 and higher mass-per-charge.

While it is unlikely that the PAH assays in this project will give the same mass profile, this can still be treated as a representative product range that can be acceptable.

4.5.2 Identification of intermediates

For this project we have defined some intermediate pathways for PAH transformation as discovered products displaying the ability to create HULIS on their own. This ability has been successfully observed for naphthol (Nap-ol) and naphthoquinone (Nap-one).

Oxidized naphthalene and anthracene clearly demonstrate HULIS character compared to SRFA data. Their many HPLC peaks appear at retention times consistent with SRFA chromatograms and UVvis absorptions have the same featureless pattern and mass spec patterns are comparable. The main differences are in the retention peaks of

HPLC and FTIR of oxidized ANT, where the ANT reactions display products on HPLC at extended retention times and its FTIR spectrum does not show a hydroxide group. This fits with field samples of atmospheric ANT correlations of many aromatics with quinone character.

Several products of NAP and ANT reactions were determined using retention times of suspected compounds, including naphthol in the naphthalene assays, naphthoquininone and a peak that matched both anthraquinone and anthracene-diol in the anthracene assays. Peaks matching benzoic and phthalic acid appeared in the assays of both PAH. These oxidation products became the reagents tested in the solar reactor to determine potential mechanism pathways.

Of the discovered products, only naphthol and naphthoquininone demonstrated HULIS-active character when subjected to sunlight. Therefore we would define these as intermediate structures in pathways of the overall mechanism.

The analyses of the resulting naphthol reaction are a nearly perfect comparison to the SRFA standard. The characteristics of UVvis absorption, FTIR evidence of functional groups, and very similar mass spread with MS. The HPLC chromatogram for this assay had an interesting difference from SRFA in that the familiar distribution of products are retained an additional five minutes, i.e. 11 to 25 minutes. This may relate to different sizes of overall structures except that the MS did not show a significant difference. So this may be due to a difference in association with water molecules creating varying ranges of hydrodynamic diameters.

The analyses of the resulting naphthoquininone reaction are favorably compared to the SRFA standard. The characteristics of HPLC retention, FTIR evidence of functional groups, and very similar mass spread with MS. The UVvis spectra for this assay had an interesting difference from SRFA in that the recognizable absorption decay for HULIS can be clearly seen in the baseline, however there now exists a should peak near the 400 nm point.

There are two intriguing takeaways from this feature within the otherwise HULIS-specific pattern. The first is that this shoulder represents a relatively high concentration of similar products with a particular difference in their structural character to the remaining products; while this doesn't seem to remove the overall HULIS character of the bulk system it would be interesting to see how this effect would alter the excitation/emission character in a fluorimeter response. The second detail to note is that this absorption bump occurs in the same region as the similar UVvis peaks observed in the SPE elution profile for anthracene in the previous study. This correlation would actually fit well considering that anthracenes in the environment are traditionally connected with higher rates of quinone products.

Given that both naphthalene derivatives have individually demonstrated HULIS production activity they must be considered as potential reaction pathways. The differences between their respective products would relate to their own reaction mechanisms. Qualitatively, the change in colorization for the naphthoquininone assays were observed to be much more rapid than the naphthol assays.

4.5.3 Identification of end products

This project has successfully identified various products which do not inherently show the ability to oxidize or grow further than their own structures or derivatives. The demonstrated lack of HULIS formation from the diol and quinone derivatives of anthracene and the benzoic and phthalic acid assays leads us to conclude that these are end products.

With extended conjugated pi systems, the oxidized anthracene derivatives were expected to have some of the more robust reactivity. However, this was not observed and these structures proved to be nearly completely unreactive. Both the anthracene diol and quinone assays displayed little to no reactions towards new products, and UVvis analysis proved inconsequential as there was no observed absorption for either assay across the entire region. Some further investigations into the HPLC fine structure of product peaks, seen in Fig. B1, have demonstrated very similar formation patterns suggesting that these compounds converge on one structure in this environment. FTIR analyses on these resulting residues, previously considered unnecessary and now seen in Fig. 4.5C and D, reveals a strong carbonyl peak at 1700 cm^{-1} as the only non-aromatic feature, suggesting that this single structure must be the quinone.

Photo-oxidation reactions of pure benzoic acid and phthalic acid demonstrate no production of products on HPLC and there was no change observed in the UVvis for these assays. At this point we could conclude that there were no HULIS materials to evaluate further.

This lack of reactivity can be explained when evaluating their structures against the suggested correlations of aromatic structure and overall stability stated by Clar (Clar and Schmidt 1975). Briefly, higher numbers of complete benzene rings observed in the Lewis structures of PAH will correlate to a higher stability. The 9,10 anthraquinone structure will afix two complete benzene structures thereby increasing its stability. The resilient nature of the benzoic and phthalic acids may be similarly explained by the high overall percent of complete aromaticity in their structures.

4.5.4 Characterization of reaction pathways

The HPLC method used in this project attained a high degree of retention and separation of product peaks in post-reaction samples. The chromatograms of naphthol (Nap-ol) and naphthoquinone (Nap-one) share features as the chromatograms seen in the previous study for NAP and ANT products. Each assay produced a distinct pattern of resolved peaks retained by our HPLC method; these peaks are observed against elevated baselines similar to the retention pattern seen from the SRFA analysis. These baselines are all presented over the course of several minutes and their respective retention times are here evaluated as signature character traits to each reagent.

Comparison of HPLC product character from Nap-ol and Nap-one to product characters produced from NAP and ANT reactions have suggested likely mechanism steps. HPLC analysis of NAP reactions show a naphthol as a major product, this is within a range of products with demonstrated retention times from 6 to 20 minutes. Despite the presence of Nap-ol in the collection of products, comparison of overall product profiles

between NAP and oxidized NAP reactions demonstrate that NAP based HULIS produces material with retention ranges closer to naphthoquininone character.

Previous HPLC analysis of ANT reactions showed anthraquinone and naphthoquininone as major products. Since a separate assay of anthraquinone demonstrated its role as an end product, our focus here will be on the naphthalene derivatives as potential intermediate structures.

ANT reactions contain products that exhibit a range of compounds with demonstrated retention times from 6 to 25 minutes. Comparison of overall product profiles between ANT and oxidized NAP reactions demonstrate that ANT based HULIS produces material with extended retention time ranges that include both naphthol and naphthoquininone character. Similar to NAP reactions, products of ANT start at retention times of six minutes but extend past the times where naphthoquininone products end. The overall range for ANT products is shown to extend into the region that includes the naphthol range of products as well, despite naphthol not being seen as a significant product. HULIS pathways for both NAP and ANT must involve both oxNAP structures, with separate kinetics for each step.

4.5.5 Suggested preliminary mechanism steps

While there are likely several reaction pathways in these reactions, the data presented in this project offer some strong evidence for some major pathways. Figure 4.7 displays our proposed preliminary mechanistic pathways of HULIS production from PAH, specifically from NAP and ANT. The shared presence of produced HULIS with Nap-one character in both NAP and ANT assays strongly suggests that the conversion of

Nap-one into HULIS is likely a faster favored reaction pathway. Conversely, the lack of HULIS similar to Nap-ol reactions in NAP assays indicates that the conversion of Nap-ol into HULIS must be a slower process than Nap-one. In Fig. 4.7A, NAP reactions are indicated as producing Nap-ol at a faster rate than they produce Nap-one. This is based on residual Nap-ol found in NAP products, which overall demonstrate HULIS with Nap-one character. The ANT proposed pathways, shown in Fig. 4.7B, are depicted with a nearly opposite trend. We propose that ANT is likely to produce Nap-one at a very rapid pace along with its HULIS products, given our previous estimation that the quinone is converted to HULIS relatively quickly. The observation that ANT also produces

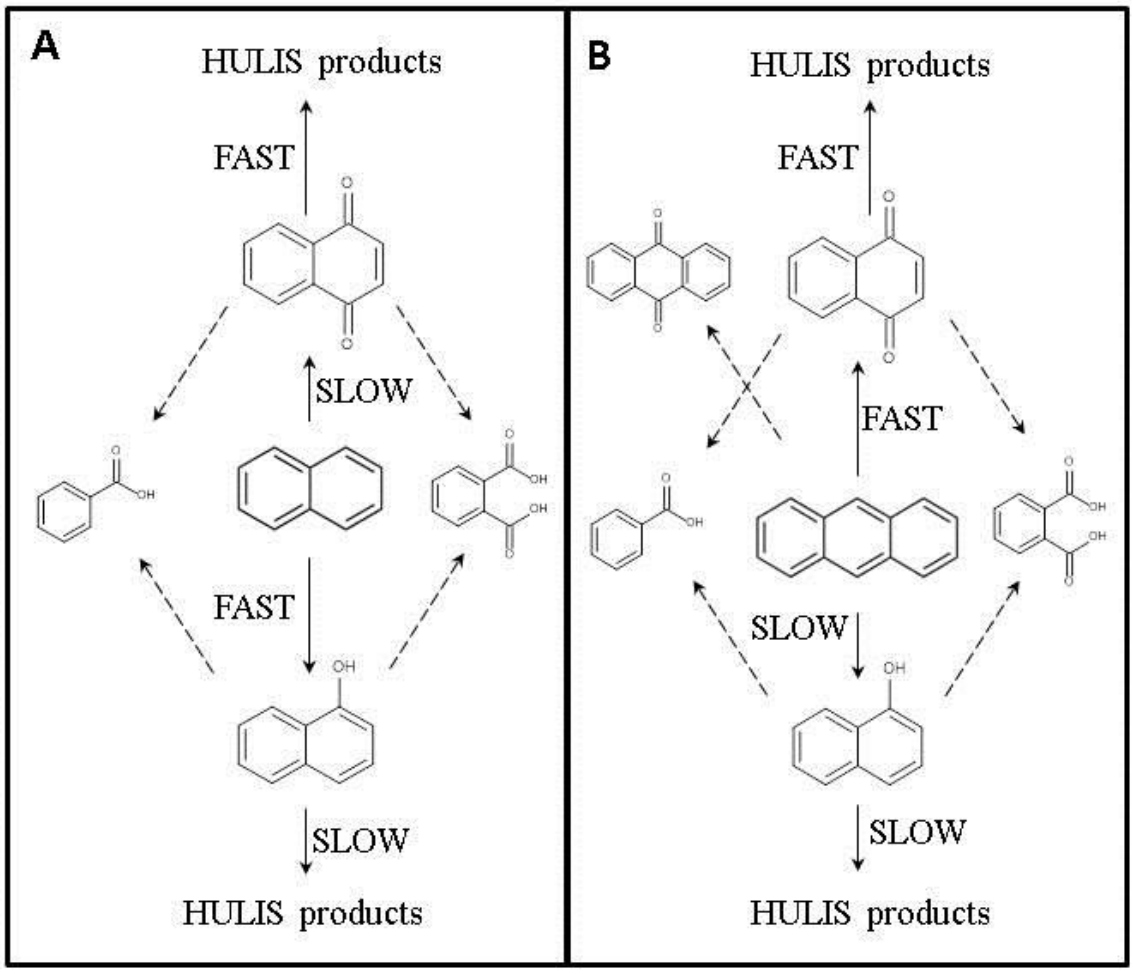

Figure 4. 7: Preliminary suggested reaction pathways.
Suggested production of HULIS from (A) naphthalene and (B) anthracene. Solid arrows represent proposed reactions involving HULIS intermediates, dashed arrows represent formation of end products. FAST and SLOW designations are based on the prominence of those compounds in the post-reaction sample.

compounds that are retained similar to Nap-ol products further suggests that Nap-ol is being produced as well, albeit at a slower rate relative to Nap-one.

Since every assay with a HULIS response have been observed to only produce this in illuminated samples, the specific impact of sunlight cannot be overstated. The excitation of dissolved oxygen or water molecules by UV radiation, thereby producing varying ROS, would be a likely component to these reactions. Here, we can suggest some reaction scenarios that may arise with produced OH and superoxide radicals. Reactions of OH typically involve the homolytic capture of acidic hydrogens to form water and a carbon centered radical. This leaves the hydrocarbon susceptible to attack and will result in a hydroxide group at the site of the attack. NAP reaction likely uses OH to produce significant Nap-ol, but may use superoxide ($\dot{O}_2^-$) to produce Nap-one which it further uses as the favored formation of HULIS. The initial Nap-ol formation must be rapid compared to the Nap-one, and Nap-one's HULIS pathway must be rapid compared to Nap-ol. ANT reaction likely uses $\dot{O}_2^-$ to produce significant Nap-one and OH to a lesser degree for Nap-ol without a specific favored pathway for HULIS. ANT's initial Nap-one formation must be rapid compared to the Nap-ol. Keeping the idea of Nap-one's HULIS pathway being rapid compared to Nap-ol fits well with ANT's overall HULIS profile.

Since both phthalic acid and anhydride are present in both NAP and ANT reactions we might conclude that they would be borne out of similar intermediate structures. Naphthol and naphthoquininone would likely have different initiation mechanisms with similar reagents. Therefore one proposed pathway could involve superoxide attack on naphthoquininone to produce the phthalic anhydride, while a

superoxide attack on naphthol, followed by OH, may lead to the phthalic acid structure. The phthalic acid and anhydride themselves may exist in equilibrium with each other as the acid may auto-condense to produce the anhydride in aqueous conditions. Each of these can be seen to go through a decarboxylation process to produce the benzoic acid.

oxANT is significantly present in only ANT reactions, therefore likely produces directly from ANT via ROS as end products. Behavior suggests that ANTdiol is quickly oxidized to ANTone. This would fit with expected Clar's rules for stability.

4.6 Conclusions

This study has successfully established some preliminary mechanism pathways into the formation of HULIS in simulated sunlight using oxidized PAH products found in a previous study. HULIS produced from the auto-oxidation of simple PAH appear to follow a mechanism using hydroxylated and quinone derivatives of naphthalene species as intermediate structures. Specifically, naphthalene appears to primarily follow a pathway using naphthoquinone as the intermediate state in HULIS formation, while anthracene reactions appear to follow multiple paths using both naphthoquinone and naphthol as intermediates for its HULIS production.

Without the influx of strong oxidizers single aromatic oxidized species, such as benzoic and phthalic acids, are seen to be end products rather than HULIS producing structures as found in other studies. Oxidized derivatives of anthracene are similarly observed to serve as overall reaction end products and may therefore serve as product standards to evaluate the kinetics of these humification reactions. These results will

greatly help in building a foundation toward studying and determining the overall mechanism of HULIS in finer detail.

CHAPTER FIVE: SUMMARY AND FUTURE WORK

This project has demonstrated some important and significant interactions that occur between persistent aromatic compounds with available metals in the environment. While these interactions have several potential outcomes, the information gathered over the course of this study suggests that the major pathways towards these interactions follow through radical generation and mediation.

Data gathered and observed in this bench study provides a glimpse into a likely chronology of events surrounding atmospheric particles both emitted by combustion processes and down-wind atmospheric dust particles. Aqueous suspensions of PAH are observed to oxidize and form HULIS material in simulated atmospheric conditions. This oxidation process is displayed with structures of PAH which are predicted to be more reactive in redox conditions and illumination of simulated sunlight. These observed HULIS formations can be considered auto-oxidation reactions since they occurred without the presence of catalysts or oxidizers. HULIS formations are observed with PAH which had previously demonstrated an effect on soluble iron. Soil-bound iron is shown to increase in solubility in the presence of short chain linear PAH expected to be redox active. This solubilization is not seen as being dependent on acidity or dissolved PAH, suggesting a surface-mediated reaction. The data herein strongly suggest that the atmospheric processing of wind-blown dust by PAH-bound particles is likely due to newly formed HULIS complexing with iron to bring it into a soluble state.

Wind-swept metals in the form of soil and dust are observed to be effective fertilizing agents for distant land and water regions. However we have determined that the solubility of these metals can be highly affected by combustion emissions even and possibly especially, in regions far removed from their sources. Bulk water samples containing suspensions of a standard soil and various individual organic reagents are subjected to a simulated sunlight source in an effort to mimic the photochemical environment of cloud water systems. These assays demonstrated a substantial increase of iron solubility in the presence of short-chain linear PAH, including naphthalene and anthracene. Conversely, this project also illustrated Clar's rules of stability by displaying the inactivity of non-linear PAH, with higher benzene-specific structural centers, with the lack of production of soluble iron. While the focus of this study was iron, there was an inherent suggestion of probable mechanism pathways, including surface-dependent catalysis based on strong differences in soluble iron among progressively soluble PAH reagents tested, and mechanisms of iron solubility involving complexations via carboxylic acids as a primary pathway versus the typical ferric reduction to the more soluble ferrous iron.

To further understand the structural basis of these reactions, continuing these assays with PAH of lower solubility but extended linearity, such as tetracene, and higher solubility but higher Clar's stabilities, such as fluorine, will greatly help complete this question. Additionally, there exists a need to elucidate the species of produced soluble iron to differentiate between free ferrous ions or ferric iron complexes by developing a method using a ferrous-specific ferrozine complex to analyze by ultra-sensitive long-

range UVvis. Finally, expanding on the reaction testing by sampling at set times during the reaction will help to determine the actual kinetics of iron solubility will be of immense interest to groups looking to hone their soluble iron models.

While current evaluations of air quality typically focus on aerosol and inorganic content, our project has brought attention to the often overlooked impact of anthropogenic aromatics in the atmosphere. There is a rather surprising and potentially concerning ability for primary PAH emissions to initiate their own secondary structure formation without the need for added anthropogenic oxidizing agents, such as NOx and sulfuric oxides. This study focused on simple PAH reagents and the evaluation of their potential photo-catalyzed transformation into a new category of humic material categorized Humic-Like Substances, or HULIS. The driver of this project was the organic analysis of PAH material resulting from the previous study into iron solubility. Sample analysis on HPLC showed that the PAH responsible for higher iron solubility were also forming a wide array of new organic products, while the iron inactive organics did not create any new products. To further determine the humic nature of these products, analysis on UV-vis demonstrated a HULIS-specific translucent brown carbon absorption curve, ATR-FTIR analysis on solid residues displayed the presence of groups highly associated with humic character, ie combination of hydroxide, carbonyl, and ether groups.

To further the impact of this phase of the project, developing methods of evaluating the exact structures being created would help sell this process and apply a set predictability to atmospheric models looking to analyze hazards of anthropogenic

emissions. This could involve one or a combination of mass spectra, LCMS to help find total parent masses, GCMS on extractions for harder ionizations to elucidate structural features which would be aided by NMR analyses also, if large and high purity solid crystals can be collected, then X-ray crystallography could complete these overall structures.

The tendency for these PAH to initiate their own oxidations in sunlight is observed to have a significant effect on their structures and will create a complex dynamic series of reactions leading to more toxic oxidized structures with several functionalities that are still not entirely understood. In this continuation of the previous study into general HULIS formation, the new focus became an attempt to enter into introductory mechanism steps in these auto-oxidation reactions. After a handful of remaining products were identified in the original reaction samples that produced HULIS materials a series of photoreactions were conducted using these products as starting materials. Of these assays any which further produced material with HULIS character are considered to be intermediate structures. Conversely, reaction assays found to be inactive toward further oxidation is then considered as an endpoint. To this, the naphthalene derivatives naphthol and naphthoquinone are concluded to be intermediate steps, likely generated via oxidation by ROS, including OH and superoxide radical, respectively, used by both naphthalene and anthracene in their production of HULIS. Additionally, anthraquinone and benzene-centered carboxylic acids, ie phthalic and benzoic acid, are seen as end products. The HULIS character in this study was completed by comparing analytical data of these assays to the closest available standard reference material to

HULIS, Suwannee River Fulvic Acid. There is further interest in the interplay of these products with their system environment. To that end, further studies into how different acidic and buffer systems affect this production will be very helpful to air quality evaluations. Overall results of interactions with soils involving soluble iron have already been established in this study, however the nature of these associations can be further understood by retention patterns on solid phase extraction columns designed for multifunctional analytes. This would couple quite well with the aforementioned ferrous ion analysis involving ferrozine reagents.

It is my hope that this information can be useful in the formation and evolution of emissions regulations and quality standard models for air in areas affected by combustion and other anthropogenic pollution sources. Further understanding of these reactions may provide significant advancements in processes governing clean energy generation, predicitive modelling of global soluble iron and light absorbing compounds, establishing source apportionment data for humic substances, and possibly planetary humification processes that would initiate primary sources of life.

REFERENCES

Aiken, A. C., P. F. Decarlo, J. H. Kroll, D. R. Worsnop, J. A. Huffman, K. S. Docherty, I. M. Ulbrich, C. Mohr, J. R. Kimmel, D. Sueper, Y. Sun, Q. Zhang, A. Trimborn, M. Northway, P. J. Ziemann, M. R. Canagaratna, T. B. Onasch, M. R. Alfarra, A. S. H. Prevot, J. Dommen, J. Duplissy, A. Metzger, U. Baltensperger and J. L. Jimenez (2008). O/C and OM/OC ratios of primary, secondary, and ambient organic aerosols with high-resolution time-of-flight aerosol mass spectrometry. *Environmental Science & Technology* **42**(12): 4478-4485.

Akhtar, U. S., R. D. McWhinney, N. Rastogi, J. P. D. Abbatt, G. J. Evans and J. A. Scott (2010). Cytotoxic and proinflammatory effects of ambient and source-related particulate matter (PM) in relation to the production of reactive oxygen species (ROS) and cytokine adsorption by particles. *Inhalation Toxicology* **22**: 37-47.

Allen, J. O., K. M. Dookeran, K. A. Smith, A. F. Sarofim, K. Taghizadeh and A. L. Lafleur (1996). Measurement of polycyclic aromatic hydrocarbons associated with size-segregated atmospheric aerosols in Massachusetts. *Environmental Science & Technology* **30**(3): 1023-1031.

Altieri, K. E., S. P. Seitzinger, A. G. Carlton, B. J. Turpin, G. C. Klein and A. G. Marshall (2008). Oligomers formed through in-cloud methylglyoxal reactions: Chemical composition, properties, and mechanisms investigated by ultra-high resolution FT-ICR mass spectrometry. *Atmospheric Environment* **42**(7): 1476-1490.

Andreae, M. O. and A. Gelencser (2006). Black carbon or brown carbon? The nature of light-absorbing carbonaceous aerosols. *Atmospheric Chemistry and Physics* **6**: 3131-3148.

Anipsitakis, G. P. and D. D. Dionysiou (2004). Radical generation by the interaction of transition metals with common oxidants. *Environmental Science & Technology* **38**(13): 3705-3712.

Arangio, A. M., H. J. Tong, J. Socorro, U. Poschl and M. Shiraiwa (2016). Quantification of environmentally persistent free radicals and reactive oxygen species in atmospheric aerosol particles. *Atmospheric Chemistry and Physics* **16**(20): 13105-13119.

Baba, Y., T. Yatagai, T. Harada and Y. Kawase (2015). Hydroxyl radical generation in the photo-Fenton process: Effects of carboxylic acids on iron redox cycling. *Chemical Engineering Journal* **277**: 229-241.

Babu, T. S., J. B. Marder, S. Tripuranthakam, D. G. Dixon and B. M. Greenberg (2001). Synergistic effects of a photooxidized polycyclic aromatic hydrocarbon and

copper on photosynthesis and plant growth: Evidence that in vivo formation of reactive oxygen species is a mechanism of copper toxicity. *Environmental Toxicology and Chemistry* **20**(6): 1351-1358.

Baek, S. O., R. A. Field, M. E. Goldstone, P. W. Kirk, J. N. Lester and R. Perry (1991). A review of atmospheric polycyclic aromatic-hydrocarbons - sources, fate and behavior. *Water Air and Soil Pollution* **60**(3-4): 279-300.

Baker, A. R., T. D. Jickells, M. Witt and K. L. Linge (2006). Trends in the solubility of iron, aluminium, manganese and phosphorus in aerosol collected over the Atlantic Ocean. *Marine Chemistry* **98**(1): 43-58.

Balachandran, S., J. E. Pachon, S. Lee, M. M. Oakes, N. Rastogi, W. Y. Shi, E. Tagaris, B. Yan, A. Davis, X. L. Zhang, R. J. Weber, J. A. Mulholland, M. H. Bergin, M. Zheng and A. G. Russell (2013). Particulate and gas sampling of prescribed fires in South Georgia, USA. *Atmospheric Environment* **81**: 125-135.

Bamforth, S. M. and I. Singleton (2005). Bioremediation of polycyclic aromatic hydrocarbons: current knowledge and future directions. *Journal of Chemical Technology and Biotechnology* **80**(7): 723-736.

Bandowe, B. A. M., H. Meusel, R. J. Huang, K. F. Ho, J. J. Cao, T. Hoffmann and W. Wilcke (2014). PM25-bound oxygenated PAHs, nitro-PAHs and parent-PAHs from the atmosphere of a Chinese megacity: Seasonal variation, sources and cancer risk assessment. *Science of the Total Environment* **473**: 77-87.

Barbas, J. T., M. E. Sigman, A. C. Buchanan and E. A. Chevis (1993). Photolysis of substitute naphthalenes on SiO2 and Al2O3. *Photochemistry and Photobiology* **58**(2): 155-158.

Barbeau, K., E. L. Rue, C. G. Trick, K. T. Bruland and A. Butler (2003). Photochemical reactivity of siderophores produced by marine heterotrophic bacteria and cyanobacteria based on characteristic Fe(III) binding groups. *Limnology and Oceanography* **48**(3): 1069-1078.

Belous, A., O. V'Yunov, M. Glinchuk, V. Laguta and D. Makovez (2008). Redox processes at grain boundaries in barium titanate-based polycrystalline ferroelectrics semiconductors. *Journal of Materials Science* **43**(9): 3320-3326.

Biermann, H. W., H. Macleod, R. Atkinson, A. M. Winer and J. N. Pitts (1985). Kinetics of the gas-phase reactions of the hydroxyl radical with naphthalene, phenanthrene, and anthracene. *Environmental Science & Technology* **19**(3): 244-248.

Boyd, P. W., A. J. Watson, C. S. Law, E. R. Abraham, T. Trull, R. Murdoch, D. C. E. Bakker, A. R. Bowie, K. O. Buesseler, H. Chang, M. Charette, P. Croot, K. Downing, R. Frew, M. Gall, M. Hadfield, J. Hall, M. Harvey, G. Jameson, J.

LaRoche, M. Liddicoat, R. Ling, M. T. Maldonado, R. M. McKay, S. Nodder, S. Pickmere, R. Pridmore, S. Rintoul, K. Safi, P. Sutton, R. Strzepek, K. Tanneberger, S. Turner, A. Waite and J. Zeldis (2000). A mesoscale phytoplankton bloom in the polar Southern Ocean stimulated by iron fertilization. *Nature* **407**(6805): 695-702.

Boyle, E. A., B. A. Bergquist, R. A. Kayser and N. Mahowald (2005). Iron, manganese, and lead at Hawaii Ocean Time-series station ALOHA: Temporal variability and an intermediate water hydrothermal plume. *Geochimica Et Cosmochimica Acta* **69**(4): 933-952.

Bridge, T. A. M. and D. B. Johnson (1998). Reduction of soluble iron and reductive dissolution of ferric iron-containing minerals by moderately thermophilic iron-oxidizing bacteria. *Applied and Environmental Microbiology* **64**(6): 2181-2186.

Canellas, L. P., F. L. Olivares, N. O. Aguiar, D. L. Jones, A. Nebbioso, P. Mazzei and A. Piccolo (2015). Humic and fulvic acids as biostimulants in horticulture. *Scientia Horticulturae* **196**: 15-27.

Cartledge, B. T., A. R. Marcotte, P. Herckes, A. D. Anbar and B. J. Majestic (2015). The Impact of Particle Size, Relative Humidity, and Sulfur Dioxide on Iron Solubility in Simulated Atmospheric Marine Aerosols. *Environmental Science & Technology* **49**(12): 7179-7187.

Cerniglia, C. E., J. R. Althaus, F. E. Evans, J. P. Freeman, R. K. Mitchum and S. K. Yang (1983). Stereochemistry and evidence for an arene oxide-NIH shift pathway in the fungal metabolism of naphthalene. *Chemico-Biological Interactions* **44**(1-2): 119-132.

Chacon, N., W. L. Silver, E. A. Dubinsky and D. F. Cusack (2006). Iron reduction and soil phosphorus solubilization in humid tropical forests soils: The roles of labile carbon pools and an electron shuttle compound. *Biogeochemistry* **78**(1): 67-84.

Chang, J. L. and J. E. Thompson (2010). Characterization of colored products formed during irradiation of aqueous solutions containing H2O2 and phenolic compounds. *Atmospheric Environment* **44**(4): 541-551.

Chen, J., F. S. Ehrenhauser, K. T. Valsaraj and M. J. Wornat (2006). Uptake and UV-photooxidation of gas-phase PAHs on the surface of atmospheric water films. 1. Naphthalene. *Journal of Physical Chemistry A* **110**(29): 9161-9168.

Cho, A. K., C. Sioutas, A. H. Miguel, Y. Kumagai, D. A. Schmitz, M. Singh, A. Eiguren-Fernandez and J. R. Froines (2005). Redox activity of airborne particulate matter at different sites in the Los Angeles Basin. *Environmental Research* **99**(1): 40-47.

Chuang, P. Y., R. M. Duvall, M. M. Shafer and J. J. Schauer (2005). The origin of water soluble particulate iron in the Asian atmospheric outflow. *Geophysical Research Letters* **32**(7).

Clar, E. and W. Schmidt (1975). Correlations between photoelectron and ultraviolet-absorption spectra of polycyclic-hydrocarbons and number of aromatic sextets. *Tetrahedron* **31**(18): 2263-2271.

Collett, J. L., P. Herckes, S. Youngster and T. Lee (2008). Processing of atmospheric organic matter by California radiation fogs. *Atmospheric Research* **87**(3-4): 232-241.

Corcoran, J., M. J. Winter and C. R. Tyler (2010). Pharmaceuticals in the aquatic environment: A critical review of the evidence for health effects in fish. *Critical Reviews in Toxicology* **40**(4): 287-304.

Cwiertny, D. M., J. Baltrusaitis, G. J. Hunter, A. Laskin, M. M. Scherer and V. H. Grassian (2008). Characterization and acid-mobilization study of iron-containing mineral dust source materials. *Journal of Geophysical Research-Atmospheres* **113**(D5).

Decesari, S., M. C. Facchini, E. Matta, M. Mircea, S. Fuzzi, A. R. Chughtai and D. M. Smith (2002). Water soluble organic compounds formed by oxidation of soot. *Atmospheric Environment* **36**(11): 1827-1832.

Diaz-Quintana, A., W. Leibl, H. Bottin and P. Setif (1998). Electron transfer in photosystem I reaction centers follows a linear pathway in which iron-sulfur cluster F-B is the immediate electron donor to soluble ferredoxin. *Biochemistry* **37**(10): 3429-3439.

Dinar, E., A. A. Riziq, C. Spindler, C. Erlick, G. Kiss and Y. Rudich (2008). The complex refractive index of atmospheric and model humic-like substances (HULIS) retrieved by a cavity ring down aerosol spectrometer (CRD-AS). *Faraday Discussions* **137**: 279-295.

Domeizel, M., A. Khalil and P. Prudent (2004). UV spectroscopy: a tool for monitoring humification and for proposing an index of the maturity of compost. *Bioresource Technology* **94**(2): 177-184.

Duce, R. A., C. K. Unni, B. J. Ray, J. M. Prospero and J. T. Merrill (1980). LONG-RANGE ATMOSPHERIC TRANSPORT OF SOIL DUST FROM ASIA TO THE TROPICAL NORTH PACIFIC - TEMPORAL VARIABILITY. *Science* **209**(4464): 1522-1524.

Duvall, R. M., B. J. Majestic, M. M. Shafer, P. Y. Chuang, B. R. T. Simoneit and J. J. Schauer (2008). The water-soluble fraction of carbon, sulfur, and crustal elements in Asian aerosols and Asian soils. *Atmospheric Environment* **42**(23): 5872-5884.

Faiola, C., A. M. Johansen, S. Rybka, A. Nieber, C. Thomas, S. Bryner, J. Johnston, M. Engelhard, P. Nachimuthu and K. S. Owens (2011). Ultrafine Particulate Ferrous Iron and Anthracene Associations with Mitochondrial Dysfunction. *Aerosol Science and Technology* **45**(9): 1109-1122.

Falkovich, A. H., G. Schkolnik, E. Ganor and Y. Rudich (2004). Adsorption of organic compounds pertinent to urban environments onto mineral dust particles. *Journal of Geophysical Research-Atmospheres* **109**(D2).

Fang, T., H. Y. Guo, L. H. Zeng, V. Verma, A. Nenes and R. J. Weber (2017). Highly Acidic Ambient Particles, Soluble Metals, and Oxidative Potential: A Link between Sulfate and Aerosol Toxicity. *Environmental Science & Technology* **51**(5): 2611-2620.

Fenoglio, I., L. Prandi, M. Tomatis and B. Fubini (2001). Free radical generation in the toxicity of inhaled mineral particles: the role of iron speciation at the surface of asbestos and silica. *Redox Report* **6**(4): 235-241.

Fu, P. P., Q. S. Xia, X. Sun and H. T. Yu (2012). Phototoxicity and Environmental Transformation of Polycyclic Aromatic Hydrocarbons (PAHs)-Light-Induced Reactive Oxygen Species, Lipid Peroxidation, and DNA Damage. *Journal of Environmental Science and Health Part C-Environmental Carcinogenesis & Ecotoxicology Reviews* **30**(1): 1-41.

Fung, I. Y., S. K. Meyn, I. Tegen, S. C. Doney, J. G. John and J. K. B. Bishop (2000). Iron supply and demand in the upper ocean. *Global Biogeochemical Cycles* **14**(1): 281-295.

Galarneau, E. (2008). Source specificity and atmospheric processing of airborne PAHs: Implications for source apportionment. *Atmospheric Environment* **42**(35): 8139-8149.

Garban, B., H. Blanchoud, A. Motelay-Massei, M. Chevreuil and D. Ollivon (2002). Atmospheric bulk deposition of PAHs onto France: trends from urban to remote sites. *Atmospheric Environment* **36**(34): 5395-5403.

Garg, S., A. L. Rose and T. D. Waite (2007). Superoxide mediated reduction of organically complexed Iron(III): Comparison of non-dissociative and dissociative reduction pathways. *Environmental Science & Technology* **41**(9): 3205-3212.

Gonzalez, D. H., C. K. Cala, Q. Y. Peng and S. E. Paulson (2017). HULIS Enhancement of Hydroxyl Radical Formation from Fe(II): Kinetics of Fulvic Acid-Fe(II)

Complexes in the Presence of Lung Antioxidants. *Environmental Science & Technology* **51**(13): 7676-7685.

Graber, E. R. and Y. Rudich (2006). Atmospheric HULIS: How humic-like are they? A comprehensive and critical review. *Atmospheric Chemistry and Physics* **6**: 729-753.

Guieu, C., S. Bonnet, T. Wagener and M. D. Loye-Pilot (2005). Biomass burning as a source of dissolved iron to the open ocean? *Geophysical Research Letters* **32**(19).

Guo, J., Y. Wang, X. H. Shen, Z. Wang, T. Lee, X. F. Wang, P. H. Li, M. H. Sun, J. L. Collett, W. X. Wang and T. Wang (2012). Characterization of cloud water chemistry at Mount Tai, China: Seasonal variation, anthropogenic impact, and cloud processing. *Atmospheric Environment* **60**: 467-476.

Hand, J. L., N. M. Mahowald, Y. Chen, R. L. Siefert, C. Luo, A. Subramaniam and I. Fung (2004). Estimates of atmospheric-processed soluble iron from observations and a global mineral aerosol model: Biogeochemical implications. *Journal of Geophysical Research-Atmospheres* **109**(D17).

Hersman, L., T. Lloyd and G. Sposito (1995). SIDEROPHORE-PROMOTED DISSOLUTION OF HEMATITE. *Geochimica Et Cosmochimica Acta* **59**(16): 3327-3330.

Hoffer, A., G. Kiss, M. Blazso and A. Gelencser (2004). Chemical characterization of humic-like substances (HULIS) formed from a lignin-type precursor in model cloud water. *Geophysical Research Letters* **31**(6).

Jenkins, B. M., A. D. Jones, S. Q. Turn and R. B. Williams (1996). Emission factors for polycyclic aromatic hydrocarbons from biomass burning. *Environmental Science & Technology* **30**(8): 2462-2469.

Jickells, T. D., Z. S. An, K. K. Andersen, A. R. Baker, G. Bergametti, N. Brooks, J. J. Cao, P. W. Boyd, R. A. Duce, K. A. Hunter, H. Kawahata, N. Kubilay, J. laRoche, P. S. Liss, N. Mahowald, J. M. Prospero, A. J. Ridgwell, I. Tegen and R. Torres (2005). Global iron connections between desert dust, ocean biogeochemistry, and climate. *Science* **308**(5718): 67-71.

Johnson, M. S., N. Meskhidze, F. Solmon, S. Gasso, P. Y. Chuang, D. M. Gaiero, R. M. Yantosca, S. L. Wu, Y. X. Wang and C. Carouge (2010). Modeling dust and soluble iron deposition to the South Atlantic Ocean. *Journal of Geophysical Research-Atmospheres* **115**.

Joss, A., E. Keller, A. C. Alder, A. Gobel, C. S. McArdell, T. Ternes and H. Siegrist (2005). Removal of pharmaceuticals and fragrances in biological wastewater treatment. *Water Research* **39**(14): 3139-3152.

Kappler, A., M. Benz, B. Schink and A. Brune (2004). Electron shuttling via humic acids in microbial iron(III) reduction in a freshwater sediment. *Fems Microbiology Ecology* **47**(1): 85-92.

Kendall, T. A. and M. F. Hochella (2003). Measurement and interpretation of molecular-level forces of interaction between the siderophore azotobactin and mineral surfaces. *Geochimica Et Cosmochimica Acta* **67**(19): 3537-3546.

Khalili, N. R., P. A. Scheff and T. M. Holsen (1995). PAH source fingerprints for coke ovens, diesel and gasoline-engines, highway tunnels, and wood combustion emissions. *Atmospheric Environment* **29**(4): 533-542.

Kim, H. Y., S. Takizawa and K. Oh (2016). Copper-catalyzed divergent oxidative pathways of 2-naphthol derivatives: ortho-naphthoquinones versus 2-BINOLs. *Organic & Biomolecular Chemistry* **14**(30): 7191-7196.

Kim, K. H., S. A. Jahan, E. Kabir and R. J. C. Brown (2013). A review of airborne polycyclic aromatic hydrocarbons (PAHs) and their human health effects. *Environment International* **60**: 71-80.

Kim, S. and D. S. Aga (2007). Potential ecological and human health impacts of antibiotics and antibiotic-resistant bacteria from wastewater treatment plants. *Journal of Toxicology and Environmental Health-Part B-Critical Reviews* **10**(8): 559-573.

Kiss, G., E. Tombacz and H. C. Hansson (2005). Surface tension effects of humic-like substances in the aqueous extract of tropospheric fine aerosol. *Journal of Atmospheric Chemistry* **50**(3): 279-294.

Knaapen, A. M., T. M. Shi, P. J. A. Borm and R. P. F. Schins (2002). Soluble metals as well as the insoluble particle fraction are involved in cellular DNA damage induced by particulate matter. *Molecular and Cellular Biochemistry* **234**(1): 317-326.

Kristensen, T. B., L. Du, Q. T. Nguyen, J. K. Nojgaard, C. B. Koch, O. F. Nielsen, A. G. Hallar, D. H. Lowenthal, B. Nekat, D. van Pinxteren, H. Herrmann, M. Glasius, H. G. Kjaergaard and M. Bilde (2015). Chemical properties of HULIS from three different environments. *Journal of Atmospheric Chemistry* **72**(1): 65-80.

Kroll, J. H., N. M. Donahue, J. L. Jimenez, S. H. Kessler, M. R. Canagaratna, K. R. Wilson, K. E. Altieri, L. R. Mazzoleni, A. S. Wozniak, H. Bluhm, E. R. Mysak, J. D. Smith, C. E. Kolb and D. R. Worsnop (2011). Carbon oxidation state as a metric for describing the chemistry of atmospheric organic aerosol. *Nature Chemistry* **3**(2): 133-139.

Lecuyer, C. and Y. Ricard (1999). Long-term fluxes and budget of ferric iron: implication for the redox states of the Earth's mantle and atmosphere. *Earth and Planetary Science Letters* **165**(2): 197-211.

Lee, J. Y., Y. P. Kim and C. H. Kang (2011). Characteristics of the ambient particulate PAHs at Seoul, a mega city of Northeast Asia in comparison with the characteristics of a background site. *Atmospheric Research* **99**(1): 50-56.

Lee, J. Y. and D. A. Lane (2009). Unique products from the reaction of naphthalene with the hydroxyl radical. *Atmospheric Environment* **43**(32): 4886-4893.

Lee, S. C., K. F. Ho, L. Y. Chan, B. Zielinska and J. C. Chow (2001). Polycyclic aromatic hydrocarbons (PAHs) and carbonyl compounds in urban atmosphere of Hong Kong. *Atmospheric Environment* **35**(34): 5949-5960.

Levar, C. E., C. L. Hoffman, A. J. Dunshee, B. M. Toner and D. R. Bond (2017). Redox potential as a master variable controlling pathways of metal reduction by Geobacter sulfurreducens. *Isme Journal* **11**(3): 741-752.

Li, P. H., Y. Wang, Y. H. Li, Z. F. Wang, H. Y. Zhang, P. J. Xu and W. X. Wang (2010). Characterization of polycyclic aromatic hydrocarbons deposition in PM2.5 and cloud/fog water at Mount Taishan (China). *Atmospheric Environment* **44**(16): 1996-2003.

Li, W. J., L. Xu, X. H. Liu, J. C. Zhang, Y. T. Lin, X. H. Yao, H. W. Gao, D. Z. Zhang, J. M. Chen, W. X. Wang, R. M. Harrison, X. Y. Zhang, L. Y. Shao, P. Q. Fu, A. Nenes and Z. B. Shi (2017). Air pollution-aerosol interactions produce more bioavailable iron for ocean ecosystems. *Science Advances* **3**(3).

Liao, X. Y., D. Zhao, X. L. Yan and S. G. Huling (2014). Identification of persulfate oxidation products of polycyclic aromatic hydrocarbon during remediation of contaminated soil. *Journal of Hazardous Materials* **276**: 26-34.

Lin, P., X. F. Huang, L. Y. He and J. Z. Yu (2010). Abundance and size distribution of HULIS in ambient aerosols at a rural site in South China. *Journal of Aerosol Science* **41**(1): 74-87.

Lin, P. and J. Z. Yu (2011). Generation of Reactive Oxygen Species Mediated by Humic-like Substances in Atmospheric Aerosols. *Environmental Science & Technology* **45**(24): 10362-10368.

Longo, A. F., Y. Feng, B. Lai, W. M. Landing, R. U. Shelley, A. Nenes, N. Mihalopoulos, K. Violaki and E. D. Ingall (2016). Influence of Atmospheric Processes on the Solubility and Composition of Iron in Saharan Dust. *Environmental Science & Technology* **50**(13): 6912-6920.

Lundstedt, S., P. A. White, C. L. Lemieux, K. D. Lynes, L. B. Lambert, L. Oberg, P. Haglund and M. Tysklind (2007). Sources, fate, and toxic hazards of oxygenated polycyclic aromatic hydrocarbons (PAHs) at PAH-contaminated sites. *Ambio* **36**(6): 475-485.

Luo, C. and Y. Gao (2010). Aeolian iron mobilisation by dust-acid interactions and their implications for soluble iron deposition to the ocean: a test involving potential anthropogenic organic acidic species. *Environmental Chemistry* **7**(2): 153-161.

Luo, C., N. Mahowald, T. Bond, P. Y. Chuang, P. Artaxo, R. Siefert, Y. Chen and J. Schauer (2008). Combustion iron distribution and deposition. *Global Biogeochemical Cycles* **22**(1).

Luo, C., N. M. Mahowald, N. Meskhidze, Y. Chen, R. L. Siefert, A. R. Baker and A. M. Johansen (2005). Estimation of iron solubility from observations and a global aerosol model. *Journal of Geophysical Research-Atmospheres* **110**(D23).

Ma, Y. Q., Y. B. Cheng, X. H. Qiu, Y. Lin, J. Cao and D. Hu (2016). A quantitative assessment of source contributions to fine particulate matter (PM2.5)-bound polycyclic aromatic hydrocarbons (PAHs) and their nitrated and hydroxylated derivatives in Hong Kong. *Environmental Pollution* **219**: 742-749.

Mahowald, N. M., A. R. Baker, G. Bergametti, N. Brooks, R. A. Duce, T. D. Jickells, N. Kubilay, J. M. Prospero and I. Tegen (2005). Atmospheric global dust cycle and iron inputs to the ocean. *Global Biogeochemical Cycles* **19**(4).

Mahowald, N. M., S. Engelstaedter, C. Luo, A. Sealy, P. Artaxo, C. Benitez-Nelson, S. Bonnet, Y. Chen, P. Y. Chuang, D. D. Cohen, F. Dulac, B. Herut, A. M. Johansen, N. Kubilay, R. Losno, W. Maenhaut, A. Paytan, J. A. Prospero, L. M. Shank and R. L. Siefert (2009). Atmospheric Iron Deposition: Global Distribution, Variability, and Human Perturbations. *Annual Review of Marine Science* **1**: 245-278.

Majestic, B. J., J. J. Schauer and M. M. Shafer (2007). Application of synchrotron radiation for measurement of iron red-ox speciation in atmospherically processed aerosols. *Atmospheric Chemistry and Physics* **7**(10): 2475-2487.

Marr, L. C., T. W. Kirchstetter, R. A. Harley, A. H. Miguel, S. V. Hering and S. K. Hammond (1999). Characterization of polycyclic aromatic hydrocarbons in motor vehicle fuels and exhaust emissions. *Environmental Science & Technology* **33**(18): 3091-3099.

Martin, J. H. and S. E. Fitzwater (1988). Iron-deficiency limits phytoplankton growth in the northeast pacific subarctic. *Nature* **331**(6154): 341-343.

McLennan, S. M. (2001). Relationships between the trace element composition of sedimentary rocks and upper continental crust. *Geochemistry Geophysics Geosystems* **2**.

Meneghini, R. (1997). Iron homeostasis, oxidative stress, and DNA damage. *Free Radical Biology and Medicine* **23**(5): 783-792.

Meskhidze, N., W. L. Chameides, A. Nenes and G. Chen (2003). Iron mobilization in mineral dust: Can anthropogenic SO2 emissions affect ocean productivity? *Geophysical Research Letters* **30**(21).

Ministry of Environment-Province of British Columbia. Polycyclic Aromatic Hydrocarbons. Retrieved Jan 7, 2016, 2016, from http://www.env.gov.bc.ca/wat/wq/BCguidelines/pahs/pahs-01.htm.

Moore, C. M., M. M. Mills, K. R. Arrigo, I. Berman-Frank, L. Bopp, P. W. Boyd, E. D. Galbraith, R. J. Geider, C. Guieu, S. L. Jaccard, T. D. Jickells, J. La Roche, T. M. Lenton, N. M. Mahowald, E. Maranon, I. Marinov, J. K. Moore, T. Nakatsuka, A. Oschlies, M. A. Saito, T. F. Thingstad, A. Tsuda and O. Ulloa (2013). Processes and patterns of oceanic nutrient limitation. *Nature Geoscience* **6**(9): 701-710.

Murakami, N., T. Chiyoya, T. Tsubota and T. Ohno (2008). Switching redox site of photocatalytic reaction on titanium(IV) oxide particles modified with transition-metal ion controlled by irradiation wavelength. *Applied Catalysis a-General* **348**(1): 148-152.

Newport. Solar Simulator Spectral Irradiance Data. Retrieved Aug 16, 2017, 2017, from https://www.newport.com/n/solar-simulator-spectral-irradiance-data.

Oakes, M., E. D. Ingall, B. Lai, M. M. Shafer, M. D. Hays, Z. G. Liu, A. G. Russell and R. J. Weber (2012). Iron Solubility Related to Particle Sulfur Content in Source Emission and Ambient Fine Particles. *Environmental Science & Technology* **46**(12): 6637-6644.

Oakes, M., R. J. Weber, B. Lai, A. Russell and E. D. Ingall (2012). Characterization of iron speciation in urban and rural single particles using XANES spectroscopy and micro X-ray fluorescence measurements: investigating the relationship between speciation and fractional iron solubility. *Atmospheric Chemistry and Physics* **12**(2): 745-756.

Paris, R. and K. V. Desboeufs (2013). Effect of atmospheric organic complexation on iron-bearing dust solubility. *Atmospheric Chemistry and Physics* **13**(9): 4895-4905.

Paris, R., K. V. Desboeufs, P. Formenti, S. Nava and C. Chou (2010). Chemical characterisation of iron in dust and biomass burning aerosols during AMMA-

SOP0/DABEX: implication for iron solubility. *Atmospheric Chemistry and Physics* **10**(9): 4273-4282.

Paris, R., K. V. Desboeufs and E. Journet (2011). Variability of dust iron solubility in atmospheric waters: Investigation of the role of oxalate organic complexation. *Atmospheric Environment* **45**(36): 6510-6517.

Pehkonen, S. O., R. Siefert, Y. Erel, S. Webb and M. R. Hoffmann (1993). Photoreduction of iron oxyhydroxides in the presence of important atmospheric organic-compounds. *Environmental Science & Technology* **27**(10): 2056-2062.

Pei, Z. G., L. Y. Li, L. X. Sun, S. Z. Zhang, X. Q. Shan, S. Yang and B. Wen (2013). Adsorption characteristics of 1,2,4-trichlorobenzene, 2,4,6-trichlorophenol, 2-naphthol and naphthalene on graphene and graphene oxide. *Carbon* **51**: 156-163.

Perraudin, E., H. Budzinski and E. Villenave (2007). Identification and quantification of ozonation products of anthracene and phenanthrene adsorbed on silica particles. *Atmospheric Environment* **41**(28): 6005-6017.

Piepenbrock, A., C. Schroder and A. Kappler (2014). Electron Transfer from Humic Substances to Biogenic and Abiogenic Fe(III) Oxyhydroxide Minerals. *Environmental Science & Technology* **48**(3): 1656-1664.

Pillar, E. A., R. C. Camm and M. I. Guzman (2014). Catechol Oxidation by Ozone and Hydroxyl Radicals at the Air-Water Interface. *Environmental Science & Technology* **48**(24): 14352-14360.

Preuss, R., J. Angerer and H. Drexler (2003). Naphthalene - an environmental and occupational toxicant. *International Archives of Occupational and Environmental Health* **76**(8): 556-576.

Prospero, J. M., K. Barrett, T. Church, F. Dentener, R. A. Duce, J. N. Galloway, H. Levy, J. Moody and P. Quinn (1996). Atmospheric deposition of nutrients to the North Atlantic Basin. *Biogeochemistry* **35**(1): 27-73.

Ravindra, K., R. Sokhi and R. Van Grieken (2008). Atmospheric polycyclic aromatic hydrocarbons: Source attribution, emission factors and regulation. *Atmospheric Environment* **42**(13): 2895-2921.

Reisen, F. and J. Arey (2005). Atmospheric reactions influence seasonal PAH and nitro-PAH concentrations in the Los Angeles basin. *Environmental Science & Technology* **39**(1): 64-73.

Ringuet, J., A. Albinet, E. Leoz-Garziandia, H. Budzinski and E. Villenave (2012). Diurnal/nocturnal concentrations and sources of particulate-bound PAHs, OPAHs

and NPAHs at traffic and suburban sites in the region of Paris (France). *Science of the Total Environment* **437**: 297-305.

Rizzolo, J. A., C. G. G. Barbosa, G. C. Borillo, A. F. L. Godoi, R. A. F. Souza, R. V. Andreoli, A. O. Manzi, M. O. Sa, E. G. Alves, C. Pohlker, I. H. Angelis, F. Ditas, J. Saturno, D. Moran-Zuloaga, L. V. Rizzo, N. E. Rosario, T. Pauliquevis, R. M. N. Santos, C. I. Yamamoto, M. O. Andreae, P. Artaxo, P. E. Taylor and R. H. M. Godoi (2017). Soluble iron nutrients in Saharan dust over the central Amazon rainforest. *Atmospheric Chemistry and Physics* **17**(4): 2673-2687.

Rose, A. L. and T. D. Waite (2003). Kinetics of iron complexation by dissolved natural organic matter in coastal waters. *Marine Chemistry* **84**(1-2): 85-103.

Santana-Casiano, J. M., M. Gonzalez-Davila and F. J. Millero (2004). The oxidation of Fe(II) in NaCl-HCO3- and seawater solutions in the presence of phthalate and salicylate ions: a kinetic model. *Marine Chemistry* **85**(1-2): 27-40.

Schroth, A. W., J. Crusius, E. R. Sholkovitz and B. C. Bostick (2009). Iron solubility driven by speciation in dust sources to the ocean. *Nature Geoscience* **2**(5): 337-340.

Searle, L. J., G. Meric, I. Porcelli, S. K. Sheppard and S. Lucchini (2015). Variation in Siderophore Biosynthetic Gene Distribution and Production across Environmental and Faecal Populations of Escherichia coli. *Plos One* **10**(3).

Sedwick, P. N., E. R. Sholkovitz and T. M. Church (2007). Impact of anthropogenic combustion emissions on the fractional solubility of aerosol iron: Evidence from the Sargasso Sea. *Geochemistry Geophysics Geosystems* **8**.

Shafer, M. M., D. A. Perkins, D. S. Antkiewicz, E. A. Stone, T. A. Quraishi and J. J. Schauer (2010). Reactive oxygen species activity and chemical speciation of size-fractionated atmospheric particulate matter from Lahore, Pakistan: an important role for transition metals. *Journal of Environmental Monitoring* **12**(3): 704-715.

Shi, Z. B., M. D. Krom, S. Bonneville and L. G. Benning (2015). Atmospheric Processing Outside Clouds Increases Soluble Iron in Mineral Dust. *Environmental Science & Technology* **49**(3): 1472-1477.

Sholkovitz, E. R., P. N. Sedwick and T. M. Church (2009). Influence of anthropogenic combustion emissions on the deposition of soluble aerosol iron to the ocean: Empirical estimates for island sites in the North Atlantic. *Geochimica Et Cosmochimica Acta* **73**(14): 3981-4003.

Sholkovitz, E. R., P. N. Sedwick, T. M. Church, A. R. Baker and C. F. Powell (2012). Fractional solubility of aerosol iron: Synthesis of a global-scale data set. *Geochimica Et Cosmochimica Acta* **89**: 173-189.

Spokes, L. J., T. D. Jickells and B. Lim (1994). SOLUBILIZATION OF AEROSOL TRACE-METALS BY CLOUD PROCESSING - A LABORATORY STUDY. *Geochimica Et Cosmochimica Acta* **58**(15): 3281-3287.

Takeda, S. (1998). Influence of iron availability on nutrient consumption ratio of diatoms in oceanic waters. *Nature* **393**(6687): 774-777.

Tang, W. W., G. M. Zeng, J. L. Gong, J. Liang, P. Xu, C. Zhang and B. B. Huang (2014). Impact of humic/fulvic acid on the removal of heavy metals from aqueous solutions using nanomaterials: A review. *Science of the Total Environment* **468**: 1014-1027.

Tipping, E., C. Rey-Castro, S. E. Bryan and J. Hamilton-Taylor (2002). Al(III) and Fe(III) binding by humic substances in freshwaters, and implications for trace metal speciation. *Geochimica Et Cosmochimica Acta* **66**(18): 3211-3224.

Tombacz, E., Z. Libor, E. Illes, A. Majzik and E. Klumpp (2004). The role of reactive surface sites and complexation by humic acids in the interaction of clay mineral and iron oxide particles. *Organic Geochemistry* **35**(3): 257-267.

Tsai, P. J., T. S. Shih, H. L. Chen, W. J. Lee, C. H. Lai and S. H. Liou (2004). Assessing and predicting the exposures of polycyclic aromatic hydrocarbons (PAHs) and their carcinogenic potencies from vehicle engine exhausts to highway toll station workers. *Atmospheric Environment* **38**(2): 333-343.

Tsapakis, M. and E. G. Stephanou (2007). Diurnal cycle of PAHs, nitro-PAHs, and oxy-PAHs in a high oxidation capacity marine background atmosphere. *Environmental Science & Technology* **41**(23): 8011-8017.

Tuomela, M., M. Vikman, A. Hatakka and M. Itavaara (2000). Biodegradation of lignin in a compost environment: a review. *Bioresource Technology* **72**(2): 169-183.

Valavanidis, A., K. Fiotakis and T. Vlachogianni (2008). Airborne Particulate Matter and Human Health: Toxicological Assessment and Importance of Size and Composition of Particles for Oxidative Damage and Carcinogenic Mechanisms. *Journal of Environmental Science and Health Part C-Environmental Carcinogenesis & Ecotoxicology Reviews* **26**(4): 339-362.

Valavanidis, A., A. Salika and A. Theodoropoulou (2000). Generation of hydroxyl radicals by urban suspended particulate air matter. The role of iron ions. *Atmospheric Environment* **34**(15): 2379-2386.

VanCappellen, P. and Y. F. Wang (1996). Cycling of iron and manganese in surface sediments: A general theory for the coupled transport and reaction of carbon, oxygen, nitrogen, sulfur, iron, and manganese. *American Journal of Science* **296**(3): 197-243.

Varga, B., G. Kiss, I. Ganszky, A. Gelencser and Z. Krivacsy (2001). Isolation of water-soluble organic matter from atmospheric aerosol. *Talanta* **55**(3): 561-572.

Verma, V., M. M. Shafer, J. J. Schauer and C. Sioutas (2010). Contribution of transition metals in the reactive oxygen species activity of PM emissions from retrofitted heavy-duty vehicles. *Atmospheric Environment* **44**(39): 5165-5173.

Vile, G. F., C. C. Winterbourn and H. C. Sutton (1987). Radical-driven Fenton reactions - studies with paraquat, adriamycin, and anthraquinone 6-sulfonate and citrate, ATP, ADP, and pyrophosphate iron chelates. *Archives of Biochemistry and Biophysics* **259**(2): 616-626.

Vione, D., V. Maurino and C. Minero (2014). Photosensitised humic-like substances (HULIS) formation processes of atmospheric significance: a review. *Environmental Science and Pollution Research* **21**(20): 11614-11622.

Voelker, B. M., F. M. M. Morel and B. Sulzberger (1997). Iron redox cycling in surface waters: Effects of humic substances and light. *Environmental Science & Technology* **31**(4): 1004-1011.

Warner, B. B., L. Stuart, S. Gebb and J. R. Wispe (1996). Redox regulation of manganese superoxide dismutase. *American Journal of Physiology-Lung Cellular and Molecular Physiology* **271**(1): L150-L158.

Wentworth, G. R. and H. A. Al-Abadleh (2011). DRIFTS studies on the photosensitized transformation of gallic acid by iron(III) chloride as a model for HULIS in atmospheric aerosols. *Physical Chemistry Chemical Physics* **13**(14): 6507-6516.

Willey, J. D., R. J. Kieber, J. J. Humphreys, B. C. Rice, M. J. Hopwood, G. B. Avery and R. N. Mead (2015). The role of fossil fuel combustion on the stability of dissolved iron in rainwater. *Atmospheric Environment* **107**: 187-193.

Willey, J. D., R. J. Kieber, P. J. Seaton and C. Miller (2008). Rainwater as a source of Fe(II)-stabilizing ligands to seawater. *Limnology and Oceanography* **53**(4): 1678-1684.

Winkelmann, G. (2002). Microbial siderophore-mediated transport. *Biochemical Society Transactions* **30**: 691-696.

Wols, B. A. and C. H. M. Hofman-Caris (2012). Review of photochemical reaction constants of organic micropollutants required for UV advanced oxidation processes in water. *Water Research* **46**(9): 2815-2827.

Yue, S. Y., H. Ren, S. Y. Fan, Y. L. Sun, Z. F. Wang and P. Q. Fu (2016). Springtime precipitation effects on the abundance of fluorescent biological aerosol particles and HULIS in Beijing. *Scientific Reports* **6**.

Yunker, M. B., L. R. Snowdon, R. W. MacDonald, J. N. Smith, M. G. Fowler, D. N. Skibo, F. A. McLaughlin, A. I. Danyushevskaya, V. I. Petrova and G. I. Ivanov (1996). Polycyclic aromatic hydrocarbon composition and potential sources for sediment samples from the Beaufort and Barents Seas. *Environmental Science & Technology* **30**(4): 1310-1320.

Zanca, N., A. T. Lambe, P. Massoli, M. Paglione, D. R. Croasdale, Y. Parmar, E. Tagliavini, S. Gilardoni and S. Decesari (2017). Characterizing source fingerprints and ageing processes in laboratory-generated secondary organic aerosols using proton-nuclear magnetic resonance (H-1-NMR) analysis and HPLC HULIS determination. *Atmospheric Chemistry and Physics* **17**(17): 10405-10421.

Zhang, Y. X. and S. Tao (2009). Global atmospheric emission inventory of polycyclic aromatic hydrocarbons (PAHs) for 2004. *Atmospheric Environment* **43**(4): 812-819.

Zhu, S. Q., A. Das, L. Bui, H. J. Zhou, D. P. Curran and M. Rueping (2013). Oxygen Switch in Visible-Light Photoredox Catalysis: Radical Additions and Cyclizations and Unexpected C-C-Bond Cleavage Reactions. *Journal of the American Chemical Society* **135**(5): 1823-1829.

APPENDIX A

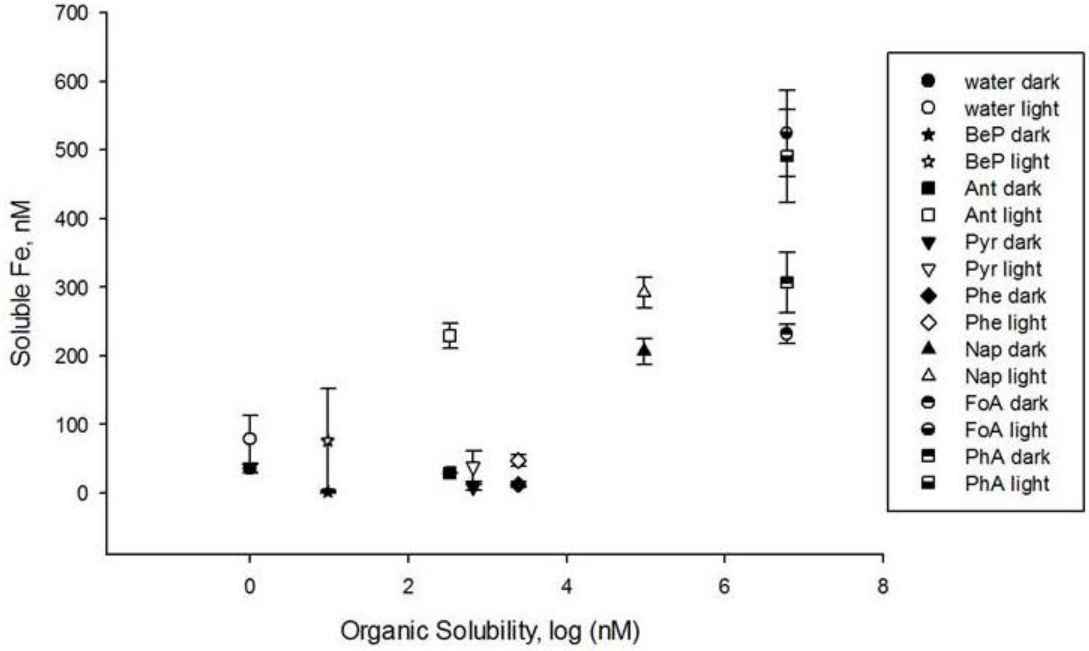

Figure A. 1 Molar comparison of dissolved organic reagents and solubilized iron. For PAH assays open markers represent light samples, filled markers represent dark samples. Split markers represent carboxylic acid assays, where open tops are light samples and closed tops are dark. Dissolved content of organics are based on listed aqueous solubilities, soluble iron data represents the total quantity of produced soluble iron over 16 hours. Both are reported in nM units with the organics plotted in log scale. "water" refers to ultrapure water samples; BeP, benzo(e)pyrene; Ant, anthracene; Pyr, pyrene; Phe, phenanthrene; Nap, naphthalene; FoA, formic acid; PhA, phthalic acid.

Supplemental Table 1: Difference in soluble metal concentrations between light and dark samples. [a] value within instrument noise region, [b] deviation below detection limits.

Organic Reagent	Δ Fe, ppb	Δ Ti, ppb	Δ Mn, ppb	Δ Ba, ppb
Ultrapure water	2.4 ± 1.98	<0.01[a] ± <0.01[b]	0.50 ± 0.60	0.25 ± 0.76
Formic Acid	16.3 ± 0.38	-0.3 ± 0.4	-2.3 ± 1.9	-1.05 ± 1.49
Phthalic Acid	10.3 ± 4.50	0.10 ± <0.01[b]	0.60 ± <0.01[b]	0.10 ± <0.01[b]
Naphthalene	4.8 ± 1.51	-0.03 ± 0.06	0.87 ± 0.12	0.87 ± 0.34
Anthracene	11.2 ± 1.06	-0.17 ± 0.29	0.23 ± 0.59	0.73 ± 0.57
Phenanthrene	1.85 ± 0.51	<0.01[a] ± <0.01[b]	1.0 ± 0.8	0.50 ± 0.23
Pyrene	1.68 ± 1.27	-0.03 ± 0.06	0.33 ± 0.34	0.37 ± 0.55
Benzo(e)Pyrene	4.15 ± 4.69	<0.01[a] ± <0.01[b]	1.4 ± 0.9	0.33 ± 0.18

Supplemental Table 2: Percent and total molar soluble iron against listed soluble availability of organic compounds in ppb and total molarity. [a] non-zero deviation below significance.

Organic Reagent	mass, g/mol	solubility, log (ppb)	solubility, log (nM)	Fe light, %	Fe dark, %	Fe light, nM	Fe dark, nM
Ultrapure water	18.02	--	--	1.75 ± 0.78	0.79 ± 0.13	78.4 ± 34.9	35.4 ± 5.8
Benzo(e)pyrene	252.3	0.38	0.98	1.71 ± 1.88	0.06 ± 0.03	76.6 ± 84.2	2.5 ± 1.3
Anthracene	178.2	1.77	2.52	5.1 ± 0.4	0.7 ± >0.0[a]	228.4±17.9	29.1± >0.0[a]
Pyrene	202.1	2.12	2.82	0.85 ± 0.50	0.18 ± 0.08	38.3 ± 22.4	8.2 ± 3.6
Phenanthrene	178.2	2.64	3.39	1.06 ± 0.19	0.29 ± 0.09	47.4 ± 8.5	12.8 ± 4.0
Naphthalene	128.2	4.10	4.99	6.5 ± 0.5	4.60 ± 0.41	291.9±22.4	205.9±18.4
Formic Acid	46.03	5.44	6.78	11.7 ± 1.4	5.2 ± 0.3	524.4±62.7	231.9±13.4
Phthalic Acid	166.14	6.00	6.78	11.0 ± 1.5	6.84 ± 0.98	491.2±67.2	306.4±43.9

APPENDIX B

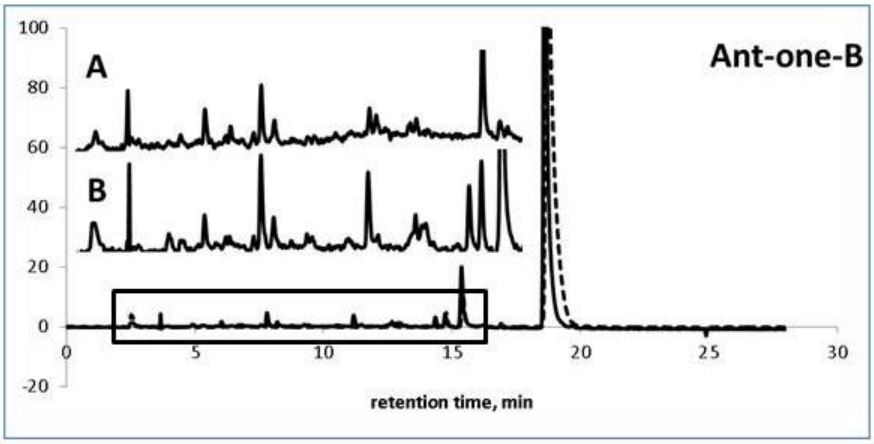

Figure B. 1 Fine structure of HPLC chromatograms of anthracene derivatives.
Box represents region of retention patterns shown in the inset. (A) 9,10-anthracene-diol, (B) 9,10-anthraquinone.